C O M M U N I C A T I O N S

FACULTY OF SCIENCES
UNIVERSITY OF ANKARA

DE LA FACULTE DES SCIENCES
DE L'UNIVERSITE D'ANKARA

Series B: Chemistry and Chemical Engineering

VOLUME: 61 **Number: 1-2** **YEAR: 2019**

Faculy of Sciences, Ankara University
06100 Beşevler, Ankara-Turkey
ISSN 1303-6017 E-ISSN 2687-4806

C O M M U N I C A T I O N S

FACULTY OF SCIENCES
UNIVERSITY OF ANKARA

DE LA FACULTE DES SCIENCES
DE L'UNIVERSITE D'ANKARA

Series B: Chemistry and Chemical Engineering

Volume: 61 **Number: 1-2** **Year: 2019**

This Journal is published two issues in a year by the Faculty of Sciences, University of Ankara. Articles and any other material published in this journal represent the opinions of the author(s) and should not be construed to reflect the opinions of the Editor(s) and the Publisher(s).

Correspondence Address:
COMMUNICATIONS
EDITORIAL OFFICE
Ankara University, Faculty of Sciences,
06100 Tandoğan, ANKARA – TURKEY
Tel: (90) 312-212 67 20 Fax: (90) 312-223 23 95
http:// https://dergipark.org.tr/en/pub/communb

Print:
Ankara University Press
İncitaş Sokak No:10 06510 Beşevler
ANKARA – TURKEY

C O M M U N I C A T I O N S

FACULTY OF SCIENCES
UNIVERSITY OF ANKARA

DE LA FACULTE DES SCIENCES
DE L'UNIVERSITE D'ANKARA

VOLUME: 61 **Number: 1-2** **YEAR: 2019**

Series B: Chemistry and Chemical Engineering

C O M M U N I C A T I O N S

FACULTY OF SCIENCES
UNIVERSITY OF ANKARA

DE LA FACULTE DES SCIENCES
DE L'UNIVERSITE D'ANKARA

Commun.Fac.Sci.Univ.Ank.Series B
Volume 61, Number 1-2, Pages 1-14(2019)
ISSN 2687-4806
http://communications.science.ankara.edu.tr/index.php?series=B

DETERMINATION OF ABSOLUTE CONFIGURATION OF 8,8,10,10-TETRACHLORO-20,21-DIHYDRO-18H,23H-6,12-EPIAZENO-6λ5,8λ5,10λ5, 12λ5-[1,3,2]BENZOXAZAPHOSPHONINO[2 ,3 :8,9][1,3,5,7,9,2,4,6,8] PENTAAZATETRAPHOSPHACYCLOUNDSYNO[2,1-B][1,3,2] BENZOXAZAPHOSPHONINE USING X-RAY CRYSTALLOGRAPHY

GAMZE ELMAS, AYTUĞ OKUMUŞ, SATİYE SEVİM İSAOĞLU, TUNCER HÖKELEK AND ZEYNEL KILIÇ

ABSTRACT. The title compound, 8, 8, 10, 10-tetrachloro-20,21-dihydro-18H, 23H-6, 12-epiazeno-6λ5, 8λ5, 10λ5, 12λ5-[1,3,2] benzoxazaphosphonino [2',3':8,9][1,3,5,7,9,2,4,6,8] pentaazatetraphosphacyclo undsyno [2,1-b] [1,3,2] benzoxazaphosphonine; C16H16Cl4N6O2P4, a cyclotetraphosphazene, has a tetrachloro-2, 4-spiro-ansa-spiro (tetrachloro-2,4-sas) architecture in which the bicyclic structure has consisted of eight-membered tetrameric N4P4 and seven-membered ansa (N1/P1/P1′/N4′/C8′/C8/N4) rings fused with a common PNP fragment. The asymmetric unit possesses one-half of the molecule. P1 and P1′ atoms are stereogenic centres. In addition, there is a mirror plane passing through the N3 and N1 atoms in the molecule, and therefore, this compound is in meso form (RS/SR). According to the checkcif result, it is found that the absolute configuration of P1 and/or P1′ phosphorus centers is RS, displaying that in the solid-state there is only one enantiomer in the unit cell. The space group is P bnm with cell parameters of a = 6.2692(2), b = 15.8111(3), c = 22.9393(4) Å.

1. INTRODUCTION

Octachlorocyclotetraphosphazene, also known as tetrameric phosphazene, N4P4Cl8, is an important starting compound in the field of phosphazene chemistry [1,2]. It has been used in the syntheses of considerable amounts of organocyclotetraphosphazene and polymeric phosphazene derivatives with different substituents, and the composed products from these reactions display various chemical and physical properties upon the types and features of the bonded groups to the four P-atoms [1-3]. Many tetrameric phosphazene derivatives were synthesized using the mono and bidentate ligands until today [4-7], however, in the literature the Cl replacement reactions with polyfunctional ligands are limited relatively [8,9]. Tetrameric products with the bidentate ligands can produce spiro, dispiro, trispiro, tetraspiro,

Received by the editors: July 11, 2019; Accepted: August 09, 2019.
Key word and phrases: Cyclotetraphosphazene, spiro-ansa-spiro-Structure, X-ray crystallography.

ansa, spiro-ansa, bino and spiro-bino derivatives, and in addition to these products N4P4Cl8 may also give spiro-ansa-spiro, ansa-spiro-ansa and di(spiro-bino) products with the polyfunctional ligands depending on the reaction conditions [4-10].

Recently, the stereogenic properties of the cyclophosphazenes have been researched as an attractive area, and some papers have been published about this topic [11,12]. For the evaluations of the stereogenic properties of the cyclophosphazenes, were used the different methods, such as X-ray crystallography, HPLC and 31P NMR spectroscopy in the presence of (R)-(+)-2,2,2-trifluoro-1-(9'-anthryl)-ethanol (CSA) [13,14].

Organocyclophosphazenes have important and different applications in the technological and biological areas; eg. ionic liquids [15], advanced elastomers [16], Li-ion batteries [17], the anti-cancer [18] and antituberculosis [19] agents, the antibacterial and antifungal activity studies [20,21], and the oxidative cleavage of DNA [22,23].

In this paper, the tetrachloro-2,4-sas cyclotetraphosphazene was synthesized from the reaction of N4P4Cl8 with N2O2 donor-type unsymmetrical tetradentate ligand according to the published paper [24], and it was crystallized from acetonitrile. The aim of the current paper is to investigate the crystallographic and stereogenic properties of tetrachloro-2,4-sas cyclotetraphosphazene derivative. Besides, the determination of the absolute configurations of this compound is an important finding.

2. Materials And Methods

2.1. X-ray crystal structure determination

The colourless single crystals of the title **tetrachloro-2,4-sas** compound was obtained from acetonitrile at room temperature. The crystallographic details are listed in Table 1, and the selected bond lengths and angles together with the selected torsion angles are presented in Table 2. The crystallographic data were recorded on a Bruker Kappa APEXII CCD area-detector diffractometer using Mo K_α radiation (λ=0.71073 Å) at T=100(2) K. Absorption correction by multi-scan [25] was applied. Structure was solved by direct methods and refined by full-matrix least squares against F^2 using all data [26]. All non-H atoms were refined anisotropically. Hydrogen atom positions were calculated geometrically at distances of 0.93 Å (CH) and 0.97 Å (CH_2) from the parent C atoms; a riding model was used during the refinement process and the U_{iso}(H) values were constrained to be 1.2U_{eq}(carrier atom).

2.2. Materials used for syntheses

The starting tetradentate ligand, 2,2'-[1,2-ethanediylbis(iminomethanediyl)]diphenol, and the **tetrachloro-sas** cyclotetraphosphazene were prepared according to the published procedures [24].

TABLE 1. Crystallographic details.

Empirical Formula	$C_{16}H_{16}Cl_4N_6O_2P_4$
Fw	590.03
Crystal System	orthorhombic
Space Group	P bnm
a (Å)	6.2692(2)
b (Å)	15.8111(3)
c (Å)	22.9393(4)
α (°)	90.00
β (°)	90.00
γ (°)	90.00
V (Å^3)	2273.81(9)
Z	4
T	100(2) K
Crystal color	colourless
Crystal size	0.18x0.28x0.29 mm
μ (mm^{-1})	0.832 (Mo K_α)
ρ (calcd) (g cm^{-3})	1.724
Number of Reflections Total	12173
Number of Reflections Unique	2883
R_{int}	0.0565
$(\Delta/\sigma)_{max}$	<0.001
$(\Delta\rho)_{max}$	0.607 e Å^{-3}
$(\Delta\rho)_{min}$	−0.838 e Å^{-3}

$2\theta_{max}$ (°)	56.64
T_{min} / T_{max}	0.896/ 0.920
Number of Parameters	148
R [$F^2>2\sigma(F^2)$]	0.0466
wR	0.1226

TABLE 2. The selected bond lengths (Å) and angles (deg) with the selected torsiyon angles (°).

P1– N1	1.5605(14)	N1– P1– N4	118.86(17)	N4– P1– N1– P1′	-81.2(3)
P1– N4	1.580(3)	N5– P1– O1	103.53(16)	N4– P4– N3– P4′	-65.8(4)
P4– N3	1.5641(14)	N5– P1– N1	112.37(14)	N1– P1– N4– P4	39.4(4)
P4– N4	1.543(3)	N4– P1– O1	103.45(15)	N3– P4– N4– P1	7.0(5)
P1– N5	1.615(3)	N3– P4– N4	122.55(17)		
P4– Cl3	2.0010(10)	N5– P1– N4	111.1(2)		
P4– Cl4	2.0107(11)	P4– N3– P4′	137.8(2)		
P1– O1	1.5882(19)	P1– N1– P1′	132.6(2)		
		P1– N4– P4	133.8(2)		
		N3– P4– Cl3	105.99(12)		
		N3– P4– Cl4	109.98(13)		
		N4– P4– Cl3	107.48(13)		
		N4– P4– Cl4	107.57(16)		

3. Result And Discussion

The title cyclotetraphosphazene (Fig. 1) has consisted of a 2,4-spiro-ansa-spiro fashion with the N_2O_2 tetradentate ligand bonded to the phosphorus atoms. The asymmetric unit of the title cyclotetraphosphazene, $C_{16}H_{16}Cl_4N_6O_2P_4$, (Fig. 2) contains only one-half of the molecule. It has a tetrachloro-2,4-spiro-ansa-spiro (**tetrachloro-2,4-sas**) architecture in which the bicyclic group contains the eight-membered tetrameric, N_4P_4, ring and the seven-membered ansa, (N1/P1/P1′/N4′/C8′/C8/N4), ring fused through a common PNP fragment, and the two symmetry related benzoxazaphosphonine groups. The oxygen atoms (O1 and O1′) bonded to the phosphorus atoms (P1 and P1′) are in *cis* fashions [symmetry code: (‘) : x, y, ½ - z]. There is a mirror plane passing through the atoms N1 and N3. The **tetrachloro-2,4-sas** cyclotetraphosphazene structure has two equivalent stereogenic P centers (P1 and P1′). It was clearly determined that the absolute configuration of these P1 and P1′ atoms is

RS with respect to the checkcif data, showing that in the unit cell there is only one enantiomer in the solid-state (Figs. 1 and 2).

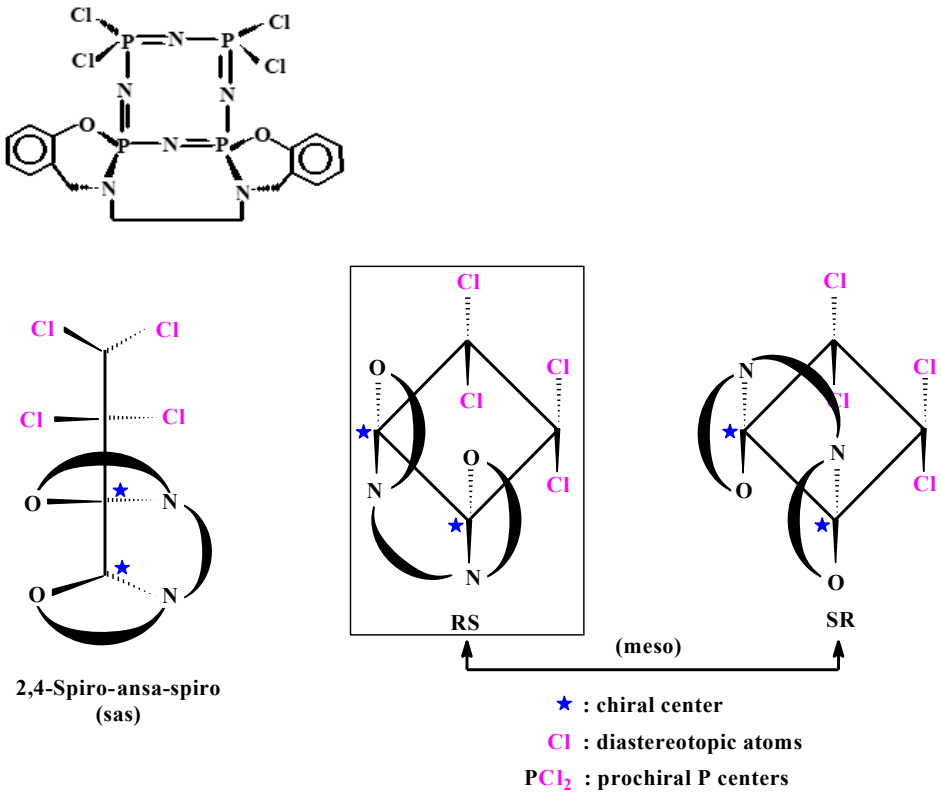

FIGURE 1. Chemical diagram and the meso forms of tetrachloro-2,4-spiro-ansa-spiro cyclotetraphosphazene.based on the ORTEP diagram *via* stick diagrams and spatial views.

The molecular and crystal structure of **tetrachloro-2,4-sas** compound along with the atom-numbering scheme is depicted in Fig. 2. The P atoms are non-coplanar and the N atoms are displaced above (+) and/or below (–) of the best least -squares plane passing through the P atoms by the following distances: N1 [–0.2957(1) Å], N3 [+0.3112(1) Å] and N4 [–0.0932(1) Å]. The conformation of the macrocyclic cyclotetraphosphazene ring is given by the torsion angles of the ring bonds (Table 2), and **tetrachloro-2,4-sas** compound comprises of a

symmetric non-planar cyclic tetrameric phosphazene ring, A (P1/N1/P1'/N4'/P4'/N3/P4/N4), in sofa conformation (Fig. 3a) with the puckering amplitude [27] Q_T of 0.5926(21) Å, while the seven-membered ansa ring, B (N1/P1/N5/C8/C8'/N5'/P1′), and the six-membered spiro ring, C (P1/O1/N5/C1/C6/C7), adopt flattened-boat (Fig. 3b) and twisted-boat (Fig. 3c) conformations with the puckering amplitudes [31] Q_T of 0.4622(32) Å and 0.5016(29) Å, respectively.

The bicyclic part of the molecule contains the eight-membered tetrameric phosphazene, A (P1/N1/P1'/N4'/P4'/N3/P4/N4), ring and the seven-membered ansa, B (N1/P1/N5/C8/C8'/N5'/P1′), precursor fused through a common PNP fragment, and it resembles the stable "adamantane" structure, with a V-shaped conformation (Fig. 4a). The orientations of the A, B and C rings constituting the spiro-ansa-spiro cyclic system is shown in Fig. 4b.

In the tetrameric, N_4P_4, phosphazene ring, the endocyclic P—N bond lengths are in the ranges of 1.580(3)-1.543(3) Å, and the average endocyclic P—N bond length is 1.562(3) Å. This value is shorter than the average exocyclic P—N bond lengths of 1.602(2) Å (Table 2). In the cyclophosphazenes, the P—N single and double bonds are generally in the ranges of 1.628-1.691 Å and 1.571-1.604 Å, respectively [28], and the obtained values of **tetrachloro-2,4-sas** compound are in consistent with these values. Besides, the exocyclic P1—N5 bond lengths is 1.615 (3) Å, and is very close to the double bond length. The shortening in this bond is probably due to the electron transfer from the N5 atom to the phosphazene ring. This value can be compared with the reported value of 1.613 (5) Å in the **sas** trimeric phosphazene, $C_{16}H_{16}Cl_2N_5O_2P_3$ [29].

Additionally, while the endocyclic P—N—P bond angles are in the ranges of 132.6(2)-137.8(2)º, and the average value is 134.7(2)º, the endocyclic N—P—N bond angles are 118.86(17)º and 122.56(17)º, and the average value is 120.71(17)º. In the standard compound, $N_4P_4Cl_8$, the endocyclic P—N—P and N—P—N bond angles are 131.3º and 121.2º [30]. These variations of the endocyclic P—N—P and N—P—N angles may reflect the steric hindrances of the bulky N_2O_2 tetradentate ligand and ought to be referred to the negative hyperconjugation [31].

On the other hand, the sum of the bond angles around the N5 atom [359.8(3)°] indicates that the N5 atom is in trigonal planar geometry. Thus, although the N5 atom bonds to three different groups, it can not be a stereogenic center. Moreover, the sum of the bond angles

around the P1 atom [438.21(17)°] can be compared with the reported value [434.4(3)°] in **sas** trimeric phosphazene [29].

Fig. 5 displays the packing diagram of title compound. The molecules are elongated along the b-axis and stacked along the a-axis. Van der Waals interactions may be considered to be effective in the unit cell packing.

The crystallographic data of the compound has been deposited with the Cambridge Crystallographic Data Centre, CCDC 1953257.

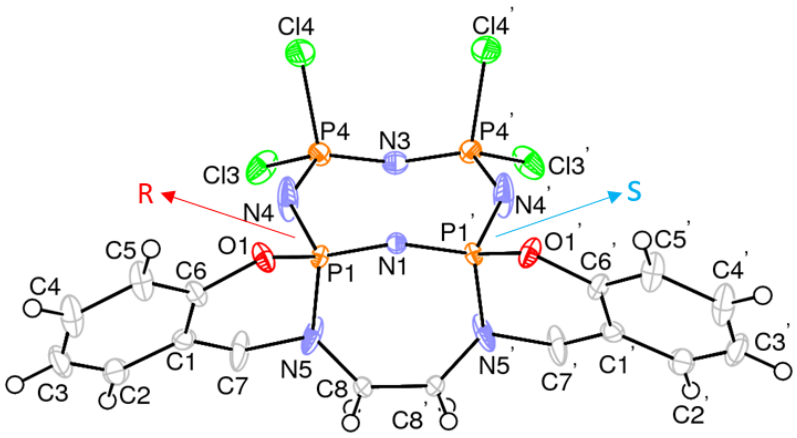

FIGURE 2. An ORTEP-3 [32] drawing of title compound with the atom-numbering scheme. Displacement ellipsoids are drawn at the 30% probability level.

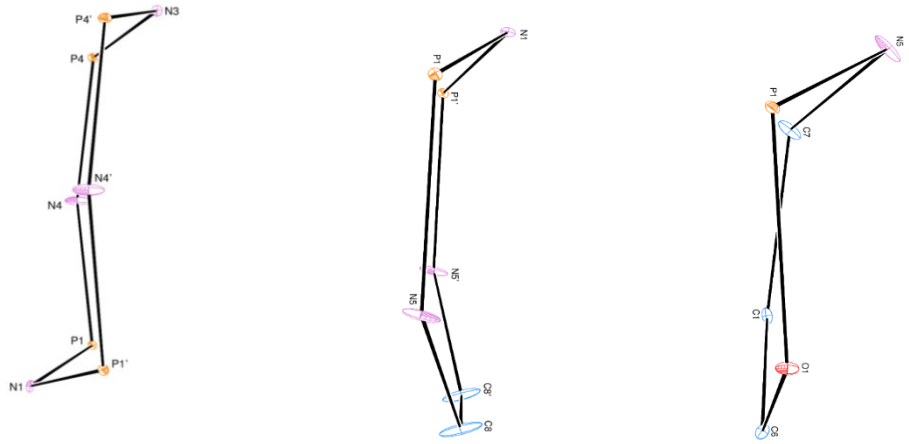

(**a**) (**b**) (**c**)

FIGURE 3. The conformations of the (**a**) cyclic tetrameric phosphazene ring, (**b**) the seven-membered ansa ring and (**c**) the six-membered spiro ring.

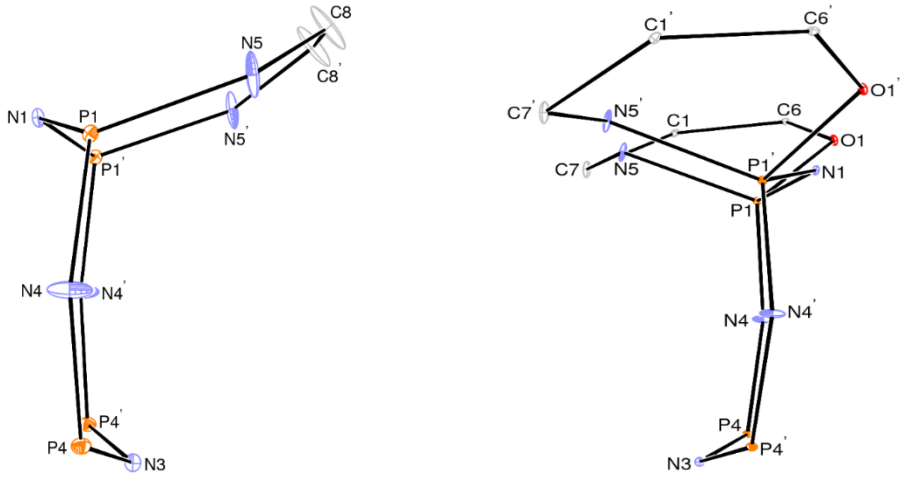

(**a**) (**b**)

FIGURE 4. The conformations of the (**a**) V-shaped bicyclic system containg the A and B rings, and (**b**) spiro-ansa-spiro cyclic system.

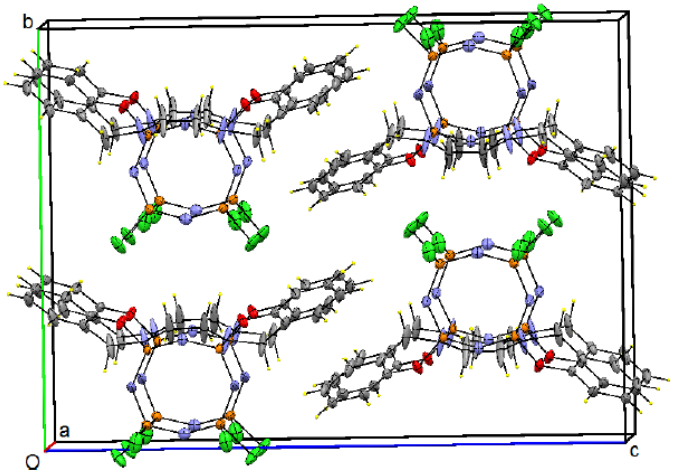

FIGURE 5. The packing diagram of tetrachloro-2,4-spiro-ansa-spiro cyclotetraphosphazene viewed down the a-axis direction.

4. Concluson

In this paper, the structure of the title **tetrachloro-2,4-sas** cyclotetraphosphazene was verified using single crystal X-ray diffraction technique. It has two equivalent chiral phosphorus (P1 and P1′) centres with respect to the X-ray structure analysis results. In addition, the molecule is a symmetric structure, and so it is in the meso form. It is undoubtedly detected that the absolute configuration of P1 and P1′ atoms is RS with checkcif data, showing that in the solid-state there is only one enantiomer in the unit cell.

Besides, the partly substituted **tetrachloro-2,4-sas** tetrameric phosphazene may be useful as the starting compounds for the preparation of the new chiral/non-chiral multi-heterocyclic cyclotetraphosphazene derivatives. All of the obtained new products may be as biologically active compounds and/or chemotherapeutic agents.

ACKNOWLEDGEMENT

The authors thank the “Scientific and Technical Research Council of Turkey” (Grant No. 211T019).

ÖZET

Bir siklotetrafosfazen olan 8,8,10,10-tetrakloro-20,21-dihidro-18*H*,23*H*-6,12-epiazeno-6λ^5,8λ^5,10λ^5,12λ^5-[1,3,2]benzoksazafosfonino[2',3':8,9][1,3,5,7,9,2,4,6,8] pentaazatetrafosfasiklound sino [2,1-*b*][1,3,2] benzoksazafosfin; $C_{16}H_{16}Cl_4N_6O_2P_4$ bileşiği, ortak bir PNP parçası ile kaynaşmış sekiz üyeli N_4P_4 tetramerik ve yedi üyeli ansa (N1/P1/P1′/N4′/C8′/C8/N4) halkalarından oluşan bisiklik yapıdaki tetrakloro-2,4-spiro-ansa-spiro (**tetrakloro-2,4-sas**) yapısına sahiptir. Asimetrik birimde yarım molekül mevcuttur. P1 ve P1′ atomları stereojenik merkezlerdir. Ayrıca, molekül içindeki N3 ve N1 atomlarından geçen bir ayna düzlemi vardır ve bu nedenle bu bileşik mezo formundadır (RS/SR). Checkcif sonucuna göre, katı halde P1 ve/veya P1′ fosfor merkezlerinin mutlak konfigürasyonunun RS olduğu bulunmuş olup bu durum katı halde birim hücrede sadece bir enantiyomer olduğunu göstermektedir. Uzay grubu, hücre parametreleri a = 6.2692(2), b = 15.8111(3), c = 22.9393(4) Å olan P bnm'dir.

REFERENCES

[1] V. Chandrasekhar and R. S. Narayanan, Phosphazenes. Organophosphorus Chemistry, (Cambridge, UK: Royal Society of Chemistry) 45 (2016) p. 375-437.

[2] V. Chandrasekhar and R. S. Narayanan, Phosphazenes. Organophosphorus Chemistry, (Cambridge, UK: Royal Society of Chemistry) 46 (2017) p. 342-417.

[3] V. Chandrasekhar and A. Chakraborty, Phosphazenes. Organophosphorus Chemistry, (Cambridge, UK: Royal Society of Chemistry) 48 (2019) p. 400-423.

[4] X. Liu, J. P. Breon, C. Chen and H. R. Allcock, Substituent exchange reactions of trimeric and tetrameric aryloxycyclophosphazenes with sodium 2,2,2-trifluoroethoxide. Dalton Transaction, 41 (2012) 2100-2109.

[5] G. Elmas, The reactions of 2-trans-6-bis(4-fluorobenzyl)spirocyclotetraphosphazene with primary amines:spectroscopic and crystallographic characterizations. Phosphorus, Sulfur, and Silicon and the Related Elements, 192 (2017) 1224-1232.

[6] G. Elmas, A. Okumuş, Z. Kılıç, M. Çam, L. Açık and T. Hökelek, Phosphorus-nitrogen compounds. Part 40. The syntheses of (4-fluorobenzyl) pendant armed cyclotetraphosphazene derivatives: Spectroscopic, crystallographic and stereogenic properties, DNA interactions and antimicrobial activities. Inorganica Chimica Acta, 476 (2018) 110-122.

[7] G. Elmas, A. Okumuş, R. Cemaloğlu, Z. Kılıç, S. P. Çelik, L. Açık, B. Ç. Tunalı, M. Türk, N. A. Çerçi, R. Güzel and T. Hökelek, Phosphorus-nitrogen compounds. Part 38. Syntheses, characterizations,cytotoxic, antituberculosis and antimicrobial activities and DNA interactions of spirocyclotetraphosphazenes with bis-ferrocenyl pendant arms. Journal of Organometallic Chemistry, 853 (2017) 93-106.

[8] G. Mutlu, G. Elmas, Z. Kılıç, T. Hökelek, L. Y. Koç, M. Türk, L. Açık, B. Aydın and H. Dal, Phosphorus-nitrogen compounds: Part 31. Syntheses, structural and stereogenic properties, in vitro cytotoxic and antimicrobial activities, DNA interactions of novel bicyclotetraphosphazenes containing bulky side group. Inorganica Chimica Acta, 436 (2015) 69-81.

[9] G. Elmas, A. Okumuş, L.Y. Koç, H. Soltanzade, Z. Kılıç, T. Hökelek, H. Dal, L. Açık, Z. Üstündağ, D. Dündar and M. Yavuz, Phosphorus-nitrogen compounds. Part 29. Syntheses, crystal structures, spectroscopic and stereogenic properties, electrochemical investigations, antituberculosis, antimicrobial and cytotoxic activities and DNA interactions of ansa-spiro-ansa cyclotetraphosphazenes. Europane Journal of Medicinal Chemistry, 87 (2014) 662-676.

[10] T. S. Cameron, A. Linden, G. Guerch, J. P. Bonnet and J. Labarre, Crystal and molecular structure of the spiransa and dispiransa cyclophosphazenic derivatives from spermidine and spermine. Journal of Molecular Structure, 212 (1989) 295-304.

[11] A. Uslu and S. Yeşilot, Chiral configurations in cyclophosphazene chemistry. Coordination Chemistry Reviews, 291 (2015) 28-67.

[12] K. Kajiyama, Y. Setone, K. Aoyagi and H. Yuge, Chiral HPLC Separation, Absolute Structural Elucidation, and Determination of Stereochemical Stability of trans- Bis[2-(2- pyridinyl)aminophenolato] Cyclotriphosphazene. Chirality, 28 (2016) 556-561.

[13] G. Elmas, Syntheses and structural characterizations of 2-pyridyl(N/O)spirocyclotriphosphazene derivatives. Phosphorus, Sulfur, and Silicon and the Related Elements,194/1-2 (2019) 13-24.

[14] A. Binici, A. Okumuş, G. Elmas, Z. Kılıç, N. Ramazanoğlu, L. Açık, H. Şimşek, B.Ç. Tunalı, M. Türk, R. Güzel and T. Hökelek. Phosphorus–nitrogen compounds. Part 42. The comparative syntheses of 2-cis-4-ansa(N/O) and spiro(N/O) cyclotetraphosphazene

derivatives: spectroscopic and crystallographic characterization, antituberculosis and cytotoxic activity studies. New Journal of Chemistry, 43 (2019) 6856-6873.

[15] T. L. Greaves and C. J. Drummond, Protic Ionic Liquids: Properties and Applications. Chemical Reviews, 108 (2008) 206-237.

[16] H. R. Allcock, Recent developments in polyphosphazene materials science. Current Opinion in Solid State and Materials Science, 10 (2006) 231-240.

[17] M. K. Harrup, K. L. Gering, H. W. Rollins, S. V. Sazhin, M. T. Benson, D. K. Jamison, C. J. Michelbacher and T. A. Luther, Phosphazene based additives for ımprovement of safety and battery lifetimes in lithium-ıon batteries. ESC Transaction, 41 (2012) 13-25.

[18] G. Elmas, A. Okumuş, P. Sevinç, Z. Kılıç, L. Açık, M. Atalan, M. Türk, G. Deniz and T. Hökelek, Phosphorus-nitrogen compounds. Part 37. Syntheses and structural characterizations, biological activities of mono and bis(4-fluorobenzyl)spirocyclotetraphosphazenes. New Journal of Chemistry, 41 (2017) 5818-5835.

[19] A. Okumuş, G. Elmas, R. Cemaloğlu, B. Aydın, A. Binici, H. Şimşek, L. Açık, M. Türk, R. Güzel, Z. Kılıç and T. Hökelek, Phosphorus–nitrogen compounds. Part 35. Syntheses, spectroscopic and electrochemical properties, and antituberculosis, antimicrobial and cytotoxic activities of mono-ferrocenyl-spirocyclotetraphosphazenes. New Journal of Chemistry, 40 (2016) 5588-5603.

[20] G. Elmas, A. Okumuş, Z. Kılıç, S.P. Çelik and L. Açık, The spectroscopic and thermal properties, antibacterial and antifungal Activity and DNA interactions of 4-(fluorobenzyl)spiro(N/O)cyclotri phosphazenium salts. Journal of the Turkish Chemical Society, Section A: Chemistry, 4/3 (2017) 993-1016.

[21] A. Okumuş, G. Elmas, Z. Kılıç, N. Ramazanoğlu, L. Açık, M. Türk and G. Akça, The reactions of N3P3Cl6 with monodentate and bidentate ligands: The syntheses and structural characterizations, In vitro antimicrobial activities and DNA interactions of 4-fluorobenzyl(N/O)spirocylotriphosphazenes. Turkish Journal of Chemistry, 41 (2017) 525-547.

[22] G. Elmas, A. Okumuş, Z. Kılıç, L. Y. Gönder, L. Açık and T. Hökelek, The Syntheses and Structural Characterizations, Antimicrobial Activity and In vitro DNA Binding of 4-fluorobenzylspıro(N/O)cyclotriphosphazenes and Their Phosphazenium salts. Journal of the Turkish Chemical Society, Section A: Chemistry, 3 (2016) 25-46.

[23]G. Elmas, Syntheses and spectroscopic investigations of 2-pyridyl(N/N)spirocyclotriphosphazenes. Journal of the Turkish Chemical Society, Section A: Chemistry, 5/2 (2018) 621-634.

[24] G. Elmas (nee Egemen), A. Okumuş, Z. Kılıç, T. Hökelek, L. Açık, H. Dal, N. Ramazanoğlu and L. Y. Koç, Phosphorus−nitrogen compounds. Part 24. Syntheses, crystal structures, spectroscopic and stereogenic properties, biological activities, and DNA interactions of novel spiro-ansa-spiro- and ansaspiro-ansa-cyclotetraphosphazenes. Inorganic Chemistry, 51 (2012) 12841-12856.

[25] Bruker SADABS, Bruker AXS Inc. Madison, Wisconsin, USA (2005).

[26] G. M. Sheldrick, SHELXS-97, SHELXL-97 University of Gottingen, Gottingen, Germany (1997).

[27] D. Cremer and J. A. Pople, General definition of ring puckering coordinates. Journal of American Chemical Society, 97 (1975) 1354-1358.

[28] F. H. Allen, O. Kennard, D. G. Watson, L. Brammer, G. Orpen and R. Taylor, Tables of bond lengths determined by X-ray and neutron diffraction. Part 1. Bond lengths in organic compounds. Journal of the Chemical Society, Perkin Transactions 2. 12 (1987) 1-19.

[29] S. Safran, T. Hökelek, S. Bilge, Ş. Demiriz, A. Natsagdorj, and Z. Kılıç, Crystal Structure of 8,8-dichloro-1,2,10,11,13,14-hexahydro-6λ5,8λ5,10λ5-6,10-nitrilo[1,3,5,7,2,4,6]tetrazatriphosphoninobis [1,3,2]oxazaphosphorine. Analytical Sciences X-ray Structure Analysis Online, 21 (2005) x77-x78.

[30] A. J. Wagner, A. Vos, The crystal structure of compounds with (N-P)n rings. IV. The stable modification (T form) of tetrameric phosphonitrilic chloride, N4P4Cl8. Acta Crystallograhica Section B. B24 (1968) 707-713.

[31] A. B. Chaplin, J. A. Harrison and P. J. Dyson, Revisiting the electronic structure of phosphazenes. Inorganic Chemistry, 44 (2005) 8407-8417.

[32] L. J. Farrugia, ORTEP-3 for Windows- a version of ORTEP-III with a Graphical User Interface (GUI). Journal of Applied Crystallography, 30 (1997) 565-566.

Current Address: GAMZE ELMAS Department of Chemistry, Ankara University, 06100 Ankara, TURKEY
E-mail Address: gegemen@ankara.edu.tr
ORCID: https://orcid.org/0000-0003-4877-3697

Current Address: AYTUĞ OKUMUŞ: Department of Chemistry, Ankara University, 06100 Ankara, TURKEY
E-mail Address: okumus@science.ankara.edu.tr
ORCID: https://orcid.org/0000-0002-2169-5695

Current Address: SATİYE SEVİM İSAOĞLU: Cebrail Neighborhood, Kuleli Street No.14A/2 Kastamonu, TURKEY
E-mail Address: satiyesevim@gmail.com

Current Address: TUNCER HÖKELEK: Department of Physics, Hacettepe University, 06800 Ankara, TURKEY
E-mail Address: merzifon@hacettepe.edu.tr
ORCID: https://orcid.org/0000-0002-8602-4382

Current Address: ZEYNEL KILIÇ (Corresponding author): Department of Chemistry, Ankara University, 06100 Ankara, TURKEY
E-mail Address: zkilic@science.ankara.edu.tr
ORCID: https://orcid.org/0000-0003-1061-8122

Commun.Fac.Sci.Univ.Ank.Series B
Volume 61, Number 1-2, Pages 15-30 (2019)
ISSN 2687-4806
http://communications.science.ankara.edu.tr/index.php?series=B

DESIGNATION OF ABSOLUTE CONFIGURATION OF MULTI-HETEREOCYCLIC 9,13-DICHLORO-22,22-DIPYRROLIDINE-1-YL-1H,2H,13H,19H-9,13-(EPIAZENOPHOSPHAZENO)-9λ5,11λ5,13λ5-[1,3,5,2,4] BENZOXADIAZADİPHOSPHONINO[4 ,5 :2,3][1,3,2]DIAZAPHOSPHOLO[2,1-D] [1,3,5,2,4]BENZOXADIAZADIPHOSPHONINE BY X-RAY CRYSTALLOGRAPHIC DATA

GAMZE ELMAS, AYTUĞ OKUMUŞ, SATİYE SEVİM İSAOĞLU, TUNCER HÖKELEK AND ZEYNEL KILIÇ

ABSTRACT. The title compound, 9,13-dichloro-22,22-dipyrrolidine-1-yl-1*H*,2*H*,13*H*,19*H*-9,13-(epiazenophosphazeno)-9λ^5,11λ^5,13λ^5-[1,3,5,2,4]benzoxadiazadiphosphonino [4',5':2,3][1,3,2]diazaphospholo[2,1-*d*][1,3,5,2,4]benzoxadiazadiphosphonine; 2($C_{24}H_{32}Cl_2N_8O_2P_4$). 0.5 C_6H_{12}, a cyclotetraphosphazene derivative, has a *geminal*-dipyrrolidino-2-*trans*-6-dichloro-*ansa*-*spiro*-*ansa* (***gem*-dipyrrolidino-2-*trans*-6-dichloro-asa**) structure in which the tricyclic parts are consisted of three eight-membered rings, containing a tetrameric N_4P_4 and two ansa rings. However, all these rings are not planar. The asymmetric unit contains two crystallographically independent molecules and one half of the cyclohexane solvent molecule. In both molecules, it is expected that two P (P1 and P3/P1′ and P3′) atoms are stereogenic centres. Both ***gem*-dipyrrolidino-2-*trans*-6-dichloro-asa** molecules have *trans* structures according to the Cl atoms, and they are in the racemic forms. Besides, it is found that the absolute configurations of P1, P3 and P1′, P3′ phosphorus centers are RR and SS, respectively. The title compound has *P-1* space group, a Sohncke chiral space group, with the cell parameters of a = 9.6682(2), b = 13.8587(3), c = 24.0250(4) Å, α = 105.249(2)°, β = 96.298(3)° and γ = 98.367(3)°.

1. INTRODUCTION

Octachlorocyclotetraphosphazene ($N_4P_4Cl_8$, tetramer) is a standard starting material for the preparation of the new cyclotetraphosphazene derivatives [1,2]. It has eight reactive P-Cl bonds, and these Cl atoms may exchange with a number of substituents, such as monodentate (amines and alkoxides), bidentate (diamines, dialkoxides and aminoalkoxides) and multidentate (polyamines, polyalkoxides and polyaminoalkoxides) ligands [3-5]. In addition, it is difficult to study the substitution reactions of $N_4P_4Cl_8$ with these ligands because of the formation of a large number of products (*cis*/*trans*-, spiro-, ansa-, bino- and optical isomers)

Received by the editors: July 22, 2019; Accepted: August 26, 2019.
Key word and phrases: Cyclotetraphosphazene, ansa-spiro-ansa-Structure, Pyrrolidine, X-ray crystallography.

and also because of the difficulties faced in the separations of these isomers from the reaction mixtures. However, in the literature, the number of the reported Cl substitution reactions with multidentate ligands containing N_2O_2 and N_2N_2 donor atoms are much less than the others [5-7].

The chiralities of the cyclophosphazenes have been researched recently as an interesting topic [8,9]. However, there are fairly a few studies researching the chiralities of the cyclotetraphosphazenes using different methods, eg. X-ray crystallography, ^{31}P NMR spectroscopy in the presence of (R)-(+)-2,2,2-trifluoro-1-(9'-anthryl)-ethanol (CSA) and HPLC in the literature [9-11].

On the other hand, in recent years, organocyclophosphazene derivatives have attracted so much attention by means of their different and special applications in some areas; such as liquid crystals [12], thermal stabilities [13], fluorescence chemosensors [14], membranes [15], the oxidative DNA cleavages [16], the antituberculosis [17], anti-cancer [18], antibacterial [19] and antifungal [20] reagents.

Herein, the title compound was prepared from the reaction of pyrrolidine with tetrachloro-2,4,6-ansa-spiro-ansa (**tetrachloro-asa)** product [21] obtained from the reaction of $N_4P_4Cl_8$ and N_2O_2 donor-type unsymmetrical tetradentate ligand with respect to the literature method. The goal of the present paper is to research the crystallographic and stereogenic properties of **dichloro-dipyrrolidino-asa** cyclotetraphosphazene.

2. Materials And Methods

2.1. X-ray crystal structure determinations

The colourless crystals of the **dichloro-dipyrrolidino-asa** compound were recrystallized from cyclohexane-THF (6:1) at room temperature. The crystallographic data are presented in Table 1, and the selected bond lengths and angles with the torsion angles are listed in Table 2. The crystallographic data were recorded on a Bruker Kappa APEXII CCD area-detector diffractometer using Mo K_α radiation (λ=0.71073 Å) at T=100(2) K. Absorption correction by multi-scan [22] was applied. Structure was solved by direct methods and refined by full-matrix least squares against F^2 using all data [23]. All non-H atoms were refined anisotropically. The remaining H atom positions were calculated geometrically at distances of 0.93 Å (CH) and 0.97 Å (CH_2) from the parent C atoms; a riding model was used during the refinement process and the U_{iso}(H) values were constrained to be $1.2U_{eq}$(carrier atom).

2.2. Materials used for syntheses

According to the published paper, the beginning N_2O_2 tetradentate ligand, {2,2'-[1,2-ethanediylbis(iminomethanediyl)]diphenol}, the starting cyclotetraphosphazene {**tetrachloro-asa**} and the title product {***gem*-dipyrrolidino-2-*trans*-6-dichloro-asa**} were synthesized again [21].

TABLE 1. Crystallographic details.

Empirical Formula	$2(C_{24}H_{32}Cl_2N_8O_2P_4).\ 0.5\ C_6H_{12}$
Fw	1360.79
Crystal System	triclinic
Space Group	*P -1*
a (Å)	9.6682(2)
b (Å)	13.8587(3)
c (Å)	24.0250(4)
α (°)	105.249(2)
β (°)	96.298(3)
γ (°)	98.367(3)
V (Å^3)	3035.54(10)
Z	2
T	100(2) K
Crystal color	colorless
Crystal size	0.15x0.35x0.43 mm
μ (mm^{-1})	0.466 (Mo Kα)
ρ (calcd) (g cm^{-3})	1.489
Number of Reflections Total	14920
Number of Reflections Unique	10169
R_{int}	0.0813
$(\Delta/\sigma)_{max}$	<0.001
$(\Delta\rho)_{max}$	1.111 e Å^{-3}
$(\Delta\rho)_{min}$	−1.282 e Å^{-3}
$2\theta_{max}$ (°)	56.74
T_{min} / T_{max}	0.825 / 0.933
Number of Parameters	748
R [$F^2 > 2\sigma(F^2)$]	0.0467
wR	0.1041

TABLE 2. The selected bond lengths (Å) and angles (°) with the torsion angles (°).

Molecule I

P1– N1	1.564(2)	N1– P1– N4	125.73(11)	N4– P1– N1– P2	-51.9(2)
P1– N4	1.547(2)	N1– P2– N2	113.54(11)	N3– P3– N2– P2	-60.0(2)
P2– N1	1.598(2)	N2– P3– N3	124.00(11)	N1– P2– N2– P3	45.3(2)
P2– N2	1.602(2)	N3– P4– N4	116.20(11)	N2– P2– N1– P1	51.76(19)
P3– N3	1.561(2)	P1– N1– P2	128.21(15)	N2– P3– N3– P4	-41.1(2)
P3– N2	1.568(2)	P3– N2– P2	126.58(15)	N4– P4– N3– P3	62.1(2)
P4– N3	1.606(2)	P1– N4– P4	133.44(15)	N1– P1– N4– P4	-33.4(3)
P4– N4	1.599(2)	P3– N3– P4	125.30(14)	N3– P4– N4– P1	18.8(3)
P1– O1	1.6046(17)	N4– P1– O1	103.67(11)		
P2– N5	1.650(2)	N6– P2– N2	114.37(11)		
P2– N6	1.639(2)	N6– P2– N1	108.32(12)		
P4– N7	1.627(2)	N5– P2– N1	115.02(11)		
P4– N8	1.646(2)	N5– P2– N6	95.22(11)		
P1– Cl1	2.0465(10)	N3– P3– O2	103.92(11)		
P3– Cl2	2.0419(9)	N7– P4– N8	103.49(11)		

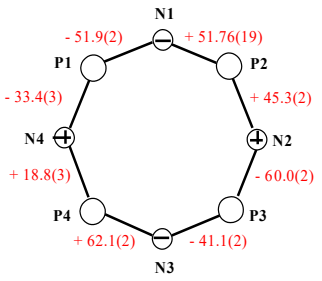

Molecule II

P1′– N1′	1.565(2)	N1′– P1′– N4′	124.34(11)	N4′– P1′– N1′– P2′	56.4(2)
P1′– N4′	1.552(2)	N1′– P2′– N2′	113.79(11)	N3′– P3′– N2′– P2′	54.4(2)
P2′– N1′	1.598(2)	N2′– P3′– N3′	125.38(11)	N1′– P2′– N2′– P3′	-47.9(2)
P2′– N2′	1.605(2)	N3′– P4′– N4′	116.43(11)	N2′– P2′– N1′– P1′	-48.8(2)
P3′– N3′	1.548(2)	P1′– N1′– P2′	127.39(15)	N2′– P3′– N3′– P4′	36.2(3)
P3′– N2′	1.562(2)	P3′– N2′– P2′	127.72(15)	N4′– P4′– N3′– P3′	-33.5(3)
P4′– N3′	1.602(2)	P1′– N4′– P4′	128.58(14)	N1′– P1′– N4′– P4′	42.3(2)
P4′– N4′	1.599(2)	P3′– N3′– P4′	132.24(15)	N3′– P4′– N4′– P1′	-50.3(2)
P1′– O1′	1.5962(18)	N4′– P1′– O1′	103.58(11)		
P2′– N5′	1.647(2)	N6′– P2′– N2′	114.45(11)		
P2′– N6′	1.648(2)	N6′– P2′– N1′	108.11(12)		
P4′– N7′	1.637(2)	N5′– P2′– N1′	114.98(11)		
P4′– N8′	1.629(2)	N5′– P2′– N6′	95.51(11)		
P1′– Cl1′	2.0483(9)	N3′– P3′– O2′	103.45(11)		
P3′– Cl2′	2.0482(10)	N7′– P4′– N8′	103.67(11)		

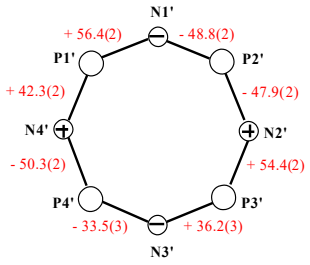

3. Result And Discussion

The title compound (Fig. 1) is a cyclotetraphosphazene derivative with a bulky N_2O_2 tetradentate ligand attached through the 2,4,6-ansa-spiro-ansa junction, where two pyrrolidine groups are bonded to the same phosphorus atom in a *geminal* position and two Cl atoms bonded to the different phosphorus atoms in a *non-geminal-trans* manner. The asymmetric unit contains two independent molecules (molecule I and molecule II) and one-half of the cyclohexane solvent molecule. The molecules, I and II, have two equivalent stereogenic P centers (P1, P3 and P1′, P3′), and it is expected that they are in the racemic mixture (RR/SS) because of the *trans*- position of two Cl atoms (Fig. 1). It is undoubtedly

found that the absolute configurations of both molecules are RR (for P1 and P3 atoms of molecule I) and SS (for P1′ and P3′ atoms of molecule II). As a result, it is determined that both enantiomers are together in the solid-state. Furthermore, the space group of ***gem*-dipyrrolidino-2-*trans*-6-dichloro-asa** is *P-1*. It is among the Sohncke space groups, and the chiral properties of them are investigated in the literature [24].

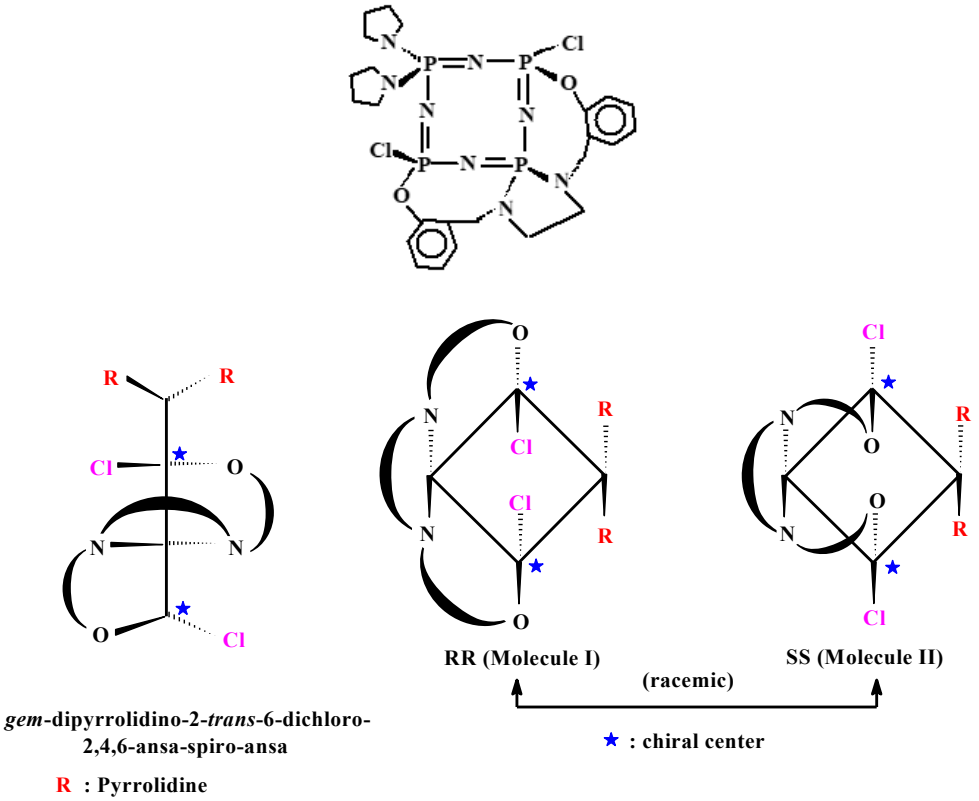

FIGURE 1. Chemical diagram and the racemic forms of ***gem*-dipyrrolidino-2-*trans*-6-dichloro-asa** cyclotetraphosphazene.based on the ORTEP diagram *via* stick diagrams and spatial views.

The molecular structure of ***gem*-dipyrrolidino-2-*trans*-6-dichloro-asa** along with the atom-numbering scheme illustrated in Fig. 2. The conformations of the tetrameric phosphazene rings depicted using the torsion angles of the ring bonds (Table 2). In both molecules, the tricyclic parts are consisted of three eight-membered rings, which are not planar having the

total puckering amplitudes, Q_T (Q'_T) [25], of 1.2071(25) Å (for tetramer ring of molecule I with unprimed atoms, Fig 3a), 1.1395(27) Å [for ansa (P1/N1/P2/N5/O1/C1/C6/C7) ring of molecule I] and 1.1317(28) Å [for ansa (P2/N2/P3/N6/O2/C10/C11/C16) ring of molecule I], 1.2457(40) Å (for tetramer ring of molecule II with unprimed atoms, Fig 4a), 1.1675(27) Å [for ansa (P1′/N1′/P2′/N5′/O1′/C1′/C6′/C7′) ring of molecule II] and 1.2843(26) Å [for ansa (P2′/N2′/P3′/N6′/O2′/C10′/C11′/C16′) ring of molecule II] (Figs.3c and 4c). Besides, the five-membered spiro rings of molecule I (P2/N5/N6/C8/C9) and molecule II (P2′/N5′/N6′/C8′/C9′) are in twisted conformations (Figs. 3b and 4b). As expected, the solvent molecule, cyclohexane, is in the chair conformation with an inversion centre.

The endocyclic P—N bond lengths of tetrameric N_4P_4 rings range from 1.547(2) to 1.606(2) Å (for molecule I) and 1.548(2) to 1.605(2) Å (for molecule II). The average endocyclic P—N bond lengths are also 1.581(2) and 1.579(2) Å for molecules I and II, respectively, and they show double bond character. These values are shorter than the average exocyclic P—N bond lengths of 1.645(2) Å (for molecule I) and 1.649(2) Å (for molecule II) (Table 2), and they are around the lower limit of the single bond length. The P—N single and double bonds are generally in the ranges of 1.628-1.691 Å and 1.571-1.604 Å, respectively, in the cyclophosphazene derivatives [26], and the obtained values of ***gem*-dipyrrolidino-2-*trans*-6-dichloro-asa** are in agreement with these values.

Furthermore, the endocyclic P—N—P bond angles of molecules I and II are in the ranges of 125.30(2)-133.44(15)º and 127.39(15)-132.24(15)º, respectively. The average values are found to be as 128.38(15)° (for molecule I) and 128.98(15)° (for molecule II). The P—N—P bond angles have spread, and the similar enlargements of these angles were seen in some cyclophosphazenes in the literature [27]. The endocyclic N—P—N bond angles range from 113.54(11) to 125.73(11)º (for molecule I) and 113.79(11) to 125.38(11)º (for molecule II). The average values are calculated as 119.87(11)° (for molecule I) and 119.99(11)° (for molecule II) as well. These variations in the endocyclic P—N—P and N—P—N bond angles of molecules I and II can reflect the steric hindrances of the bulky N_2O_2 tetradentate ligand and may attribute to the negative hyperconjugation [28,29].

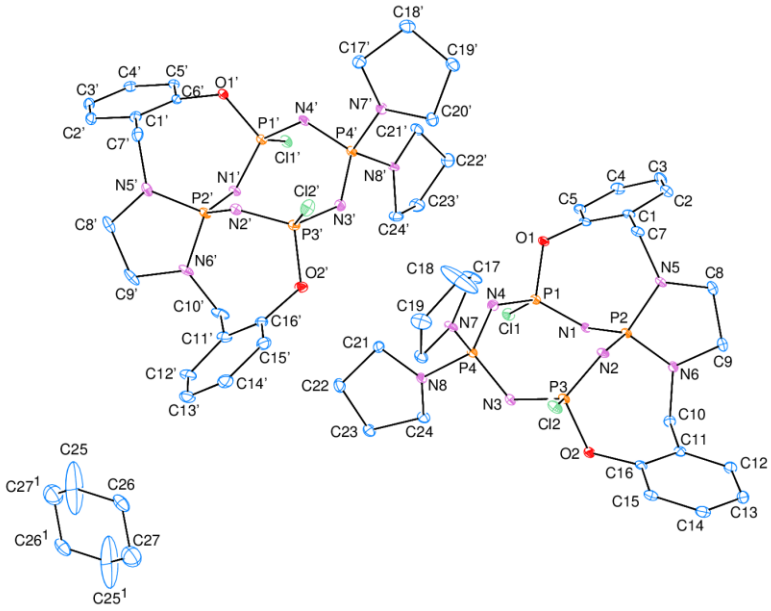

FIGURE 2. An ORTEP-3 [30] drawing of ***gem*-dipyrrolidino-2-*trans*-6-dichloro-asa** with the atom-numbering scheme. Displacement ellipsoids are drawn at the 30% probability level [symmetry code 1: -x, -y, -z].

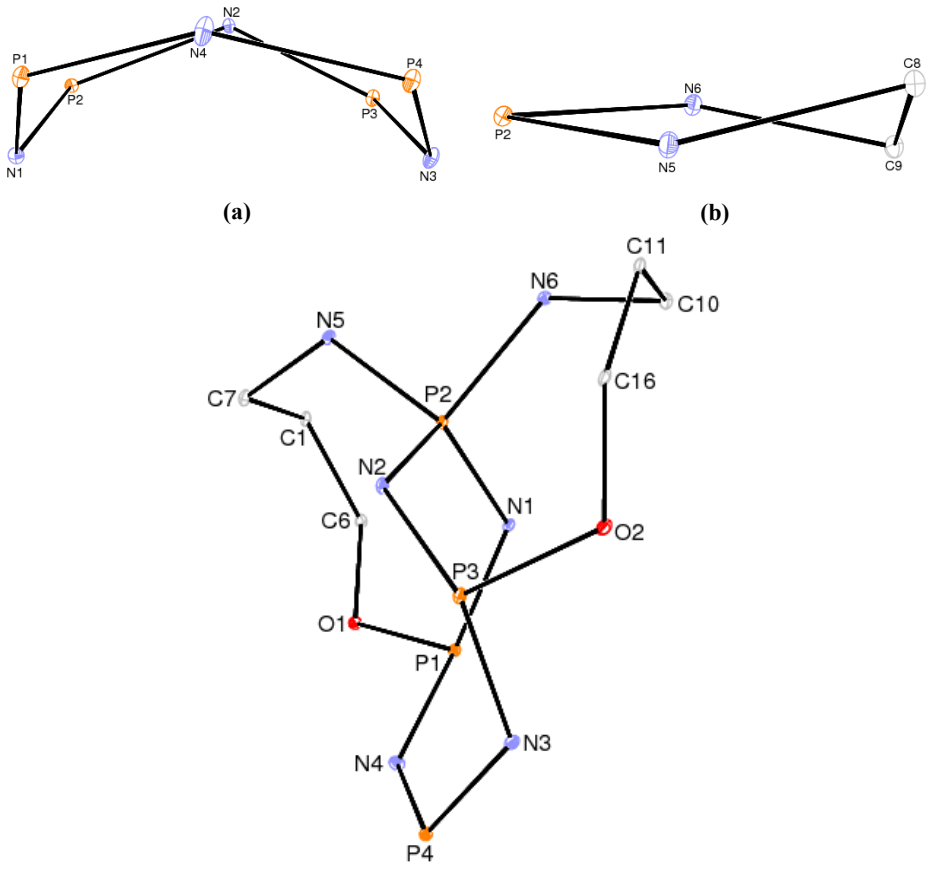

FIGURE 3. The conformations of (**a**) the tetramer ring, (**b**) the five-membered spiro-ring and (**c**) the all rings of molecule I.

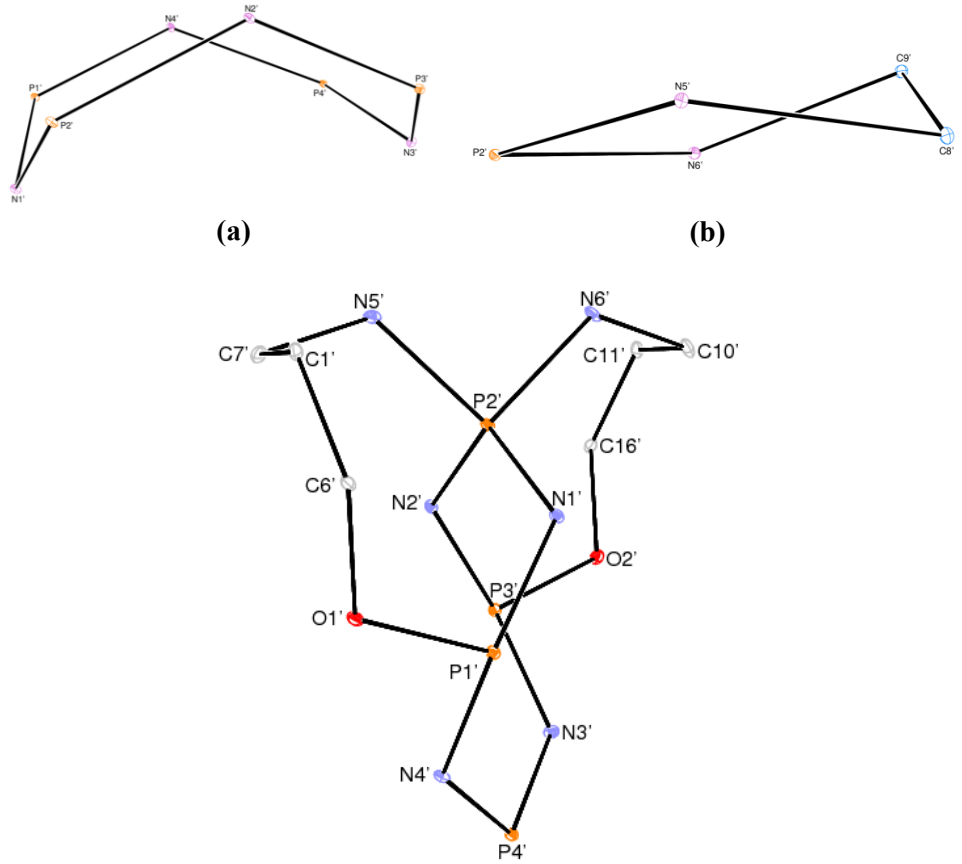

FIGURE 4. The conformations of (**a**) the tetramer ring, (**b**) the five-membered spiro-ring and (**c**) the all rings of molecule II.

The packing diagram of the ***gem*-dipyrrolidino-2-*trans*-6-dichloro-asa** compound is depicted in Fig. 5. The molecules are elongated along the c-axis direction and stacked along the a-axis direction. Cyclohexane molecules are located in the intermolecular spaces. It can be considered that Van der Waals interactions are effective in molecular packing, and especially in keeping the guest cyclohexane molecules in the inner holes.

The crystallographic data of the compound has been deposited with the Cambridge Crystallographic Data Centre, CCDC 1953256.

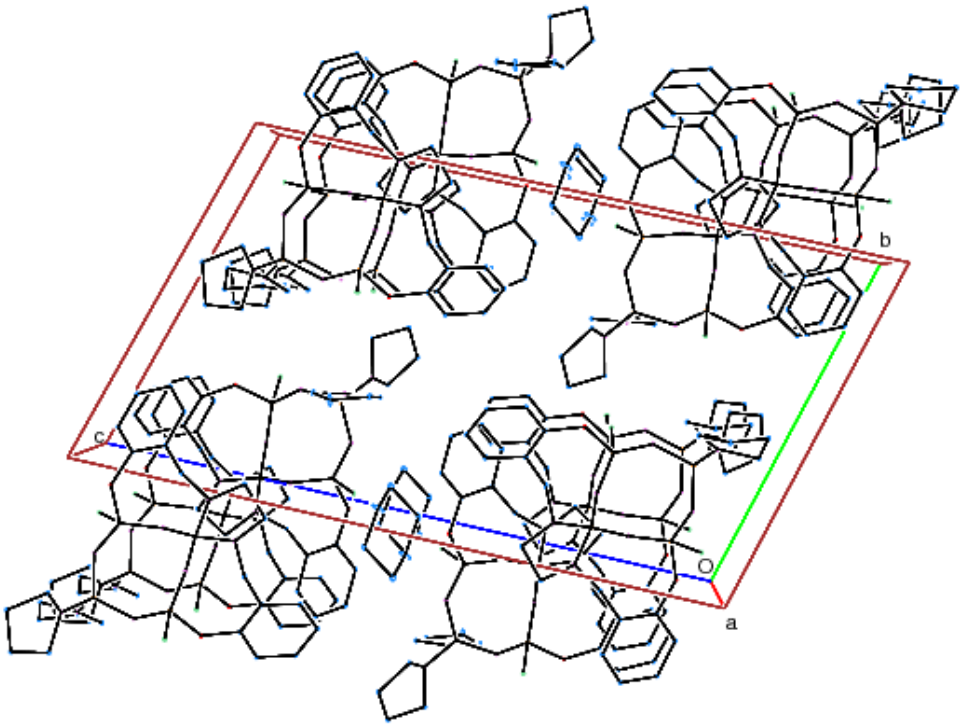

FIGURE 5. The partial packing diagram of ***gem*-dipyrrolidino-2-*trans*-6-dichloro-asa** compound.

4. Conclusion

In the current paper, the structure of the title ***gem*-dipyrrolidino-2-*trans*-6-dichloro-asa** cyclotetraphosphazene was confirmed by X-ray crystallography. It has two crystallographically independent molecules and one half of the cyclohexane solvent molecule in the asymmetric unit. Both molecules have two equivalent chiral phosphorus (P1 and P3/P1′

and P3′) centres according to X-ray crystallographic data. Moreover, these molecules are in the racemic forms on account of the *trans* manner of the two Cl atoms. It is clearly determined that the absolute configurations of P1, P3 and P1′, P3′ atoms are RR and SS, respectively.

Additionally, the pyrrolidine substituted **asa** tetrameric phosphazene may have important applications in many fields, eg. chemistry, material science, biology and medicine. For example, it can be useful for the preparation of the new chiral products, as ligating agents for the metal cations and as biologically active agents.

ACKNOWLEDGEMENT

The authors thank the "Scientific and Technical Research Council of Turkey" (Grant No. 211T019).

ÖZET

Bir siklotetrafosfazen türevi olan 9,13-dikloro-22,22-dipirolidin-1-il-1*H*,2*H*,13*H*,19*H*-9,13-(epiazenofosfazeno)-9λ^5,11λ^5,13λ^5-[1,3,5,2,4]benzoksadiazadifosfinino[4',5':2,3][1,3,2] diazafosfolo [2,1-*d*] [1,3,5,2,4]benzoksadiazadifosfin, 2($C_{24}H_{32}Cl_2N_8O_2P_4$). 0.5 C_6H_{12} bileşiği, bir tetramerik N_4P_4 ve iki ansa halkası içeren üç sekiz üyeli halkadan oluşan trisiklik yapıdaki *geminal*-dipirolidino-2-*trans*-6-dikloro-*ansa*-*spiro*-*ansa* (***gem*-dipirolidino-2-*trans*-6-dikloro-asa**) yapısına sahiptir. Bununla birlikte, tüm bu halkalar düzlemsel değildir. Asimetrik birimde kristallografik açıdan iki bağımsız fosfazen molekülü ve yarım molekül siklohekzan çözücüsü içerir. Her iki molekülde, iki P (P1 and P3/P1′ and P3′) atomlarının stereojenik merkez olması beklenmektedir. Her iki ***gem*-dipirolidino-2-*trans*-6-dikloro-asa** molekülü Cl atomlarına göre *trans* yapıya sahiptir ve rasemik karışım halindedir. Ayrıca, P1, P3 ve P1′, P3 fosfor merkezlerinin mutlak konfigürasyonlarının sırasıyla RR ve SS olduğu bulunmuştur. Uzay grubu, hücre parametreleri a = 9.6682(2), b = 13.8587(3), c = 24.0250(4)Å, α = 105.249(2)°, β = 96.298(3)° ve γ = 98.367(3)° olan *P-1* olup Sohncke uzay grupları arasındadır.

REFERENCES

[1] F. F. Stewart, Phosphazenes. Organophosphorus Chem. (Cambridge, UK: Royal Society of Chemistry) 44 (2015) p. 397-430.

[2] V. Chandrasekhar and A. Chakraborty, Phosphazenes. Organophosphorus Chemistry, (Cambridge, UK: Royal Society of Chemistry) 48 (2019) p. 400-423.

[3] G. Elmas, The reactions of 2-trans-6-bis(4-fluorobenzyl)spirocyclotetraphosphazene with primary amines:spectroscopic and crystallographic characterizations. Phosphorus, Sulfur, and Silicon and the Related Elements, 192 (2017) 1224-1232.

[4] G. Elmas, A. Okumuş, Z. Kılıç, M. Çam, L. Açık and T. Hökelek, Phosphorus-nitrogen compounds. Part 40. The syntheses of (4-fluorobenzyl) pendant armed cyclotetraphosphazene derivatives: Spectroscopic, crystallographic and stereogenic properties, DNA interactions and antimicrobial activities. Inorganica Chimica Acta, 476 (2018) 110-122.

[5] H. İbişoğlu, Ç. G. Yenilmez, A. Kılıç, E. Tanrıverdi, İ. Ün, H. Dal and T. Hökelek, Formation of novel spiro, spiroansa and dispiroansa derivatives of cyclotetraphosphazene from the reactions of polyfunctional amines with octachlorocyclotetraphosphazatetraene. Journal of Chemical Sciences. 121 (2009) 125-135.

[6] G. Mutlu, G. Elmas, Z. Kılıç, T. Hökelek, L. Y. Koç, M. Türk, L. Açık, B. Aydın and H. Dal, Phosphorus-nitrogen compounds: Part 31. Syntheses, structural and stereogenic properties, in vitro cytotoxic and antimicrobial activities, DNA interactions of novel bicyclotetraphosphazenes containing bulky side group. Inorganica Chimica Acta, 436 (2015) 69-81.

[7] G. Elmas, A. Okumuş, L.Y. Koç, H. Soltanzade, Z. Kılıç, T. Hökelek, H. Dal, L. Açık, Z. Üstündağ, D. Dündar and M. Yavuz, Phosphorus-nitrogen compounds. Part 29. Syntheses, crystal structures, spectroscopic and stereogenic properties, electrochemical investigations, antituberculosis, antimicrobial and cytotoxic activities and DNA interactions of ansa-spiro-ansa cyclotetraphosphazenes. Europane Journal of Medicinal Chemistry, 87 (2014) 662-676.

[8] D. Kumar, J. Singh and A. J. Elias, Chiral multidentate oxazoline ligands based on cyclophosphazene cores: synthesis, characterization and complexation studies. Dalton Transaction, 43 (2014) 13899-13912.

[9] G. Elmas, A. Okumuş, R. Cemaloğlu, Z. Kılıç, S. P. Çelik, L. Açık, B. Ç. Tunalı, M. Türk, N. A. Çerçi, R. Güzel and T. Hökelek, Phosphorus-nitrogen compounds. Part 38. Syntheses, characterizations,cytotoxic, antituberculosis and antimicrobial activities and DNA interactions of spirocyclotetraphosphazenes with bis-ferrocenyl pendant arms. Journal of Organometallic Chemistry, 853 (2017) 93-106.

[10] G. Elmas, Syntheses and structural characterizations of 2-pyridyl(N/O)spirocyclotriphosphazene derivatives. Phosphorus, Sulfur, and Silicon and the Related Elements,194/1-2 (2019) 13-24.

[11] A. Binici, A. Okumuş, G. Elmas, Z. Kılıç, N. Ramazanoğlu, L. Açık, H. Şimşek, B.Ç. Tunalı, M. Türk, R. Güzel and T. Hökelek. Phosphorus–nitrogen compounds. Part 42. The comparative syntheses of 2-cis-4-ansa(N/O) and spiro(N/O) cyclotetraphosphazene derivatives: spectroscopic and crystallographic characterization, antituberculosis and cytotoxic activity studies. New Journal of Chemistry, 43 (2019) 6856-6873.

[12] J. Jimenez, I. Pintre, E. Gascon, C. Sanchez-Somolinos, R. Alcala, E. Cavero, J. L. Serrano and L. Oriol, Photoresponsive liquid-crystalline dendrimers based on a cyclotriphosphazene core. Macromolecular Chemistry and Physics, 215 (2014) 1551-1532.

[13] G. Elmas, A. Okumuş, Z. Kılıç, S.P. Çelik and L. Açık, The spectroscopic and thermal properties, antibacterial and antifungal Activity and DNA interactions of 4-(fluorobenzyl)spiro(N/O)cyclotriphosphazenium salts. Journal of the Turkish Chemical Society, Section A: Chemistry, 4/3 (2017) 993-1016.

[14] R. Xu and Y. Xu, Modern Inorganic Synthetic Chemistry, Second Edition, 11 (2017) p. 295.

[15] R. Gutru, S.G. Peera, S.D. Bhat and A.K. Sahu, Synthesis of sulfonated poly(bis(phenoxy)phosphazene) based blend membranes and its effect as electrolyte in fuel cells. Solid State Ionics, 296 (2016) 127-136.

[16] G. Elmas, Syntheses and spectroscopic investigations of 2-pyridyl(N/N)spirocyclotriphosphazenes. Journal of the Turkish Chemical Society, Section A: Chemistry, 5/2 (2018) 621-634.

[17] A. Okumuş, G. Elmas, R. Cemaloğlu, B. Aydın, A. Binici, H. Şimşek, L. Açık, M. Türk, R. Güzel, Z. Kılıç and T. Hökelek, Phosphorus–nitrogen compounds. Part 35. Syntheses, spectroscopic and electrochemical properties, and antituberculosis, antimicrobial and cytotoxic activities of mono-ferrocenyl-spirocyclotetraphosphazenes. New Journal of Chemistry, 40 (2016) 5588-5603.

[18] G. Elmas, A. Okumuş, P. Sevinç, Z. Kılıç, L. Açık, M. Atalan, M. Türk, G. Deniz and T. Hökelek, Phosphorus-nitrogen compounds. Part 37. Syntheses and structural characterizations, biological activities of mono and bis(4-

fluorobenzyl)spirocyclotetraphosphazenes. New Journal of Chemistry, 41 (2017) 5818-5835.

[19] A. Okumuş, G. Elmas, Z. Kılıç, N. Ramazanoğlu, L. Açık, M. Türk and G. Akça, The reactions of N3P3Cl6 with monodentate and bidentate ligands: The syntheses and structural characterizations, In vitro antimicrobial activities and DNA interactions of 4-fluorobenzyl(N/O)spirocylotriphosphazenes. Turkish Journal of Chemistry, 41 (2017) 525-547.

[20] G. Elmas, A. Okumuş, Z. Kılıç, L. Y. Gönder, L. Açık and T. Hökelek, The Syntheses and Structural Characterizations, Antimicrobial Activity and In vitro DNA Binding of 4-fluorobenzylspıro(N/O)cyclotriphosphazenes and Their Phosphazenium salts. Journal of the Turkish Chemical Society, Section A: Chemistry, 3 (2016) 25-46.

[21] G. Elmas (nee Egemen), A. Okumuş, Z. Kılıç, T. Hökelek, L. Açık, H. Dal, N. Ramazanoğlu and L. Y. Koç, Phosphorus−nitrogen compounds. Part 24. Syntheses, crystal structures, spectroscopic and stereogenic properties, biological activities, and DNA interactions of novel spiro-ansa-spiro- and ansaspiro-ansa-cyclotetraphosphazenes. Inorganic Chemistry, 51 (2012) 12841-12856.

[22] Bruker SADABS, Bruker AXS Inc. Madison, Wisconsin, USA (2005).

[23] G. M. Sheldrick, SHELXS-97, SHELXL-97 University of Gottingen, Gottingen, Germany (1997).

[24] E. Pidcock, Achiral molecules in non-centrosymmetric space groups. Chemical Communications, (2005) 3457.

[25] D. Cremer and J. A. Pople, General definition of ring puckering coordinates. Journal of American Chemical Society, 97 (1975) 1354-1358.

[26] F. H. Allen, O. Kennard, D. G. Watson, L. Brammer, G. Orpen and R. Taylor, Tables of bond lengths determined by *X*-ray and neutron diffraction. Part 1. Bond lengths in organic compounds. Journal of the Chemical Society, Perkin Transactions 2. 12 (1987) 1-19.

[27] T. Hökelek, E. Kılıç and Z. Kılıç, Trans-2,6-Bis(ethylamino)-2,4,4,6,8,8-hexapiperidinocyclo-2□^{5},4□^{5},6□^{5},8□^{5}-tetraphosphazatetraene. Acta CrystallogrAPHİCA, C55 (1999) 983-985.

[28] A. B. Chaplin, J. A. Harrison and P. J. Dyson, Revisiting the electronic structure of phosphazenes. Inorganic Chemistry, 44 (2005) 8407-8417.

[29] E. W. Ainscough, A. M. Brodie, A. B. Chaplin, A. Derwahl, J. A. Harrison and C. A. Otter, Conformational flexibility in 2,2‘-dioxybiphenyl-chloro-cyclotetraphosphazenes and its relevance to polyphosphazene analogues. Inorganic Chemistry, 46 (2007) 2575-2583.

[30] L. J. Farrugia, ORTEP-3 for Windows- a version of ORTEP-III with a Graphical User Interface (GUI). Journal of Applied Crystallography, 30 (1997) 565-566.

Current Address: GAMZE ELMAS Department of Chemistry, Ankara University, 06100 Ankara, TURKEY
E-mail Address: gegemen@ankara.edu.tr
ORCID: https://orcid.org/0000-0003-4877-3697

Current Address: AYTUĞ OKUMUŞ: Department of Chemistry, Ankara University, 06100 Ankara, TURKEY
E-mail Address: okumus@science.ankara.edu.tr
ORCID: https://orcid.org/0000-0002-2169-5695

Current Address: SATİYE SEVİM İSAOĞLU: Cebrail Neighborhood, Kuleli Street No.14A/2 Kastamonu, TURKEY
E-mail Address: satiyesevim@gmail.com

Current Address: TUNCER HÖKELEK: Department of Physics, Hacettepe University, 06800 Ankara, TURKEY
E-mail Address: merzifon@hacettepe.edu.tr
ORCID: https://orcid.org/0000-0002-8602-4382

Current Address: ZEYNEL KILIÇ (Corresponding author): Department of Chemistry, Ankara University, 06100 Ankara, TURKEY
E-mail Address: zkilic@science.ankara.edu.tr
ORCID: https://orcid.org/0000-0003-1061-8122

Commun.Fac.Sci.Univ.Ank.Series B
Volume 61, Number 1-2, Pages 31-54 (2019)
ISSN 2687-4806
http://communications.science.ankara.edu.tr/index.php?series=B

DFT CALCULATIONS OF BENZOISOXAZOLE DERIVATIVES

EZGİ ÖZEN, MELİKE KALKAN AND PERVİN ÜNAL CİVCİR

ABSTRACT. In this work, we carried out theoretical calculations to determine the structure-activity relationship and the properties of two benzoisoxazole derivatives. For the quantum chemical calculations, the Density Functional Theory (DFT) with B3LYP (Becke three-parameter hybrid correlation functional combined with Lee–Yang–Parr correlation functional) and 6-311+G(d,p) basis set were employed both in the gas phase and in different solvents such as toluene, chloroform, THF, DCM, acetone, DMSO. The CPCM (conductor-like polarizable continuum) solvation model was also used to compute condensed-phase energies in solvent systems. The structural parameters (bond lengths, bond angles, and dihedral angles), energetics (the total energies, the zero-point vibrational energies, the frontier orbital energies (E_{HOMO}, E_{LUMO}), and the bandgap energies) and the spectroscopic characteristics (UV, IR, ^{1}H-NMR, and ^{13}C-NMR) of the target molecules were also determined. The results of the calculations were compared with experimental values for molecule 1, which exists in literature. The calculated geometries (bond length, bond angle and dihedral angle) were in a good agreement with the experimental data. In the case of IR frequencies, the scaled calculated frequencies agreed reasonably well with the experimental results. Moreover, there is a good correlation between experimental and calculated proton signals ($R^2 = 0.9769$) and carbon signals ($R^2 = 0.9972$) of molecule 1.

1. INTRODUCTION

Heterocyclic compounds are very important in chemistry because of their biological activities. These type of compounds are used commonly in medicinal chemistry and they used to build therapeutic agents. Benzoxazole and benzoisoxazole compounds are the significant class of heterocyclic compounds. Benzoisoxazole derivatives bearing various substituents are known to have diverse biological activities in pharmaceutical and agricultural areas [1]. Some derivatives are also used as semiconductors and as corrosion inhibitors in fuels and lubricants [2]. They are also important intermediates in the synthesis of many complex natural products [3]. Among these compounds, 3-substituted-1,2-benzoisoxazole and its derivatives have significant pharmacological and biological activities such as analgesics [4], anticonvulsant [5,6], antipsychotic [7,8], anticancer [9], antimicrobial [10] and also show an affinity for serotonergic and dopaminergic receptors. For example, 1,2-benzoxazole-3-methanesulfonamide, known as zonisamide, is an effective commercially

Received by the editors: August 02, 2019; Accepted: August 23, 2019.
Key word and phrases: Benzoisoxazoles, Density Functional Theory, IR, UV, NMR.

available antiepileptic. Therefore, synthesis of nitrogen, oxygen and sulfur-containing heterocyclic compounds are of interest to researchers.

In this work, theoretical investigations of 3-(chloromethyl)-6,7-dimethylbenzo[d]isoxazole **1** and 3-(bromomethyl)-6,7-dimethyl benzo[d]isoxazole **2** were performed and their structures and IUPAC names are presented in Fig. 1. In 2011, molecule **1** was synthesized by Arava et al. [11]. However, there is not a synthesis of molecule **2** in literature. Literature survey also reveals that to the best of our knowledge, neither structural properties nor spectral properties of the molecules (**1** and **2)** by quantum chemical calculations have been reported so far. In this context, we aimed to illuminate the structure of the target molecules with the help of quantum chemical calculations considering the biological properties mentioned above and to see how the properties of the bromine-linked derivative of the benzoisoxale ring change concerning the chlorine derivative. Also, we wanted to test the accuracy and reliability of the level of theory and the basis set, which we used in the calculations, by comparing the experimental values to the calculated values of molecule **1**. For these purposes, the structural properties (bond lengths, bond angles, and dihedral angles), energetics (the total energies, the zero-point vibrational energies, the frontier orbital energies (E_{HOMO}, E_{LUMO}), and the bandgap energies), and spectroscopic characteristics (UV-VIS, FT-IR, ^{1}H-NMR, and ^{13}C-NMR) of compounds **1** and **2** were calculated and the results of the calculations were compared with experimental ones for molecule **1,** which exists in the literature [11].

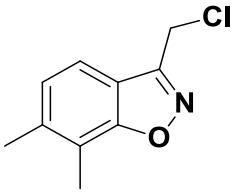

3-(Chloromethyl)-6,7-dimethylbenzo[d]isoxazole **1**

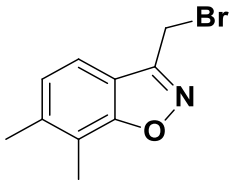

3-(Bromomethyl)-6,7-dimethylbenzo[d]isoxazole **2**

FIGURE 1. Molecular structures and IUPAC names of the studied compounds.

2. Computational Methods

The Density Functional Theory (DFT) [12] calculations presented in this work were carried out by using the Gaussian 09W (Revision D.01) program package [13] and Gauss View 5.0.8 molecular visualization program [14]. Conformation analysis was performed by using B3LYP (Becke three-parameter hybrid functional combined with Lee–Yang–Parr correlation functional) method [15, 16] and the 6-311+G(d,p) basis set [17]. Once the stable conformers

of the target molecules were verified, full geometry optimizations for only the most stable (global minimum on the potential energy surface) conformers were carried using the B3LYP with 6-311+G (d, p) basis set in the gas phase. The B3LYP /6-311+G (d, p) level of theory was selected according to literature examples for this type of molecules [18].

Geometry optimizations were performed with the full analytical Hessian calculated at every geometry step and without any geometrical or symmetry constraints. The vibrational analysis shows that all optimized configurations have no imaginary frequencies and were minima on potential energy surfaces. Harmonic frequencies were used to calculate the zero-point vibrational energies (ZPVE) which was scaled by a factor of 0.967 (B3LYP/6-311+G(d,p)) [18]. This was necessary due to the very complicated structure of the PES, particularly for the larger molecular species. All reported energies are 0 K values including ZPVEs unless otherwise stated. Based on these approaches, the following sections are arranged and our results provide a better understanding of the energetics, structural and spectroscopic properties of the benzoisoxazole derivatives.

3. Results And Discussion

3.1. Structural Analysis

Firstly, the scan analysis was performed with B3LYP/6-311+G(d,p) level of theory. A potential energy surface (PES) scan was done by minimizing the potential energy in all geometrical parameters by changing the dihedral angle at every 30° (from 0° to 360°) with the rotation around the single bond (N1,C9—C10, X11; **X:** Cl, Br). The general representation of the dihedral angle (φ_1) determined from the scan analysis is given in Fig. 2.

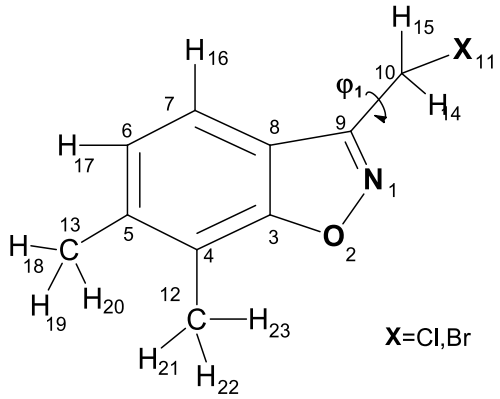

FIGURE 2. Numbering atoms for the definition of the bond lengths, bond angles, and dihedral angles.

From the scan analysis results, for each of the target molecules, we selected only one conformation which had the lowest energy value and hence the most stable conformer. The lowest energy conformers are shown in Fig. 3, along with the graph of change of total energy with dihedral angle. According to the conformational analysis results, the heteroatoms (oxygen and nitrogen) of the benzoisoxazole ring were on the different side to the halogen atoms in the 3- position of the benzoisoxazole. The conformational analysis results also show that the whole molecule is planar for both compounds and the minimum energies were obtained at 300º on the potential energy curve and the energy values for the compounds **1** and **2** are -3091.31 and -977.39 Hartree, respectively.

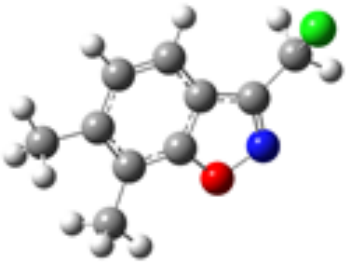

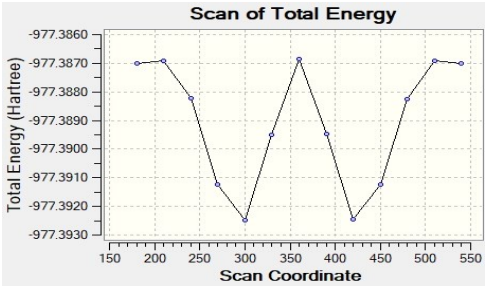

Energy: -3091.31 Hartree
Dihedral Angle: 0.86º

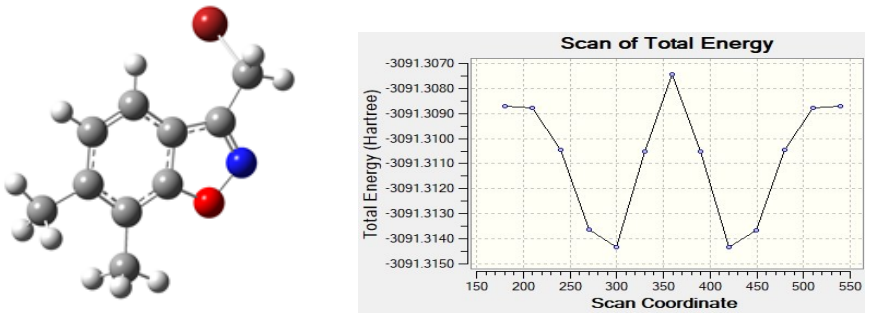

Energy: -977.39 Hartree
Dihedral Angle:-60,0º

FIGURE 3. Most stable conformers of the molecules and potential energy graph.

After determining the most stable conformers of the target compounds with the conformational analysis, we continued with the lowest conformers in next calculations and the geometry optimization of these conformers were performed by B3LYP/6-311+G(d,p) level of theory. The optimized structures of the studied compounds were given in Fig. 4. A search of the literature revealed that the molecule **1** was studied experimentally [11, 19], but that compound **2** was not present in any published computational or experimental studies. Experimental and calculated bond lengths of the studied compounds are given in Table 1.

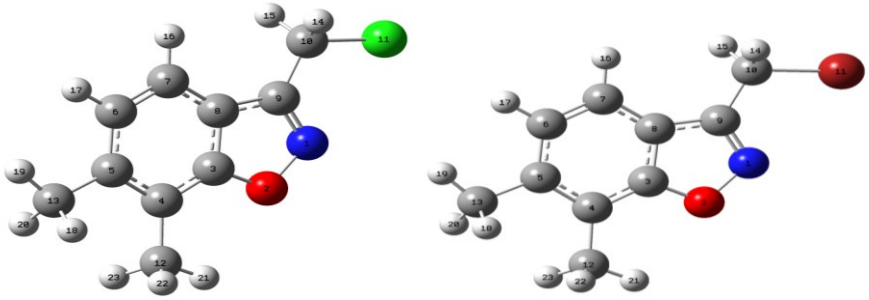

1 **2**

FIGURE 4. The optimized geometries of the target molecules.

As can be seen from the Table 1, after the geometry optimization, the calculated average bond lengths of the target molecules were 1.50 Å (C-C), 1.36 Å (C-O), 1.30 Å (C=N), 1.41 Å (O-N), 1.80 Å (C-Cl), 1.96 Å (C-Br) and between 1.39-1.44 Å (C = C). Due to the

conjugation in the aromatic heterocyclic benzoisoxale ring, all C=C bonds had an average C-C single and C=C double bond lengths values, as expected. Since only the experimental bond lengths of the molecule **1** were found in the literature, only the calculated values for molecule **1** were compared with the experimental values (X-Ray) [19]. The correlation coefficient (R^2) of experimental and calculated bond lengths for molecule **1** was found to be 0.861 (Fig. 5). Similarly, the correlation coefficient (R^2) between experimental and calculated bond angles for the title molecule **1** were 0.9658 (Fig. 5). Therefore, we can say that the calculated all bond lengths and bond angles of molecule **1** are in good agreement with the results obtained from X-ray analyses. We can conclude that the B3LYP/6-311+G(d,p) level of theory used in the calculation gives the correct results for these type molecules.

TABLE 1. Calculated bond lengths, bond angles and dihedral angles of the target compounds.

Bond Lengths (Å)				***Bond Angles (°)***			
Bond Type	**1 Expt***	**1 Calc.**	**2 Calc.**	**Bond Type**	**1 Expt***	**1 Calc.**	**2 Calc.**
N(1)-O(2)	1.417	1.407	1.407	N(1)-O(2)-C(3)	107.37	108.4	108.4
O(2)-C(3)	1.363	1.357	1.357	C(3)-C(4)-C(5)	114.78	115.3	115.3
C(3)-C(4)	1.387	1.396	1.396	C(4)-C(5)-C(6)	120.40	120.6	120.6
C(4)-C(5)	1.389	1.403	1.402	C(5)-C(6)-C(7)	123.19	122.5	122.5
C(5)-C(6)	1.406	1.414	1.414	C(6)-C(7)-C(8)	117.15	117.3	117.3
C(6)-C(7)	1.361	1.385	1.385	C(7)-C(8)-C(3)	118.97	119.5	119.5
C(7)-C(8)	1.397	1.399	1.399	C(8)-C(3)-C(4)	125.48	124.5	124.5
C(8)-C(9)	1.420	1.440	1.441	C(3)-C(8)-C(9)	103.89	103.2	103.2
C(8)-C(3)	1.372	1.395	1.395	C(8)-C(9)-N(1)	112.04	111.5	111.4
C(9)-C(10)	1.488	1.496	1.493	C(9)-N(1)-O(2)	106.82	107.2	107.2
C(9)-N(1)	1.295	1.301	1.301	C(9)-C(10)-X(11)	110.08	114.4	115.0
C(10)-X(11)	1.776	1.799	1.961	C(3)-C(4)-C(12)	121.25	121.3	121.3
C(4)-C(12)	1.498	1.506	1.506	C(5)-C(4)-C(12)	123.97	123.2	123.2
C(5)-C(13)	1.505	1.509	1.509	C(4)-C(5)-C(13)	120.5	119.9	119.9
C(6)-H(17)	0.930	1.084	1.084	C(6)-C(5)-C(13)	119.09	119.4	119.4
C(7)-H(16)	0.930	1.083	1.083	***Dihedral angles (°)***			
C(10)-H(14)	0.970	1.090	1.089	N(1)-O(2)-C(3)-C(4)	-178.95	180	179.99
C(10)-H(15)	0.970	1.090	1.089	O(2)-C(3)-C(4)-C(5)	177.83	-179.99	179.99
C(12)-H(21)	0.960	1.086	1.089	C(3)-C(4)-C(5)-(C6)	1,80	0.005	-0.001
C(12)-H(22)	0.960	1.094	1.094	C(4)-C(5)-(C6)-C(7)	-1.20	-0.002	0
C(12)-H(23)	0.960	1.094	1.094	C(5)-C(6)-C(7)-C(8)	-0.20	-0.003	0
C(13)-H(18)	0.960	1.094	1.094	C(6)-C(7)-C(8)-C(9)	-178.2	-179.9	179.99

C(13)-H(19)	0.960	1.090	1.090	N(1)-O(2)-C(3)-C(8)	0.20	0.0	-0.002
C(13)-H(20)	0.960	1.094	1.094	O(2)-C(3)-C(8)-C7)	-179.26	179.99	-179.99
-	-	-	-	C(8)-C(9)-C(10)-X(11)	58.8	179.9	179.9
-	-	-	-	N(1)-C(9)-C(10)-X(11)	-121.31	0.0	0.1

* Taken from reference 19

When we examine the rotation angles, it is observed that the results of the dihedral angles found by the geometry optimization of molecule **1** supported the results found by conformation analysis. However, there is a difference between experimental and calculated rotation angles of the molecule. Our calculation results show also that the benzoisoxazole ring and even the whole molecule are planar and the dihedral angle (φ_1) is almost 180°.

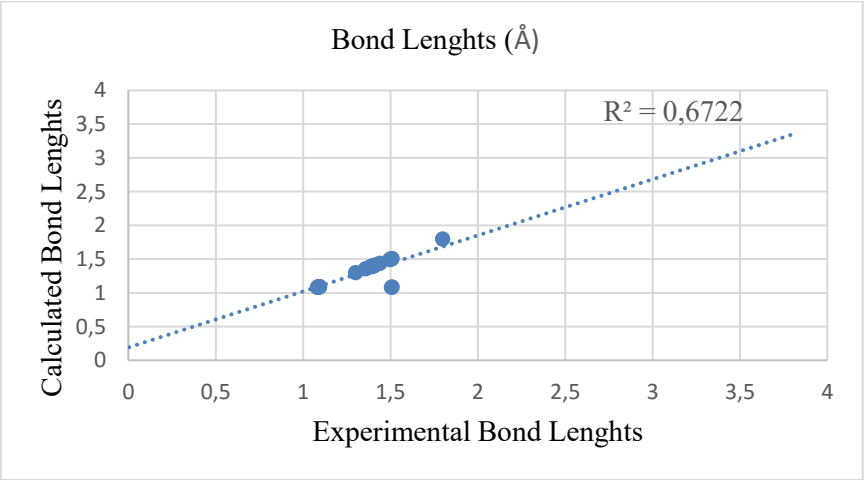

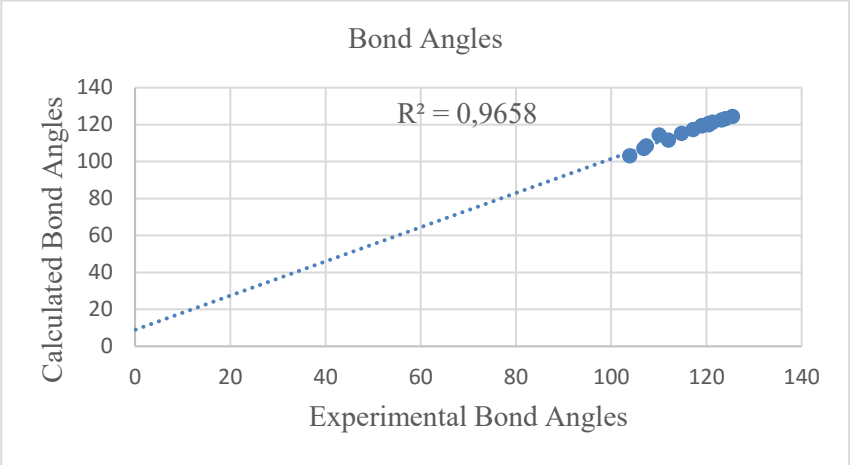

FIGURE 5. Bond lengths (upper) and bond angles (lower) correlation graphs for molecule **1**.

The X-Ray results of the molecule **1** show that the benzoisoxazole ring is planar and the torsion angle (φ_1) is 121.31° and the side chain is anticlinal looking down the C9—C10 bond [19]. The difference between computed and measured values can be explained that X-ray measurement is taken in a solid phase while calculation performed in the gas phase.

3.2. Energetics

The energies of the target molecules were based on the ground state and calculated with B3LYP/6-311+G(d,p) theory level in the gas phase and different solvents such as toluene, chloroform, THF, DCM, acetone, DMSO. The CPCM (conductor-like polarizable continuum) solvation method was used to compute condensed-phase energies in solvent systems. The total energies (E_T), the highest filled molecular orbital energies (E_{HOMO}) and the lowest empty molecular orbital (E_{LUMO}) energies, and the LUMO - HOMO energy difference (E_{gap}) were calculated. The zero point vibration energies (E_{ZPVEs}) were determined to convert the total electronic energy obtained from DFT calculations to 0 K total energy. The E_{ZPVEs} were corrected by a scaling factor of 0.967 for the B3LYP/6-311+G (d, p). Our energetic results are presented in Table 2. The results show that for both compounds, the zero point vibrational energies and the total energies in CPCM method are changed depending on the polarity of the solvent. In other words, both compounds have the lowest energy in DMSO, which has a higher dielectric constant. This can be explained by strong solvent-solute interactions in polar solvents. The calculation results revealed that all the energies, except the total energies (E_T), for both molecules are almost identical.

TABLE 2. Computed energies (E_{ZPVE}, $E_{T,}$ E_{HOMO}, $E_{LUMO,}$ and E_{gap}) of the studied molecules in the gas and different solvents.

Molecule 1	**Gas**	**Toluene**	**$CHCl_3$**	**THF**	**DCM**	**Acetone**	**DMSO**
$\mathbf{E_{ZPVE}}$ (kcal mol^{-1})	108.241	108.246	108.249	108.241	108.246	108.249	108.241
$\mathbf{E_T}$ (kcal mol^{-1})	-613211.460	-613215.001	-613216.536	-613217.151	-613217.336	-613217.866	-613218.101
$\mathbf{E_{HOMO}}$ (eV)	-6.821	-6.796	-6.785	-6.780	-6.779	-6.775	-6.774
$\mathbf{E_{LUMO}}$ (eV)	-1.543	-1.545	-1.550	-1.552	-1.553	-1.556	-1.557
$\mathbf{E_{gap}}$ (eV)	5.279	5.251	5.235	5.228	5.226	5.219	5.216
Molecule 2							
$\mathbf{E_{ZPVE}}$ (kcal mol^{-1})	107.728	107.764	107.778	107.782	107.784	107.788	107.787
$\mathbf{E_T}$ (kcal mol^{-1})	-1939717.861	-1939721.355	-1939722.864	-1939723.469	-1939719.973	-1939724.170	-1939724.405
$\mathbf{E_{HOMO}}$ (eV)	-6.820	-6.795	-6.784	-6.779	-6.778	-6.774	-6.772
$\mathbf{E_{LUMO}}$ (eV)	-1.542	-1.545	-1.549	-1.551	-1.552	-1.554	-1.556
$\mathbf{E_{gap}}$ (eV)	5.278	5.250	5.234	5.228	5.226	5.219	5.216

The HOMO and LUMO are named as frontier molecular orbitals (FMOs). The FMOs play an important role in the optical and electrical properties, as well as in UV–VIS spectra [20]. The energy difference (E_{gap}) characterizes the chemical reactivity and kinetic stability of molecules. A molecule with a small E_{gap} is usually associated with a high chemical reactivity and also termed as soft molecule [20]. As mentioned above, the HOMO and LUMO energies and their energy difference (E_{gap}) of the target molecules were computed and their HOMO and LUMO graphs in the gas phase were generated from the optimized geometry using GaussView 05 program and are depicted in Fig. 6. The HOMO and LUMO graphics show π molecular orbital characteristics and the electronic cloud distribution of both molecular orbitals are mainly localized on the benzoisoxazole ring system as seen from Fig. 6. The calculation results show that the band gaps are very similar for both optimized molecules. In the case of solvent systems, in going from low-polarity solvent to high-polarity solvent, the HOMO energy increases while the LUMO energy decreases. As a natural consequence of this, the E_{gap} values decrease in the same polarity order for both compounds.

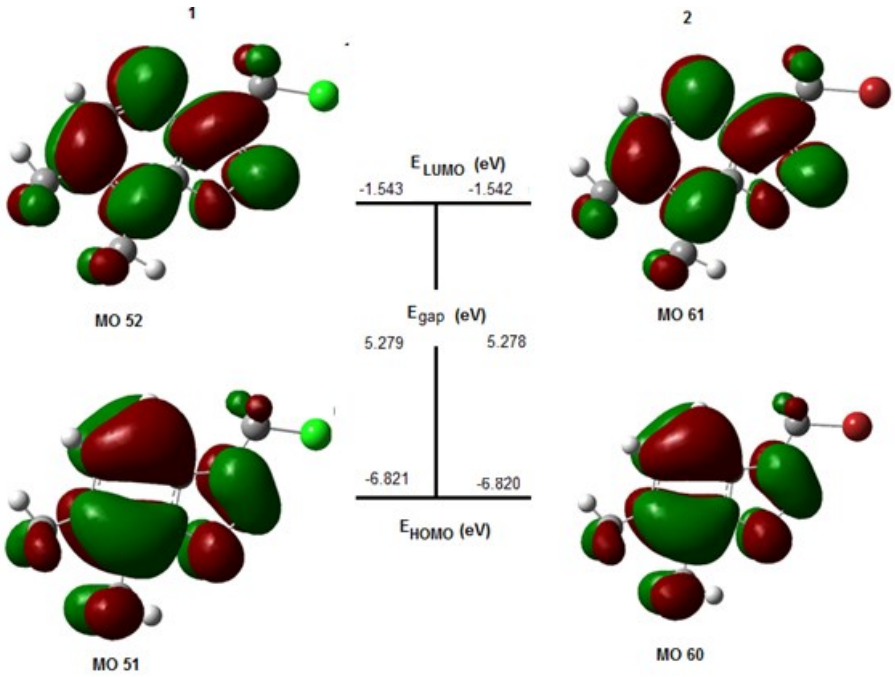

FIGURE 6. HOMO and LUMO graphs of the title compounds in the gas phase

3.3. Spectroscopic Analysis

In this part, UV, IR, ^{1}H-NMR and ^{1}3C-NMR spectra calculated by B3YLP/6-311+ G (d,p) theory level for the target molecules **1** and **2** are described.

UV Analysis

The maximum absorption wavelengths (λ_{max}) in the ultraviolet spectra of the title compounds in the gas phase and different solvents were calculated using the TD-DFT with B3LYP functional and 6-311+G(d,p) basis set. To observe solvent effects Conductor-like Polarizable Continuity Model (CPCM) [21] was used in TD-DFT calculations and dichloromethane, chloroform, tetrahydrofuran, acetone, ethanol, and dimethyl sulfoxide were chosen as solvents. The computed λ_{max1} and λ_{max2} values of the title compounds in the gas phase and the solvent systems are presented in Table 3 and their electronic absorption spectra are given in Fig. 7. There is not experimental UV spectral data of the title compounds, the benzoisoxazole without substituent and 6,7-dimethylbenzoisoxazole in the literature, therefore we could not compare our calculation results to the experimental values and we

evaluated our UV calculation results for gas phase and different solvent systems. From the results, it is revealed that the absorption maxima of the compounds exhibited two distinct absorption bands, attributed to $\pi \rightarrow \pi^*$ transitions. The calculated characteristic peaks (λ_{max1}) of benzoisoxazoles in the gas phase are sharp and observed at 203.5 and 249.5 nm for the molecules **1** and **2**, respectively**.** In gas-phase calculations, the moderate absorbance peak (λ_{max2}) for molecule **1** was found at 252.0 nm, while the same peak was not found for molecule **2**. Since the Cl atom is more electronegative than Br, the λ_{max1} wavelength of molecule **1** were obtained at a lower wavelength than that of molecule **2** in the gas phase.

TABLE 3. Calculated wavelengths λ_{max1} and λ_{max2} (in nm) for title molecules.

Phase/Solvent	**1**		**2**	
	λ_{max1}	**λ_{max2}**	**λ_{max1}**	**λ_{max2}**
Gas	203.5	252.0	249.5	-
Chloroform	188.0	228.0	189.5	227.5
Tetrahydrofuran	206.5	250.0	189.0	227.5
Dichloromethane	188.0	227.5	189.0	227.5
Acetone	189.5	227.5	189.0	227.5
Dimethyl sulfoxide	190.0	227.5	189.5	228.0
Ethanol	189.5	227.5	188.5	227.5

In all solvent systems, two characteristic peaks for both compounds were obtained one sharp and the other broad, as in the gas phase. In all solvent systems except THF, the absorption bands at almost the same wavelengths for both compounds were also obtained. Namely, the λ_{max1} wavelengths in all solvent systems, except THF, for both compounds, were found in the range of 188-190 nm, while the broad absorption bands (λ_{max2}) were determined as 228 nm. The λ_{max1} and λ_{max2} for molecule **1** in THF are 206.5 and 250.0 nm, respectively. Molecule **1** in THF shows a bathochromic shift (~17-22 nm) resulting in absorption in the UV region. In all other solvent systems, the λ_{max1} and λ_{max2} absorption bands shifted to the lower wavelengths than the wavelengths found in the gas phase. In the case of both compounds, the λ_{max1} and λ_{max2} wavelengths varied little with solvent type, except THF for molecule **1**.

Analysis of the wave functions indicates that the electron absorption (λ_{max1}) corresponds to the transition from the ground to the first excited state and is generally described by the one-electron transition from HOMO energy level to LUMO energy level. The calculation results

showed that $E_{HOMO} \rightarrow E_{LUMO}$ transition, which is the most fundamental transitions, were 51→52 for molecule **1** and 60→61 for molecule **2** (see Fig. 6).

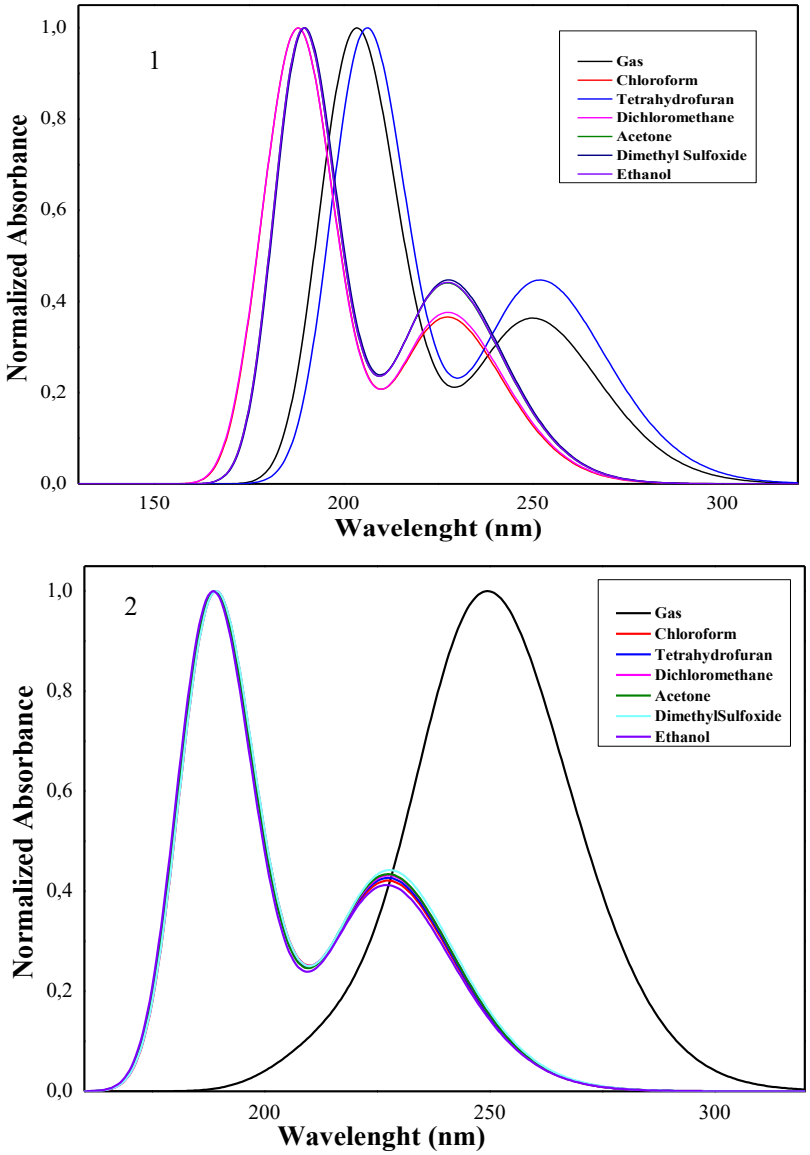

FIGURE 7. Calculated UV spectra for molecules **1** and **2** in gas and various solvents.

IR Analysis

In this section, the calculated vibrations of the target compounds are discussed and the calculation results for molecule **1** are compared with its experimental values. All frequency values calculated with B3YLP/6-311+G(d,p) method were obtained with the harmonic approximation in the gas phase. The calculated IR spectra of the title molecules are given in Fig. 8.

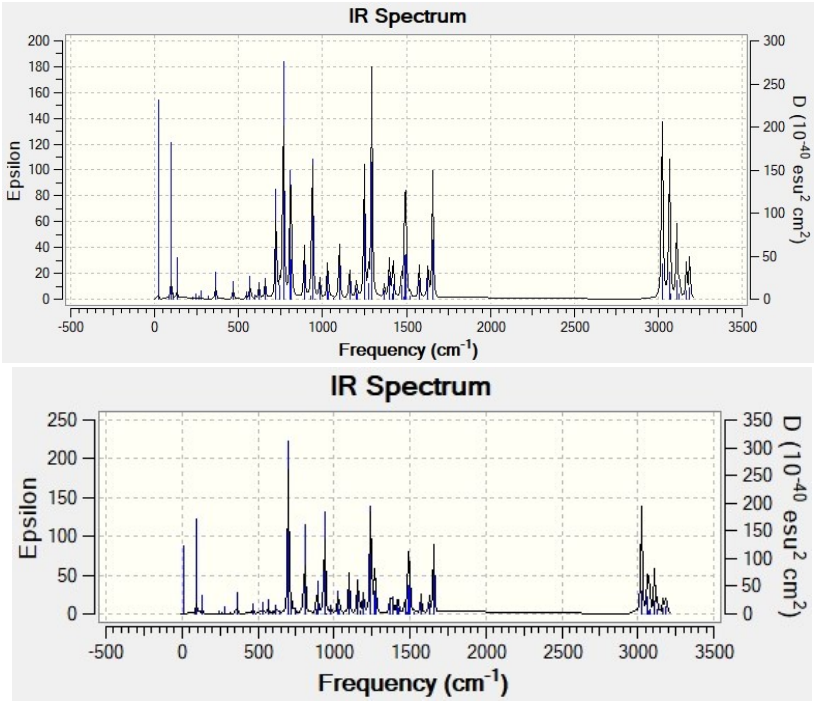

FIGURE 8. Calculated IR spectra of the title compounds.

The vibrational wavenumbers obtained by DFT calculations are generally overestimated than the experimental values due to the neglect of anharmonicity in the real system. These discrepancies can be corrected either by computing with anharmonic approximation or by multiplying with a scaling factor. To compensate these systematic errors the calculated vibrational frequencies for the target compounds in the gas phase are corrected by using a scaling factor (0.9688) [22] for B3LYP/6-311+G(d,p) level of theory. Both molecules have 23 atoms and hence there are 63 normal modes of vibrations. Instead of discussing all

individual modes, the most characteristic peaks are selected and unscaled and scaled vibrational frequencies for the molecules **1** and **2** are presented in Table 4.

TABLE 4. Selected IR absorption bands (cm^{-1}) for molecules **1** and **2**.

	1			**2**		
N	**Expt.***	**Unscaled**	**Scaled**	**Unscaled**	**Scaled**	**Assignments**
1	3019	3167.9	3069.1	3168.1	3069.3	Aromatic C-H
2	2970	3070.0	2974.2	3081.8	2985.6	Aliphatic X-C-H
3	2923	3022.4	2928.1	3022.5	2928.2	Aliphatic C-H
4	1604	1656.9	1605.2	1656.3	1604.6	Aromatic C=C
5	-	1575.4	1526.2	1574.0	1524.9	Aromatic C=N
6	1390	1423.5	1379.1	1423.4	1379.0	C-C stretching
7	-	1273.6	1233.9	1274.2	1234.4	C-O stretching
8		940.0	910.7	938.9	909.6	N-O stretching
9	697	767.1	743.2	-	-	C-Cl stretching
10	-	-	-	699.4	677.6	C-Br stretching

***** Taken from reference 19

The heteroaromatic rings have highly extremely characteristic peaks such as aromatic C-H and aromatic C=C stretching vibrations. Aromatic C-H stretching vibrations are normally observed in the range of 3100-3000 cm^{-1} [23]. The experimental value for molecule **1** is 3019 cm^{-1} while our calculated value of this mode is 3069.1 cm^{-1}. There is a little difference between experimental and calculated vibrational frequencies because experimental results are taken in solvent phase while theoretical results are obtained in the gas phase. It is thought that another reason for this difference is the harmonic approach used for calculations while many modes have anharmonic character, experimentally. Aromatic C = C stretching vibrations are generally observed between 1600-1400 cm^{-1}. The experimental aromatic C = C vibration for molecule **1** was 1604 cm^{-1} and the corresponding calculated value is 1605.2 cm^{-1}. The calculated remaining bands of the benzoisoxazole ring at 1526.2, 1233.9 and 910.7 cm^{-1} are assigned for C = N, C-O, and N-O ring stretching vibrations, respectively.

Aliphatic C-H vibrational frequencies of the methyl and methylene groups connected aromatic rings are normally expected in the range of 3100-2900 cm^{-1} and the experimental aliphatic C-H stretching vibration of the molecule **1** is observed at 2923 cm^{-1} and the

vibrational wavenumber computed at 2928.1 cm^{-1} is assigned to aliphatic C-H stretching. Similarly, aliphatic X-C-H stretching vibration of molecule **1** is experimentally observed at 2970 cm^{-1} and the band calculated at 2974.2 cm^{-1} is assigned as X-C-H stretching. Finally, experimental C-Cl stretching vibration is observed at 697 cm^{-1} and the calculated corresponding value is 743.2 cm^{-1}. The result computed by B3LYP/6-31+G(d,p) presents that the vibrational wavenumber at 677.6 cm^{-1} is assigned to the C-Br stretching vibration for molecule **2**. Also, according to the computed results, the vibrational frequencies of molecules **1** and **2** are very similar and the difference in the electronegativity of the substituents had little effect on other vibrations. To make a comparison with the experimental and computed IR frequencies for molecule **1**, we made a correlation graph shown in Fig. 9. As can be seen in Fig. 9, there is a good correlation between the experimental and the calculated scaled fundamental vibrational of molecule **1** (R^2=0.9993).

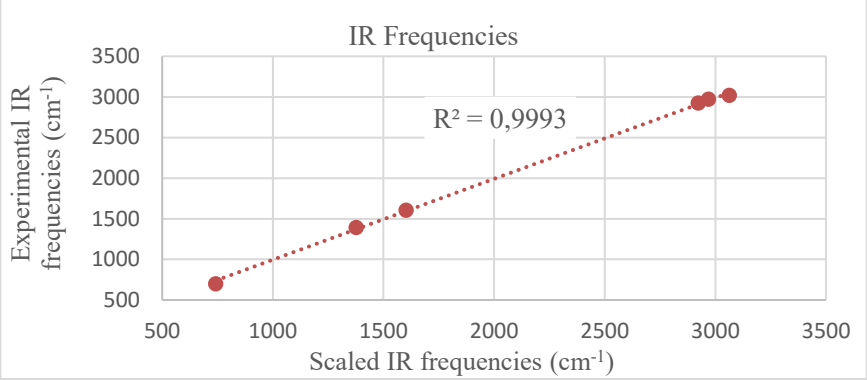

FIGURE 9. IR correlation graph for molecule **1**

NMR Analysis

The ^{1}H and ^{13}C-NMR chemical shifts of the title molecules optimized by B3YLP/6-311+G (d,p) were calculated at the same level of theory by the GIAO (Gauge-Independent Atomic Orbital) [24, 25] approach and referenced by TMS. First, the shielding of tetramethylsilane (TMS), which is used as a general standard, was computed using the B3YLP/6-311+G(d,p) level of theory. Then, the chemical shifts of the title compounds were calculated with the theory used in the geometry optimization of the molecules. The subtracting of two evaluated values ($\sigma_{TMS} - \sigma_{comp.}$) gives the desired chemical shifts of the molecules. The calculated ^{1}H and ^{13}C isotropic chemical shielding of TMS at the B3LYP/6-311+G(d,p) level in the gas phase are 31.98 and 183.96 ppm, respectively. The numbering of atoms in the molecules for

^{1}H-NMR and ^{13}C-NMR is presented in Fig. 10. The ^{1}H-NMR spectra of both compounds were calculated in a $CDCl_3$ solvent are presented in Fig. 11. The calculated values of ^{1}H and ^{13}C chemical shifts in the gas phase together with experimental values, only available in the literature for compound **1**, are presented in Table 5.

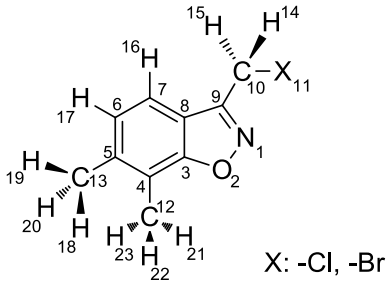

FIGURE 10. Numbering atoms for ^{1}H-NMR and ^{13}C-NMR.

Both molecules have three types of protons, which are aromatic, methyl and methylene. In calculated ^{1}H-NMR spectra, the aromatic protons (H16 and H17) of benzoisoxazole ring appeared in the range of 7.2-7.6 ppm and the corresponding experimental values are at 7.17 and 7.52 ppm for the molecule **1**. For both molecules, the calculated methyl protons (H18-H23) bound to the benzoisoxazole ring at positions 6 and 7 were found in the range 2.1- 3.4 ppm and experimentally observed methyl protons were at 2.43 and 2.47 ppm for molecule **1**. The signals calculated at 5.2 ppm for molecule **1** and 4.6 ppm for molecule **2** were assigned as methylene protons (H14 and H15) of both compounds and the corresponding methylene protons were experimentally observed at 4.88 ppm for molecule **1**. There is a good correlation between experimental and calculated proton signals of molecule **1** and the maximum deviation is 0.53 ppm, except H23 proton of the methyl group. However, the deviation of the experimental and calculated value of H23 proton was 0.93 ppm. This may be due to the weak H bond between the oxygen (O2) and methyl hydrogen (H23) of the benzoisoxazole ring. According to the calculation results, the length of this H bond is 2.53 Å.

1

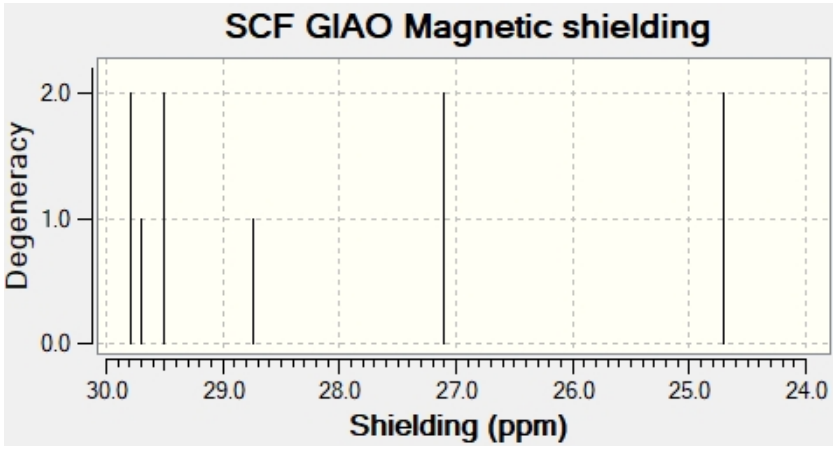

2

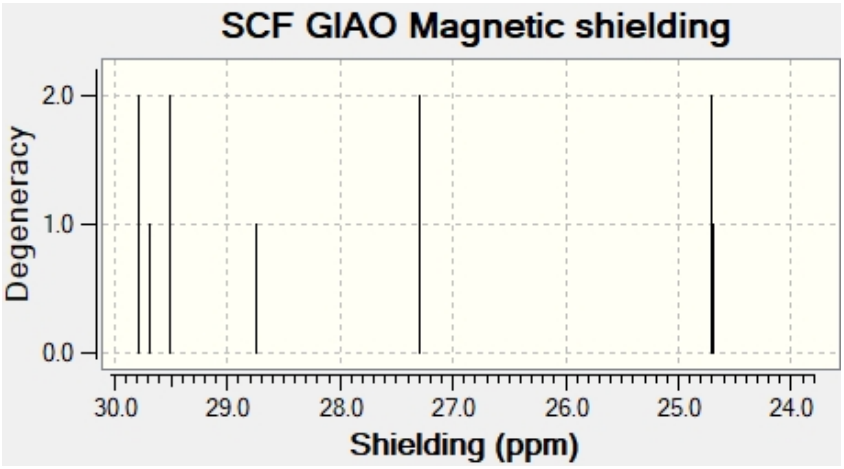

FIGURE 11. Calculated ^{1}H-NMR spectra of the title compounds.

TABLE 5. Experimental and calculated ^{1}H-NMR and ^{13}C-NMR isotropic chemical shifts (ppm) for title molecules.

Atom	**1**		**2**
	Cal.	**Expt.***	**Cal.**
H-14	5.2	4.88	4.6
H-15	5.2	4.88	4.6
H-16	7.6	7.52	7.2
H-17	7.5	7.17	7.2
H-18	2.5	2.43	2.4
H-19	2.4	2.43	2.2
H-20	2.5	2.43	2.4
H-21	3.0	2.47	3.2
H-22	2.3	2.47	2.1
H-23	3.4	2.47	2.1
C-3	171.5	163.5	171.8
C-4	126.8	118.7	126.8
C-5	146.8	139.0	146.8
C-6	131.2	126.5	131.3
C-7	120.9	117.5	121.1
C-8	124.1	117.7	124.6
C-9	160.6	155.1	160.7
C-10	47.3	35.1	39.8
C-12	13.3	11.7	13.3
C-13	22.1	19.1	22.1

*Taken from reference 19

The ^{13}C NMR spectra of both compounds were calculated in a $CDCl_3$ solvent and are presented in Fig. 12. In the ^{13}C NMR spectra of the compounds, calculated signals at δ 120.9, 124.1, 126.8, 131.2, 146.8, 160.6, and 171.5 ppm are corresponding to carbon atoms (C3-C9) of the benzoisoxazole ring. The corresponding experimental values for molecule **1** are 117.5, 117.7, 118.7, 126.5, 155.1, and 163.5 ppm in the literature [19]. The values of the methyl carbons (C12 and C13) linked to benzoisoxazole ring were calculated as 13.3 and 22.1 ppm for both molecules and experimental values of these carbon peaks are observed at

11.7 and 19.1 ppm [19]. The signal for methylene carbon (C10) linked to chlorine atom is experimentally observed at 35.1 ppm and theoretically at 47.3 ppm for molecule **1**. The peak of the same carbon in molecule **2** was calculated as 39.8 ppm because this carbon in molecule **2** is bound to the bromine, whose electronegativity less than chlorine. Hence, it gives a signal in an upfield. The maximum deviation between the calculated and experimental carbon signals of molecule **1** is 8.1 ppm, except C10 carbon of the methylene. However, the maximum deviation in ^{13}C-NMR is higher than ^{1}H NMR chemical shifts.

1

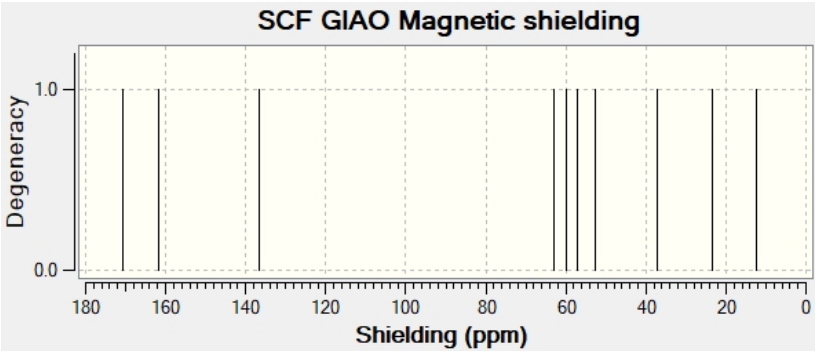

2

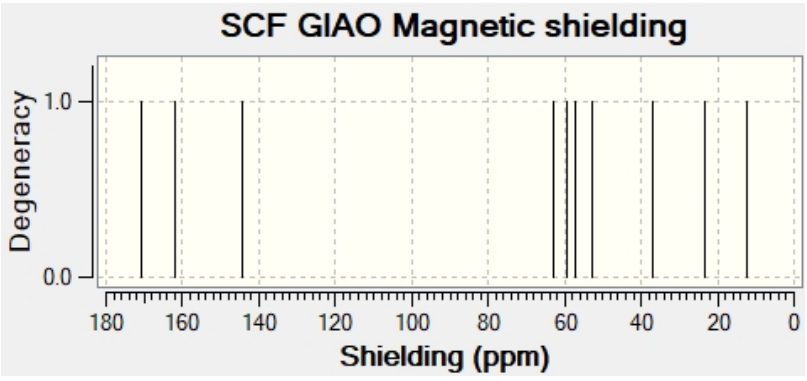

FIGURE 12. Calculated ^{13}C-NMR spectra of the title compounds.

The correlation graphs obtained from the comparison of the experimental and calculated results of ^{1}H-NMR and ^{13}C-NMR for molecule **1** are depicted in Fig. 13. The results show that the calculated chemical shifts are in line with the experimental values of compound **1**. The correlation coefficients (R^2) found for molecule **1** are 0.9769 and 0.9972 for ^{1}H and ^{13}C-NMR, respectively. However, small differences may be because the calculations were done

in the gas phase, while the experimental values measured in the $CDCl_3$ solution, where the molecular interactions are important. Even so, it can be concluded that the GIAO method and B3LYP/6-311+G(d,p) level of theory is sufficient to calculate ^{1}H and ^{13}C-NMR chemical shifts of the studied compounds.

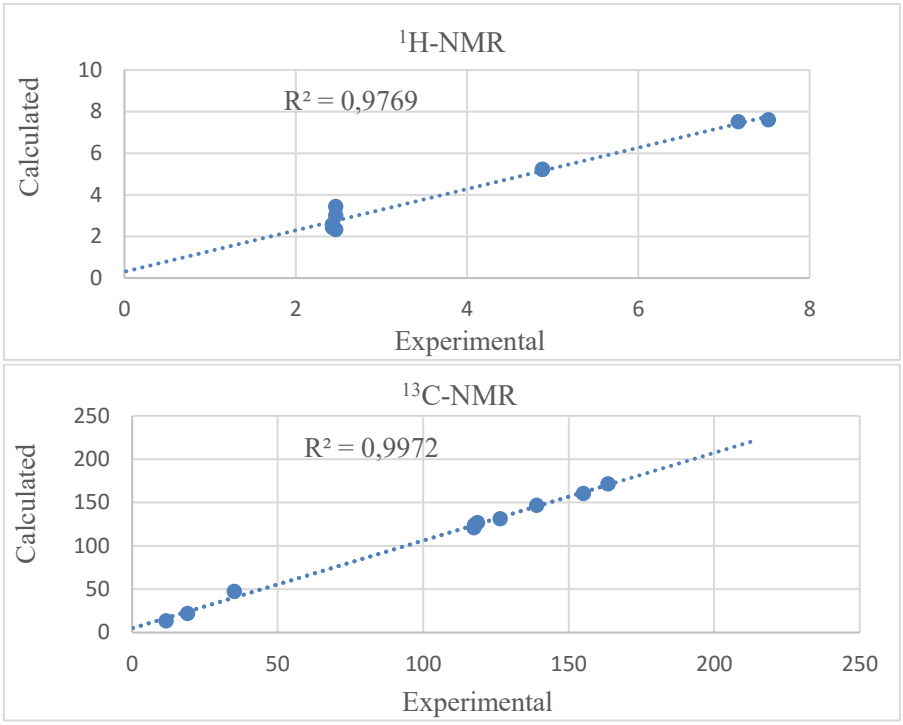

FIGURE 13. Comparison of the experimental and calculated ^{1}H (upper) and ^{13}C-NMR (lower) values of the compound **1**.

4. Conclusion

In this work, firstly the molecular structural parameters such as bond length, bond angle, and dihedral angle for two benzoisoxale derivatives were calculated and compared to the experimental values of molecule **1**. Calculations done by DFT method were carried out with the gas phase and in various solvent systems. The calculated geometric parameters by using density functional theory (DFT) with the 6-311+G(d,p) basis set are in good agreement with the X-ray structure of the molecule **1**. Then, the energies and spectroscopic properties of the molecules were computed. The B3LYP/6-311+G(d,p) level of theory was used to determine

the most stable conformations, energetics, the structural and spectral properties. The total energies, the highest filled molecular orbital energies, the lowest empty molecular orbital energies, and the LUMO - HOMO energy difference were calculated. It is found that the zero-point vibrational energies and the total energies in CPCM method varied depending on the polarity of the solvent. The calculated HOMO, LUMO energies and band gaps of both molecules are very similar for both compounds. Then, the maximum absorption wavelengths (λ_{max}) in the ultraviolet spectra of the title compounds in the gas phase and different solvents were calculated using the TD-DFT with B3LYP/6-311+G(d,p). Two characteristic peaks for both compounds were obtained one sharp and the other broad. In all solvent systems except THF, the absorption bands at almost the same wavelengths for both compounds were also obtained. The vibrational band assignments were performed at B3LYP/6-311++G(d,p) theory level to compare the experimental (FT-IR) and calculated vibrational frequencies of the compound **1**. A good correlation between the observed and scaled IR frequencies was obtained for compound **1**. Scaled results seem to be in good agreement with the experimental ones. Finally, the ^{1}H and ^{13}C-NMR chemical shifts of the title molecules were calculated at the same level of theory by the GIAO approach. The results show that the calculated chemical shifts are in good agreement with the experimental values of compound **1**. Because of the compatibility of the calculated and experimental results of molecule **1**, the B3LYP level with 6-311+G(d,p) basis set can be considered as a suitable method for similar molecules to understanding the energetics, structural and spectral properties.

ÖZET

Bu çalışmada, iki benzisoksazol türevinin özelliklerini belirlemek için teorik hesaplamalar yapılmıştır. Kuantum kimyasal hesaplamalarda, 6-311+G(d,p) temel seti ile Yoğunluk Fonksiyonel Teorisi (DFT) kullanılmıştır. Hesaplamalar, gaz fazında ve toluen, kloroform, THF, DCM, aseton, DMSO gibi farklı çözücü sistemlerinde gerçekleştirilmiştir. Çözücü sistemlerde enerjileri hesaplamak için CPCM (conductor-like polarizable continuum) solvasyon modeli kullanılmıştır. Hedef moleküllerin yapısal parametreler (bağ uzunlukları, bağ açıları ve dönme açılar), enerjileri (toplam enerjiler, sıfır noktası titreşim enerjileri, sınır orbital enerjileri (E_{HOMO}, E_{LUMO} ve bant aralığı enerjileri) ve spektroskopik özellikleri (UV, IR, ^{1}H-NMR ve ^{13}C-NMR) belirlenmiştir. Molekül 1 için deneysel değerler literatürde bulunduğu için hesaplama sonuçları literatür değerleri ile karşılaştırılmıştır. Molekül 1 için hesaplanan geometriler deneysel verilerle hata sınırları içinde uyuşmaktadır. IR frekansları durumunda ise, ölçeklendirilmiş hesaplanan frekansların deneysel sonuçlarla uyuştuğu anlaşılmıştır. Ayrıca, molekül 1'in deneysel ve hesaplanmış proton sinyalleri (R^2 = 0.9769) ve karbon sinyalleri (R^2 = 0.9972) arasında iyi bir ilişki bulunmuştur.

References

[1] K. Ha, H. S. Lim and H. J. Kim, 5-(4-Chlorophenyl)-6-isopropyl-5,6-dihydro-4H-pyrrolo[3,4-c]isoxazole. Acta Crystallographica, E66 (2010) o2483.

[2] K. V. N. Raju, M. Krishnaiah, N. J. Kumar and S. N. Rao, Structure conformation of 4-(4-methoxyphenyl)-5-phenyl isoxazole. Acta Crystallographica, A58 (2002) c128.

[3] M. Krishnaiah, R. R. Kumar, T. Oo and P. Kaung, 4-(4-Chlorophenyl)-5-phenylisoxazole. Acta Crystallographica, E65 (2009) o2324.

[4] H. Hasegawa, Utilization of zonisamide inpatients with chronic pain orepilepsy refractory to other treatments: a retrospective, open label, uncontrolled study in a VA hospital. Current Medical Research and Opinion, 20/5 (2004) 577-580.

[5] Y. Masuda, Y. Utsui, Y. Sharashi, T. Karasawa, K. Yoshida and M. Shimizu, Relationships between plasma concentrations of diphenylhydantoin, phenobarbital, carbamazepine, and 3-sulfamoylmethyl-1,2-benzoisoxazole (AD-810), a new anticonvulsant agent, and their anticonvulsant or neurotoxic effects in experimental animals. Epilepsia, 20/6 (1979) 623-633.

[6] H. Uno, M. Kurukova, Y. Masuda and H. Nishimura, Studies on 3-substituted 1,2-benzoisoxazole derivatives. 6. Syntheses of 3-(sulfamoylmethyl)-1,2-benzoisoxazole derivatives and their anticonvulsant activities. Journal of Medicinal Chemistry, 22/2 (1979) 180-183.

[7] G. V. Bossche, Y. G. Gelders and S. L. Heylen, Development of new antipsychotic drugs. Acta psiquiátrica y psicológica de América Latina, 36 (1990) 13-25.

[8] M. Shimizu, T. Karasawa, M. Masuda and M. Oka, 1,2-Benzoisoxazole-3-acetamidoxime hydrochloride, a new psychotropic agent. Experientia, 30/4 (1974) 405-405.

[9] M. Jain and C. H. Kwon, 1,2-Benzoisoxazole Phosphorodiamidates as Novel Anticancer Prodrugs Requiring Bioreductive Activation. Journal of Medicinal Chemistry, 46/25 (2003) 5428-5436.

[10] K. A. Thakar and B. M. Bhawal, Synthesis and Antimicrobial screening of amino-1, 2-Benzoisoxazoles and sulphanilamido-1, 2 benzoisoxazoles. Current Science, 47/24 (1978) 950-952.

[11] V. R. Arava, G. Laxminarasimhulu, U. B. R. Siripalli and P. K. Dubey, An efficient synthesis of 3-chloromethyl-1,2-benzoisoxazoles via modified Boekelheide rearrangement. Indian Journal of Chemistry, 50B/1 (2011) 119-125.

[12] W. Kohn and L.J. Sham, Self-Consistent Equations Including Exchange and Correlation Effects. Physical Review, 140A (1965) 1133–1138.

[13] M. J. Frisch, G. W. Trucks, H. B. Schlegel, G. E. Scuseria, M. A. Robb, J. R. Cheeseman, G. Scalmani, V. Barone, B. Mennucci, G. A. Petersson, H. Nakatsuji, M. Caricato M, X. Li, H. P. Hratchian, A. F. Izmaylov, J. Bloino, G. Zheng, J. L. Sonnenberg, M. Hada, M. Ehara, K. Toyota, R. Fukuda, J. Hasegawa, M. Ishida, T. Nakajima, Y. Honda, O. Kitao, H. Nakai, T. Vreven, J. A. Montgomery, J. E. Peralta, F. Ogliaro, M. Bearpark, J. J. Heyd, E. Brothers, K. N. Kudin, V. N. Staroverov, R. Kobayashi, J. Normand, K. Raghavachari, A. Rendell, J.C. Burant, S. S. Iyengar, J. Tomasi, M. Cossi, N. Rega, J. M. Millam, M. Klene, J. E. Knox, J. B. Cross, V. Bakken, C. Adamo, J. Jaramillo, R. Gomperts, R. E. Stratmann, O. Yazyev, A. J. Austin, R. Cammi, C. Pomelli, J. W. Ochterski, R. L. Martin, K. Morokuma, V. G. Zakrzewski, G. A. Voth, P. Salvador, J. J. Dannenberg, S. Dapprich, A. D. Daniels, Ö. Farkas, J. B. Foresman, J. V. Ortiz, J. Cioslowski and D. J. Fox (2009) Gaussian 09, Revision D.01. Gaussian, Inc., Wallingford CT.

[14] R. Dennington, T. Keith, and J. Millam, (2009) GaussView, Version 5.0.8.

[15] A. D. Becke, Density-functional exchange-energy approximation with correct asymptotic behavior. Physical Review A, 38 (1988) 3098–3100.

[16] C. Lee, W. Yang and R. G. Parr, Development of the Colle-Salvetti correlation-energy formula into a functional of the electron density. Physical Review B, 37 (1988) 785–789.

[17] K. Raghavachari, J. S. Binkley, R. Seeger and J. A. Pople, Self consistent molecular orbital methods. XX. A basis set for correlated wave functions. Journal of Chemical Physics, 72 (1980) 650-654.

[18] P. Ü. Civcir**,** G. Kurtay and K. Sarıkavak, Experimental and theoretical investigation of new furan and thiophene derivatives containing oxazole, isoxazole, or isothiazole subunits. Structural Chemistry, 28/3 (2017) 773–790.

[19] M. Kayalvizhi, G. Vasuki, A. Veerareddy and G. Laxminarasimha, 3-Chloromethyl-6,7-dimethyl-1,2-benzoxazole. Acta Crystallographica Section E, 68/10 (2012) o3008-o3008.

[20] I. Fleming, Frontier Orbitals and Organic Chemical Reactions. Wiley, London, 1976.

[21] R. E. Stratmann, G. E. Scuseria and M. J. Frisch, An efficient implementation of time-dependent density-functional theory for the calculation of excitation energies of large molecules. Journal of Chemical Physics, 109/19 (1998) 8218-8224.

[22] J. P. Merrick, D. Moran and L. Radom, An Evaluation of Harmonic Vibrational Frequency Scale Factors. Journal of Physical Chemistry A, 111/45 (2007) 11683–11700.

[23] E. Erdik, Organik Kimyada Spektroskopik Yöntemler. Gazi Kitabevi, Ankara, 2015.

[24] K. Wolinski, J. F. Hinton and P. Pulay, Efficient implementation of the gauge-independent atomic orbital method for NMR chemical shift calculations. Journal of the American Chemical Society, 112/23 (1990) 8251–8260.
[25] R. Ditchfield, Self-consistent perturbation theory of diamagnetism. Molecular Physics, 27/4 (1974) 789–807.

Current Address: EZGİ ÖZEN: Department of Chemistry, Ankara University, 06100 Ankara, TURKEY
E-mail Address: ozenezgi@ankara.edu.tr
ORCID: http://orcid.org/0000-0002-4433-813X

Current Address: MELİKE KALKAN: Department of Chemistry, Ankara University, 06100 Ankara, TURKEY
E-mail Address: mkalkan@ankara.edu.tr
ORCID: http://orcid.org/0000-0001-5461-7151

Current Address: PERVİN ÜNAL CİVCİR (Corresponding author): Department of Chemistry, Ankara University, 06100 Ankara, TURKEY
E-mail Address: civcir@science.ankara.edu.tr
ORCID: https://orcid.org/0000-0003-0331-4091

Commun.Fac.Sci.Univ.Ank.Series B
Volume 61, Number 1-2, Pages 55-68(2019)
ISSN 2687-4806
http://communications.science.ankara.edu.tr/index.php?series=B

PROBING THE STRUCTURE-CORROSION INHIBITION PROPERTY RELATIONSHIP OF PYRROLE OLIGOMERS WITH DFT CALCULATIONS

GÖKHAN GECE, SEMRA BİLGİÇ

ABSTRACT. Density functional theory (DFT) calculations on pyrrole oligomers were carried out at the B3LYP/6-311+G(d,p) level to search the relationship between the molecular structure and corrosion inhibition. The electronic properties such as the highest occupied molecular orbital (HOMO), the lowest unoccupied molecular orbital (LUMO) energy levels, energy gap (LUMO-HOMO) and dipole moment were computed. It was found that these electronic values can explain some features of the inhibition phenomena.

1. INTRODUCTION

The annual cost of corrosion and of protection against corrosion in the world is staggering. A recent study estimates that the annual cost of corrosion in the U.S. alone is $276 billion [1]. Protection of oxidizable metals against corrosion is one application that has been intensively investigated [2]. Many corrosion control methods such as coating and conversion films have been proposed, but all such methods involve environmentally hazardous materials [3,4]. Therefore, there is a rigorous search underway for an environmentally friendly alternative to be used in corrosion control coatings [5,6]. One possible alternative are electroactive conducting polymers such as polypyrrole.

Following Deberry's work [7] on the corrosion-protective properties of polyaniline on stainless steel, several papers have been published describing corrosion studies of conducting polymers on various active metals [8-10]. It has been shown that polypyrrole coatings can prevent corrosion of oxidizable metals [11]. However, the protection mechanism is too complex and still under debate.

Recently, quantum chemical methods have become an effective way to study the corrosion inhibition [12] and much achievement was reached [13-15]. It is generally

Received by the editors: October 30, 2019; Accepted: December 03, 2019.
Key word and phrases: Pyrrole, Polypyrrole, Corrosion, Inhibition, Density Functional Theory

accepted that conducting polymers operate as corrosion inhibitors since they have multiple adsorption sites in their molecular structure [16], and there appears to be no reported work involving an adequate treatment of the quantum mechanics to understand of the role of pyrrole oligomers in corrosion inhibition.

On the basis of the above considerations, the aim of the present work was to investigate the underlying physical behavior for corrosion inhibition properties of small pyrrole oligomers up to heptapyrrole as models of the polypyrrole chain by using density functional theory (DFT) calculations.

2. Computational Methods

The calculations were performed by using the *Gaussian09* program [17] with the 6-311+G(d,p) basis set. The Becke three-parameter exchange-functional with non-local correction provided by the Lee-Yang-Parr (B3LYP) method was used. The molecular geometries were fully optimized. After geometry optimizations, harmonic vibrational frequencies have been calculated at the same level. Harmonic frequency analysis indicated that all stationary points were found to be true minima. It is very difficult to calculate parameters directly for an entire polymer molecule due to high molecular weights. However, oligomers can be used in such studies of polymers since all the properties depend on the chemical structure of the polymer molecule, and all this structure is conditioned by the oligomer structure. Therefore, in this study, oligomers composed from the central fragment (pyrrole) were accreted symmetrically and polypyrrole was modelled as a finite chain length of seven structural repeating units. The following quantum chemical indices were considered: the energy of the highest occupied molecular orbital (E_{HOMO}), the energy of the lowest unoccupied molecular orbital (E_{LUMO}), energy band gap, $\Delta E=E_{LUMO}-E_{HOMO}$ and dipole moment (μ).

3. Results And Discussion

The optimized molecular structure for pyrrole unit as a major and a repeat constituent of polypyrrole is depicted in Fig. 1. Experimental structural information on oligopyrroles is scarce, much theoretical discussion of π-conjugated systems such as polypyrrole begins with their representation as a linear, flat molecule. The important structural property of these structures is their planarity, which is directly related to the conjugation of π bond systems. Polypyrrole itself is planar in the solid [18] and gas-phase data are restricted to the microwave results of the pyrrole monomer [19]. In all cases, the geometry is found to be planar. This

geometry is consistent with the expectation of an uncharged π-conjugated system and with the results obtained for the oligomer versions of these polymers [20].

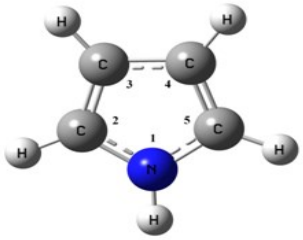

FIGURE 1. Optimized structure of pyrrole.

It is still controversial if polypyrrole exists only in the *anti* form or *syn* form at experimental conditions. The *anti* form has been found to be energetically more favorable [21], thus our theoretical calculations were conducted on planar *anti* structures of the pyrrole oligomers (Fig. 2). The geometrical parameters of the *anti* form of pyrrole are reported in Table 1 together with the experimental planar *anti* structure in the solid for comparison. In our case the structural parameters obtained by B3LYP/6-311+G(d,p) method are in the reasonable agreement with the relevant experimental results. It should be noted that in the case of the lowest molecular symmetries the results of calculations are closer to the experimental ones.

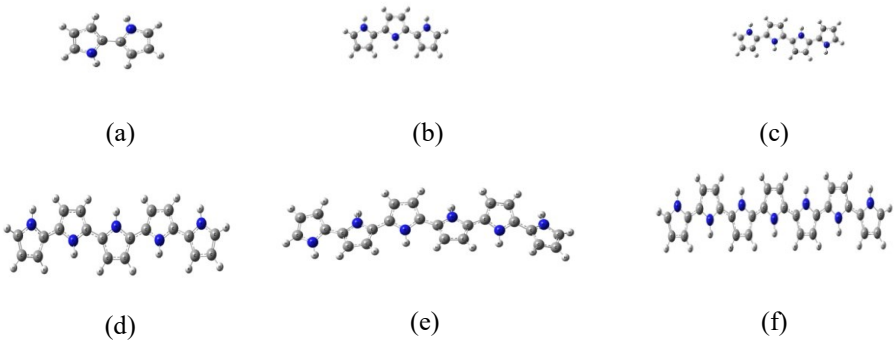

FIGURE 2. Optimized structures for (a) bipyrrole, (b) terpyrrole, (c) quarterpyrrole, (d) pentapyrrole, (e) hexapyrrole, (f) heptapyrrole.

TABLE 1. Optimized and experimental geometric parameters of pyrrole in the ground state.

	B3LYP/6-311+G(d,p)	Exp.[b]
Bond length (Å)[a]		
N1-C2	1.374	1.370
C2-C3	1.376	1.382
C3-C4	1.424	1.417
N1-H	1.006	0.996
C2-H	1.078	1.076
C3-H	1.077	1.077
Bond angle (º)[a]		
C2-N1-C5	109.8	109.8
N1-C2-C3	107.7	107.7
C2-C3-C4	107.4	107.4
H-C2-C3	131.1	130.8
H-C3-C2	125.7	125.5

[a] For numeration please see Fig. 1.
[b] Ref.[19].

According to the frontier molecular orbital theory, the formation of a transition state is due to an interaction between the frontier orbitals (HOMO and LUMO) of reactants [22]. The highest occupied molecular orbitals (HOMO) of the repeat units form the occupied π-band (valence band) of the polypyrrole and the lowest unoccupied molecular orbitals (LUMO) of the repeat unit form the π*-band (conduction band) of the polypyrrole. The energy distance between these two bands is defined as the band gap (ΔE), and in neutral conjugated polymers refers to the onset energy of the π-π* transition [23]. Accordingly, the energy of the highest occupied molecular orbital (E_{HOMO}), the energy of the lowest unoccupied molecular orbital (E_{LUMO}) and the energy gap ($\Delta E = E_{LUMO}$-E_{HOMO}) are important electronic properties that are related to the inhibition efficiency of polypyrrole. In the present work, these properties were examined. It is well known that the value of E_{HOMO} is often associated with the electron donating ability of the inhibitor molecule, higher values of E_{HOMO} indicate the greater ease of donating electrons to the unoccupied d orbital of the metal. The value of E_{LUMO} is related to the ability of the molecule to accept electrons, lower values of E_{LUMO} show the acceptance of

electrons by the inhibitor molecule. Consequently, the value of ΔE provides a measure for the stability of the formed complex [12].

E_{HOMO}, E_{LUMO} and ΔE data for the studied structures are summarized in Table 2. Table 3 shows the comparison of the values of ΔE for pyrrole, bipyrrole and polypyrrole with experimental data [24]. From these results it appears that the E_{HOMO} level increases and the E_{LUMO} level and the energy gap decrease with increasing chain length. This tendency also provides evidence that resulting from the molecular structure, the higher the HOMO energy of the polypyrrole, the greater the ease of offering electrons to unoccupied d orbitals of metal surface. The lower the LUMO energy, the easier the acceptance of electrons from the metal surface, which decreases HOMO-LUMO energy gap and improves the efficiency of the polypyrrole. The plots of E_{HOMO}, E_{LUMO} and ΔE as a function of the reciprocal of inverse chain length (CL=1/n) are given in Fig. 3. Plotting the calculated results against the inverse chain length is a commonly applied approach to discuss the polymer properties [25,26].

TABLE 2. Energetic data for the studied structures versus to the increasing chain length (CL).

Structure	E_{HOMO} (eV)	E_{LUMO} (eV)	$\Delta E(E_L-E_H)$ (eV)	CL (1/n)
Pyrrole	-5.946	-0.085	5.861	1
Bipyrrole	-5.098	-0.378	4.720	0.50
Terpyrrole	-4.782	-0.390	4.392	0.33
Quarterpyrrole	-4.676	-0.814	3.862	0.25
Pentapyrole	-4.573	-0.928	3.645	0.20
Hexapyrrole	-4.507	-1.004	3.503	0.16
Heptapyrrole	-4.432	-1.096	3.336	0.14

In order to calculate the effects of E_{HOMO}, E_{LUMO} and ΔE variables on the CL (1/n), a first-order design model was used according to the results given in Table 2. The general form of the first-order model in k independent variables $X_1,X_2,...,X_k$ is

$$Y = \beta_0 + \sum_{i=1}^{k} \beta_i X_i + \varepsilon \tag{3.1}$$

Where Y is an observable dependent variable, $\beta_o, \beta_1, \ldots, \beta_k$ are the unknown parameters and ε is a random error term [27]. In this study, CL $(1/n)$ is taken as a dependent variable and E_{HOMO}, E_{LUMO} and ΔE are considered as independent variables.

TABLE 3. Comparison of the ΔE values for pyrrole, bipyrrole and polypyrrole.

Structures	B3LYP/6-311+G(d,p)	Exp.[a]
Pyrrole	5.86	5.97
Bipyrrole	4.72	4.35
Polypyrrole	3.34	3.00

[a] Ref.[24].

The parameters of the model in equation (3.1) are estimated from the calculated results by applying the least squares method in Minitab 14 statistical software. Firstly, the effects of E_{HOMO}, E_{LUMO} and ΔE on the CL (1/n) are calculated individually. Then the relationship between all the independent variables and CL (1/n) is probed. The predicted models are given in the following equations:

$$CL = -2.44 - 0.577E_{HOMO} \quad (R^2 = 99.9\ \%) \tag{3.2}$$

$$CL = 0.841 + 0.705E_{LUMO} \quad (R^2 = 79.2\ \%) \tag{3.3}$$

$$CL = -1.04 + 0.336\,\Delta E \quad (R^2 = 95.9\ \%) \tag{3.4}$$

$$CL = -2.46 - 0.581E_{HOMO} - 0.0053E_{LUMO} \quad (R^2 = 99.9\ \%) \tag{3.5}$$

The obtained equations (3.3) and (3.4) show that E_{LUMO} and ΔE values increase with increasing values of CL $(1/n)$. Conversely, an increase in E_{HOMO} values causes a significant decrease in CL $(1/n)$ as in equation (3.2). In order to gain a better understanding of the results, the predicted models (3.2)-(3.4) are presented in Fig. 3. The slope of the line shows the negative correlation between the CL $(1/n)$ and E_{HOMO} variables in Fig. 3(a). It can be seen from the Fig. 3(b) and Fig. 3(c) that there is a positive correlation between the CL $(1/n)$ and independent variables.

When the effects of all independent variables are taken into consideration, the equation (3.5) gives a good predicted model. The ΔE has been neglected in this predicted model due to the

multicollinearity of ΔE with the E_{HOMO} and E_{LUMO}. Besides, the coefficient of E_{LUMO} is too small, -0.0053, to explain the variation on CL ($1/n$). It can be said that the coefficient of determination, R^2, is sufficient enough to explain the effect of E_{HOMO} on CL ($1/n$) for the models given in equations (3.2) and (3.5).

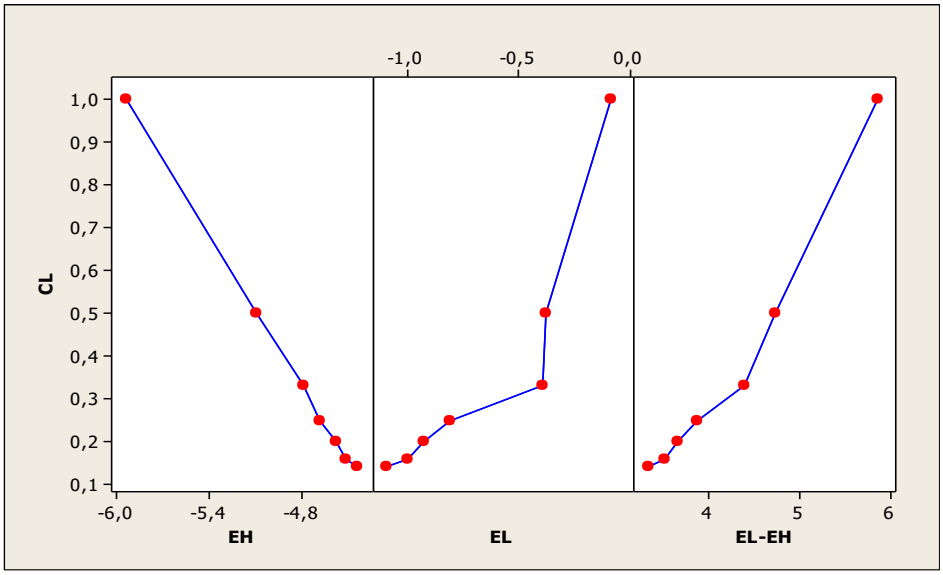

(a) b) (c)

FIGURE. 3. Predicted models of equations (3.2) - (3.4).

The observed and predicted values of CL ($1/n$) which are obtained using predicted model equations (3.2)-(3.5) are presented in Fig. 4. As can be seen, there is a good agreement between predicted values of equation (3.2), Pre2_CL, and observed data points, CL ($1/n$). Also, equation (3.5) gives good agreement with observed CL ($1/n$). The regression analysis shows that the E_{HOMO} is the most efficient variable on the CL ($1/n$).

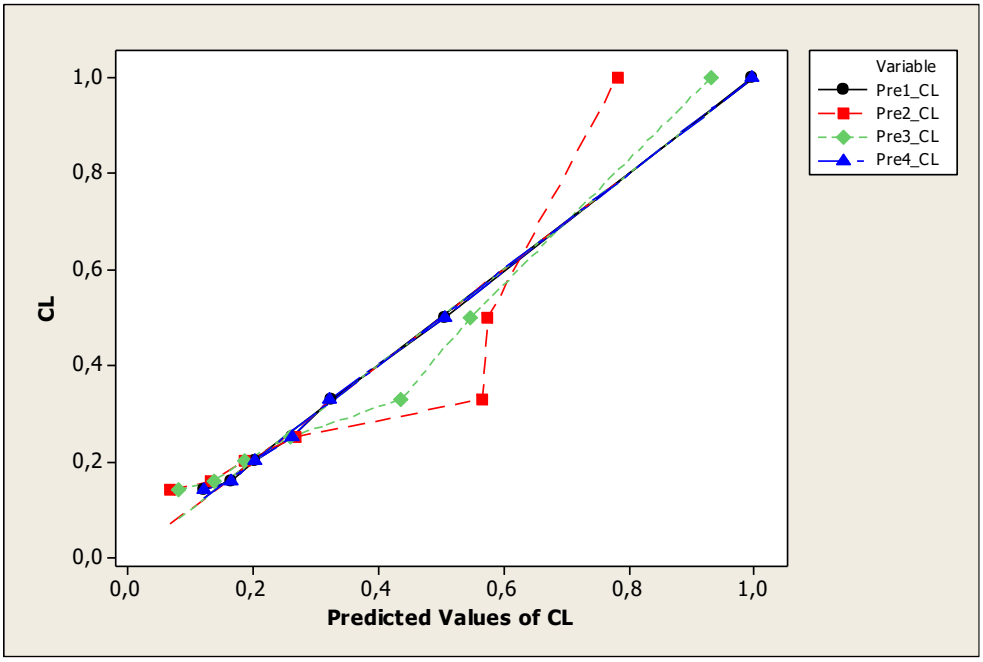

FIGURE 4. Relationship between experimental and predicted values of equations (3.2) - (3.5).

To determine the type of interaction between iron and the studied structures by a molecular approach, the energy differences of frontier orbitals of iron and pyrrole derivatives are considered in Table 4. The energies of HOMO and LUMO of iron were taken from the literature [28] equal to -7.81 and -0.25 eV, respectively. Since the gap of $E_{LUMO(Fe)}$ - $E_{HOMO(polypyrrole)}$ has much less value compared to, $E_{LUMO(polypyrrole)}$ - $E_{HOMO(Fe)}$, there is a strong possibility of electrons from polypyrrole to be given to iron, further strengthening the adsorption.

TABLE 4. HOMO-LUMO gap for the interaction of iron – polypyrrole.

	E_{HOMO} (eV)	E_{LUMO} (eV)	ΔE (eV)	
polypyrrole	-4.43	-1.09	6.72[a]	4.18[b]
iron	-7.81	-0.25		

[a] $E_{LUMO\ polypyrrole}$ - $E_{HOMO\ Fe}$

[b] $E_{LUMO\ Fe}$ - $E_{HOMO\ polypyrrole}$

The polarity of a molecule is well known to be important far various physicochemical properties and the most often used quantity to describe the polarity is the dipole moment (μ) of the molecule [29]. Pyrrole has a medium polarity with an experimental gas-phase dipole moment of 1.74 D [19]. In order to compare the polarization of pyrrole quantitatively with those of oligomers, the dipole moments (μ) were calculated by 6-311+G(d,p) DFT method. To validate the accuracy of the obtained values, the data from the literature [19,30,31] were also given in Table 5.

TABLE 5. Dipole moments (μ/Debye) of the studied structures.

	HF/6-31G(d)	MP2/6-31G(d)	B3LYP/6-31G(d)	B3LYP/6-311+G(d,p)	Exp.
Pyrrole	1.90[a]	1.98[a]/1.84[b]	1.91[a]	1.88	1.74[c]
Bipyrrole	1.80[a]		1.81[a]	0.85	
Terpyrrole				2.28	
Quarterpyrrole				1.59	
Pentapyrrole				2.32	
Hexapyrrole				2.61	
Polypyrrole				1.84	

[a] Ref. [30].
[b] Ref. [31].
[c] Ref. [19].

The dipole moment is essential in the transfer process of inhibitors to the metal surface and its effect on corrosion inhibition is an ambiguous issue. Some researchers assert the contributions of higher dipole moments to the physical adsorption of inhibitory acting molecules [32,33] while some affirm the effect of the lowest dipole moments [34,35]. As can be seen from Table 5, there is an irregularity in the values of dipole moment. Nevertheless, this irregular change proves the fact that the adsorption might not be arisen from the intermolecular electrostatic force.

There is also a dicrepancy in the literature for the calculated dipole moment (μ) values of pyrrole by ab initio methods. Millefiori and Alparone [30] reported the overestimation of dipole moment by a somewhat greater amount (14%) in MP2/6-31G* calculations, while Seio et al. [31] overestimated it by 5-6%. HF/6-31G* and B3LYP/6-31G* calculations also overestimate the dipole moment (μ) by 9-10%. It is evident that the theoretical data suffer from the lack of diffuse functions in the basis set and the difference is probably due to the use of basis set in which the exponents of the d-polarization functions were reduced to 0.25 to improve the accuracy of the dispersion attractions.

4. Conclusion

The calculations provide a theoretical explanation to some extent for the evaluation of corrosion inhibition efficiency of polypyrrole. It is found that the inhibiting action of pyrrole oligomers depends strongly on the electronic structure of the molecules and corrosion inhibition efficiency has certain relationships to the highest occupied molecular orbital (HOMO), the lowest unoccupied molecular orbital (LUMO) energy levels, and the energy gap (LUMO-HOMO).

Özet

Pirol oligomerlerinde yoğunluk fonksiyonel teorisi (DFT) hesaplamaları, moleküler yapı ve korozyon inhibisyonu arasındaki ilişkiyi araştırmak için B3LYP/6-311+G(d,p) seviyesinde yapılmıştır. En yüksek dolu moleküler orbital (HOMO), en düşük boş moleküler orbital (LUMO) enerji seviyeleri, enerji boşluğu (LUMO-HOMO) ve dipol moment gibi elektronik özellikler hesaplanmıştır. Bu elektronik değerlerin inhibisyon olayının bazı özelliklerini açıklayabildiği bulunmuştur.

References

[1] G. H. Koch, M. P. H. Brongers, N. G. Thompson, Y. P. Virmani and J. H. Payer, Corrosion costs and preventive strategies in the United States. U.S. Federal Highway Administration Report, 2002.

[2] F. Presuel-Moreno, M. A. Jakab, N. Tailleart, M. Goldman and J. R. Scully, Corrosion-resistant metallic coatings. Materials Today 11 (2008) 14-23.

[3] G. O. Ilevbare, J. Yuan, R. G. Kelly and J. R. Scully, Inhibition of the corrosion of AA 2024: chromate conversion coating versus chromate additions. Corrosion 56 (2000) 227-242.

[4] I. M. Zin, R. L. Howard, S. J. Badger, J. D. Scantlebury and S. B. Lyon, The mode of action of chromate inhibitor in epoxy primer on galvanized steel. Progress in Organic Coatings 33 (1998) 203-210.

[5] M. Bazzaoui, J. I. Martins, E. A. Bazzaoui, T. C. Reis and L. Martins, Pyrrole electropolymerization on copper and brass in a single-step process from aqueous solution. Journal of Applied Electrochemistry 34 (2004) 815-822.

[6] B. N. Grgur, N. V. Krstajić, M. V. Vojnović, Č. Lačnjevac and Lj. Gajić-Krstajić, The influence of polypyrrole films on the corrosion behavior of iron in acid sulfate solutions. Progress in Organic Coatings 33 (1998) 1-6.

[7] D. W. Deberry, Modification of the electrochemical and corrosion behavior of stainless steels with an electroactive coating. Journal of the Electrochemical Society 132 (19859 1022-1026.

[8] A. Michalik and M. Rohwerder, Conducting polymers for corrosion protection: a critical view. Zeitschrift für Physikalische Chemie, 219 (2005) 1547-1559.

[9] P. Zarras, N. Anderson, C. Webber, D. J. Irwin, A. Guenthner and J.D. Stenger-Smith, Progress in using conductive polymers as corrosion-inhibiting coatings. Radiation Physics and Chemistry 68 (2003) 387-394.

[10] H. Nguyen Thi Le, M. C. Bernard, B. Garcia-Renaud and C. Deslouis, Raman spectroscopy analysis of polypyrrole films as protective coatings on iron. Synthetic Metals, 140 (2004) 287-293.

[11] J. Reut, A. Öpik and K. Idla, Corrosion behavior of polypyrrole coated mild steel. Synthetic Metals, 102 (1999) 1392-1393.

[12] G. Gece, The use of quantum chemical methods in corrosion inhibitor studies. Corrosion Science, 50 (2008) 2981-2992.

[13] L. T. Jr. Sein, Y. Wei and S. A. Jansen, The role of adsorption of aniline trimers on the corrosion inhibition process : a ZINDO/1 study. Computational and Theoretical Polymer Science, 11 (2001) 83-88.

[14] L. T. Jr. Sein, Y. Wei and S. A. Jansen, Corrosion inhibition by aniline oligomers through charge transfer: a DFT approach. Synthetic Metals 143 (2004) 1-12.

[15] A. Yurt, V. Bütün and B. Duran, Effect of the molecular weight and structure of some novel water-soluble triblock copolymers on the electrochemical behaviour of mild steel. Materials Chemistry and Physics 105 (2007) 114-121.

[16] R. Hasanov, S. Bilgiç and G. Gece, Experimental and theoretical studies on the corrosion properties of some conducting polymer coatings. Journal of Solid State Electrochemistry 15 (2011) 1063-1070.

[17] M. J. Frisch, G. W. Trucks, H. B. Schlegel, G. E. Scuseria, M. A. Robb, J. R. Cheeseman, G. Scalmani, V. Barone, G. A. Petersson, H. Nakatsuji, X. Li, M. Caricato, A. Marenich, J. Bloino, B. G. Janesko, R. Gomperts, B. Mennucci, H. P. Hratchian, J. V. Ortiz, A. F. Izmaylov, J. L. Sonnenberg, D. Williams-Young, F. Ding, F. Lipparini, F. Egidi, J. Goings, B. Peng, A. Petrone, T. Henderson, D. Ranasinghe, V. G. Zakrzewski, J. Gao, N. Rega, G. Zheng, W. Liang, M. Hada, M. Ehara, K. Toyota, R. Fukuda, J. Hasegawa, M. Ishida, T. Nakajima, Y. Honda, O. Kitao, H. Nakai, T. Vreven, K. Throssell, J. A. Montgomery, Jr., J. E. Peralta, F. Ogliaro, M. Bearpark, J. J. Heyd, E. Brothers, K. N. Kudin, V. N. Staroverov, T. Keith, R. Kobayashi, J. Normand, K. Raghavachari, A. Rendell, J. C. Burant, S. S. Iyengar, J. Tomasi, M. Cossi, J. M. Millam, M. Klene, C. Adamo, R. Cammi, J. W. Ochterski, R. L. Martin, K. Morokuma, O. Farkas, J. B. Foresman and D. J. Fox, Gaussian 09, Revision B.01, Gaussian, Inc., Wallingford CT, 2009.

[18] T. A. Skotheim, R. L. Elsenbaumer and J. R. Reynolds, Handbook of conducting polymers, Marcel Dekker Inc. New York, 1998.

[19] L. Nygaard, J.T. Nielsen, J. Kirchheiner, G. Maltesen, J. Rastrup-Andersen and G.O. Sørensen, Microwave spectra of isotopic pyrroles. Molecular structure, dipole moment, and ^{14}N quadrupole coupling constants of pyrrole. Journal of Molecular Structure, 3 (1969) 491-506.

[20] G. R. Hutchison, M. A. Ratner and T. J. Marks, Accurate prediction of band gaps in neutral heterocyclic conjugated polymers. Journal of Physical Chemistry A, 106 (2002) 10596-10605.

[21] T. Tamm, J. Tamm and M. Karelson, Theoretical study of the effect of counterions on the structure of pyrrole oligomers. International Journal of Quantum Chemistry, 88 (2002) 296-301.

[22] K. Fukui, Theory of orientation and stereoselection, Springer-Verlag, New York, 1975.

[23] J. Casanovas, E. Armelin, J. I. Iribarren, C. Alemán and F. Liesa, La modelización molecular como herramienta para el diseño de nuevos polímeros conductores. Polimeros, 15 (20059 239-244.

[24] J. L. Brédas, R. Silbey, D. S. Boudreaux and R. R. Chance, Chain-length dependence of electronic and electrochemical properties of conjugated systems - polyacetylene, polyphenylene, polythiophene, and polypyrrole. Journal of the American Chemical Society, 105 (1983) 6555-6559.

[25] G. Zotti, S. Martina, G. Wegner and A. D. Schlüter, Well-defined pyrrole oligomers: electrochemical and UV/vis studies. Advanced Materials, 4 (1992) 798-801.

[26] P. Audebert, J. M. Catel, G. L. Coustumer, V. Duchenet and P. Hapiot, Electrochemical oxidation of five-unit heterocycles: a discussion on the possible dimerization mechanisms. Journal of Physical Chemistry, 99 (1995) 11923-11929.

[27] A. I. Khuri and J. A. Cornell, Response surfaces: Designs and analyses, 2nd ed., (Marcel Dekker Inc., New York, 1996).

[28] P. Mutombo and N. Hackerman, The effect of some organophosphorus compounds on the corrosion behaviour of iron 6 M HCl. Anti-Corrosion Methods and Materials, 45 (1998) 413-418.

[29] M. Karelson and V. S. Lobanov, Quantum chemical descriptors in QSAR/QSPR studies. Chemical Reviews, 96 (1996) 1027-1043.

[30] S. Millefiori and A. Alparone, Ab initio and density functional theory study of the structure and torsional potential of pyrrole oligomers. Journal of Chemical Society Faraday Transactions, 94 (1998) 25-32.

[31] K. Seio, H. Ukawa, K. Shohda and M. Sekine, Computational evaluation of intermolecular interactions of a universal base 3-nitropyrrole in stacked dimers and DNA duplexes. Journal of Biomolecular Structure and Dynamics, 22 (2005) 735-746.

[32] A. Stoyanova, G. Petkova and S. D. Peyerimhoff, Correlation between the molecular structure and the corrosion inhibiting effect of some pyrophthalone compounds. Chemical Physics, 279 (2002) 1-6.

[33] X. Pang, B. Hou, W. Li, F. Liu, and Z. Yu, 2,3,5-triphenyl-2h-tetrazolium chloride and 2,4,6-tri(2-pyridyl)-s-triazine on the corrosion of mild steel in HCI. Chinese Journal of Chemical Engineering, 15 (2007) 909-915.

[34] M. Finšgar, A. Lesar, A. Kokalj and I. Milošev, A comparative electrochemical and quantum chemical calculation study of BTAH and BTAOH as copper corrosion inhibitors in near neutral chloride solution. Electrochimica Acta, 53 (2008) 8287-8297.

[35] Y. Yan, W. Li, L. Cai and B. Hou, Electrochemical and quantum chemical study of purines as corrosion inhibitors for mild steel in 1 M HCl solution. Electrochimica Acta, 53 (2008) 5953-5960.

Current Address: GÖKHAN GECE (Corresponding author): Department of Chemistry, Bursa Technical University, 16310 Bursa, Turkey.
E-mail Address: gokhangc@gmail.com
ORCID: https://orcid.org/0000-0001-9310-5407

Current Address: SEMRA BİLGİÇ: Department of Chemistry, Ankara University, 06100 Ankara, Turkey.
E-mail Address: bilgic@science.ankara.edu.tr
ORCID: https://orcid.org/0000-0001-9730-0146

Commun.Fac.Sci.Univ.Ank.Series B
Volume 61, Number 1-2, Pages 69-87(2019)
ISSN 2687-4806
http://communications.science.ankara.edu.tr/index.php?series=B

SYNTHESIS AND CHARACTERIZATION OF PURE SILICA POWDER FROM A K-FELDSPAR SILICATE ORE FOR INDUSTRIAL VALUE ADDITION

KURANGA I. AYINLA, ALAFARA A. BABA, SUBRAT KU. PADHY, OSENI ADIO, KEHINDE A. ODELEYE, BANKIM CH. TRIPATHY

ABSTRACT. Nigeria is one of the African countries endowed with abundant varieties of solid mineral resources. Despite huge mineral abundance in all States of the Federation, these resources to boost the country's economy, aid industrialization and revenue generation has been far less utilized. Thus, the utilization of a Nigerian k-feldspar ore containing an admixture of orthoclase (KAlSiO8 : 96-740-9031), albite (AlSiO8 : 96-940-0741) and quartz (SiO2 : 96-900-9667) impurities to produce pure silica powder (PSP) was investigated using roast-leaching and co-precipitation method. During leaching, parameters such as leachant concentration, effect of particle size and reaction temperature on the synthesis yield were accordingly examined. At optimal leaching conditions (2.0 mol/L NaOH, 90°C), 87% of the initial 10g/L ore reacted within 120 minutes. The un-reacted product (~13.0%) analyzed by XRD was found to contain siliceous impurities which could serve as a valuable by-product for some defined industries. The leachate at optimal leaching was accordingly co-precipitated using concentrated H2SO4 to obtain pure silica powder (PSP) of industrial value.

1. INTRODUCTION

Silica is a mineral that consists of silicon and oxygen, two of the most common elements on the planet. It comes in several forms, although by far the most common is crystalline silica [1]. The crystalline form of silica is so abundant that it makes up over 12% of the earth's crust, making it the second-most common mineral on the planet [2]. Silica occurs in nature as seven distinct polymorphs: quartz, cristobalite, tridymite, coesite, stishovite, lechatelerite (silica glass), and opal. Disordered cristobalite commonly occurs in soils; tridymite is rare in soils and usually associated with siliceous volcanic rocks; and coesite, stishovite, and lechatelerite are rare polymorphic forms. Opal is hydrated, amorphous silica and is not uncommon, but, of these minerals, quartz is the most abundant in soil environments [3,4].

Silica (SiO2) is so common in such a way that, it is known as a building block of modern life. Products containing silica are used in a vast array of industries, which has made it a key component in the manufacture of millions of products. It is an

Received by the editors: May 22, 2019; Accepted: December 03, 2019.
Key word and phrases: Silica, K-feldspar, Leachant, Optimal leaching, Orthoclase, Kinetics

irreplaceable ingredient in lots of high technology applications such as: precision casting, fibre-optic cables, and the raw materials for computer chips. The presence of silica in our computers and phones cannot be over emphasize because it is a key to the infrastructure of the internet, renewable energy and telecommunications [5]. It is a key part of how we get around our cars and buses, roads and railways. Our homes are even made from it, rocks, glass and ceramics, and many of the things we use every day contain or rely on one form of silica or more [6].

To meet the increasing demand for pure silica powder, it is important to unravel variations of silica production precursor and cheaper production technologies. In the recent time two, main techniques are used for the manufacturing of PSP, this include: Pyrometallurgical method and hydrometallurgical or wet methods [7]. The pyrometallurgical method involved in large scale precipitation of PSP from sodium silicate which is continually produced by high temperature fusion of sodium carbonate and quartz sand while the hydrometallurgical method utilized different lixiviants such as acid/base and their salts to extract silica in the form either silica acid or alkali metal silicate solutions, which are later neutralized to give PSP. This method is of high advantages because it does not require elevated temperature reaction and thus require low energy input than the pyrometallurgical route [8].

Based on the aforementioned merit of hydrometallurgy over pyrometallurgy, various efforts have been exerted to find alternative raw materials for the production of PSP by this method. Many materials such as: rice husk, rice straw, bagasse ash, naturally occurring silicate rocks and photonic industrial waste have been employed [9-13]. However, the choices of these raw materials have been governed by various factors to achieve good commercially produced PSP. These factors include abundance, availability and relative concentration of impurity of the material [8]. Despite the abundance being recorded of rice husk, rice straw and bagasse, their use as a source of material for PSP production require high energy consumption and additional purification steps for the removal of impurities. Secondly, the use of photonic waste cannot meet the high global demand for PSP.

A good number of reports have been reported on the application of the hydrometallurgical process for silica recovery from various types of silicate rock using acid or alkaline solution through the optimization of reaction conditions such as: system temperature, concentration of acid or base solution and material particle

sizes [7,14]. However, it has been reported by Chen and Brantley [14] reported that the dissolution of olivine in HCl depend on the pH and reaction temperature. In another report, sulphuric acid was adopted as a lixiviant to investigate the effect of olivine particle size on the porosity and surface area of nano-silica [15]. Their research gave silica with very small particle size ranging from 8-25 μm. But no attention was given over other kinetic parameters that affect the dissolution rate of olivine and the resulting texture properties of the produced silica powder. Lazaro et al., also achieve 95% purity of silica powder using sulphuric acid as lixiviant. They concluded that the olivine dissolution process in dilute acid could be a convenient alternative to the traditional pyrometallurgy method used for bulky production of nano-silica due to its fewer energy consumptions. Also, no attention was given to deduce the rate-determining step in the acid dissolution of olivine. Despite the fact that mineral acids as proven to be a good lixiviant they exhibit a greater tendency to dissolve impurities like iron from silicate minerals along with the compound of interest, leading to contamination of the product. This has made the use of an alkaline extracting agent is advantageous to compare to that of acid.

Global market demand for silica powder has reported that the worldwide demand for precipitated silica is expected to expand at a 5.5% compound annual growth rate between 2015 and 2023. According to this report, the global precipitated silica market was US$2.22 billion in 2015 and will increase to US$3.49 billion by 2023 [16]. The prospect of this increase in demand is envisaged which is in collaboration with the present regime seven-point economic agenda to diversify Nigeria. Therefore, the study aimed to maximize the synthesis efficiency of PSP by focusing on the alkaline extraction efficiency through an evaluation of the effects of various experimental parameters, including the concentration of sodium hydroxide, liquid to solid ratio, temperature and particle sizes. The determination of optimal reaction conditions through reaction kinetics and rate-limiting steps is vital for the large scale commercial production of various chemicals. Therefore, the kinetics of K-feldspar dissolution in sodium hydroxide media are also analyzed to determine the rate-controlling step and to optimize the reaction conditions. Hence, this study is expected to contribute to economic diversification, as the country is working out some alternative proposal from the present crude oil exploration as a major means of foreign exchange earnings.

2. Materials and Methods

2.1. Materials

The K-Feldspar ore used for this study was sourced from Giri village, Municipal Local Government Area of Abuja (Federal Capital Territory) of Nigeria. The ore was crushed, grinded and pulverized into three different particle sizes: 75+63 μm, -63+75 μm and -75+90 μm fractions. All reagents used were of analytical grade (BDH grades) and deionize water was used to prepare all aqueous solution.

2.2. K- feldspar dissolution process

Leaching experiments were performed in a 1 L glass reactor equipped with a mechanical stirrer, a reaction temperature control unit and a bulk-cooler. For each experiment, 150 mL of aqueous sodium hydroxide solution of pre-determined molarity (0.5 – 2.5 M) and 2 g ore were mixed in the reactor vessel making 20 g/L bulk density. The contents of the reactor were initially heated with mild agitation during heating stage and on attaining the set temperature, the leaching duration start from this point. Sample was collected at an interval of 10, 15, 30, 60 and 120 min. after the desired reaction time, the leached slurry was immediately separated by filtration. The effect of concentration on the extent of K- feldspar dissolution was studied in the NaOH concentration range between 0.5 to 2.5 M at temperature 55°C, particle size -110+75 μm and 300 rpm stirring speed. Considering the temperature dependency, the effect of leaching temperature on phosphate leaching was studied in the temperature range 27 - 90 °C under standard condition of 2.0 M NaOH, -110 +75 μm particle size and atmosphere pressure. To ascertain the effect of particle size on the rate of K-feldspar dissolution, experiments were performed using three different size fractions in the range of -75+63 μm, -63+75 μm and -75+90 μm fractions. The chemical reaction that occurred can be written as follows:

$$KAlSiO_3(s) + 2NaOH(s) + H_2O(l) \rightarrow Al(OH)_3(s) + KOH(aq) + Na_2SiO_3(aq) \quad (2.1)$$

2.3. Pure silica precipitation

The resulting slurry from optimal leaching process was then filtered through an ashless filter (Whatman No 41) and washed with the minimum necessary amount of boiled distilled water. Silica starts to precipitate when the pH of the mixture falls to less than 10 using 0.5 M Hydrochloric acid (HCl); thus, the acidic conditions were maintained until the complete precipitation of silica was achieved. An acidification and neutralization of the transparent filtrate solution was performed to form a silica gel; therefore, the solution was titrated with H2SO4 (1M) to pH 7 under vigorously stirring. The reaction that yields silicic acid can be written as follows:

$$Na_2SiO_3(aq) + H_2SO_4(aq) \rightarrow H_2SiO_3(s) + Na_2SO_4(aq) \quad (2.2)$$

The soft, white aqua gel that formed was allowed to stand at room temperature for 24 hours, before being filtered and washed with distilled water to remove the sulphate salt. The solid residue was dried at 80°C for 24 hours. The silica purification was carried out against impurity such as: Al, Ca, Fe and Mg, by refluxing the powder with a solution of 1M HCl at 110°C for three hours. The suspension was filtered and washed with copious amount of distilled water, and oven dried at 110°C for 2 hours, follow by Calcinations at 800 °C for two hours in a muffle furnace. The fine silica powder was obtained with an excellent mass yield of 94% [8]. The reaction which yields pure silica was given as:

$$H_2SO_4(s) \rightarrow SiO_2(s) + H_2O(g) \quad (2.3)$$

The percent recovery of PSP from K-feldspar was calculated using the following equation:

$$\% \text{ recovery of SPS} = \frac{\propto silica\ obtained}{\propto silica\ calculated} \quad (2.4)$$

Where, α-silica obtained is the fraction of PSP obtained experimentally from the dissolution of K-feldspar, while α-silica calculated indicates the theoretical concentration of silica contained in given amount of K-feldspar based on the chemical analysis.

2.4. Sample/product characterization

The initial raw k-feldspar ore and the PSP produced after precipitation was analyzed by X-ray fluorescent (XRF) with model No: X-MET800. X-ray powder diffraction (XRD) analysis

of both k-feldspar and PSP was carried out using an APD 2000 diffractometer manufactured by Ital Structures (Riva Del Garda, Italy) and Scanning electron microscopy (SEM) techniques was used for microstructure analysis. pH values were measured with a pHM-26 instrument and a combined glass electrode with an operating range of up to pH ~ 14, both manufactured by Radiometer (Denmark). The Fourier transform IR spectrum was recorded using a Perkin-Elmer spectrometer (Model 2000). The specimen was pressed using a spectroscopically pure KBr matrix.

3. Results And Discussion

3.1. Ore characterization

The raw mineral used in this study as examined by XRF gave 18.61 % quartz, 1.32 % iron, 12.05 % aluminium, 12.15 % potasium, 0.69 % sulphur, 0.14 % calcium and 0.55 % calcium. The mineral phase of the ore detected by XRD supported the XRF result, comprised mainly of *quartz* ($Si_{3.00}$ $O_{6.00}$: 96-900-2700) albite ($AlSi_{3.00}O_{8.00}$: 96-900-9076), and orthoclase (KAlSi3.00O5.00 : 96-900-9567). The SEM analysis indicated that the raw ore consists of an-hedral to sub-hedral with two distinct scattered crystals of potassium and aluminium silicate (Fig. 1) varieties [18]

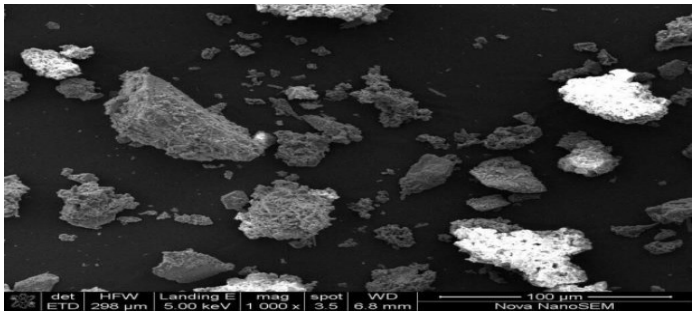

FIGURE 1. Micro structural image of raw K-feldspar.

The photomicrography of the thin section also indicated the main metallic minerals present in ore as aluminum oxide, potassium oxide, iron oxide (haematite) with associated gangues identified as quartz (Fig. 2).

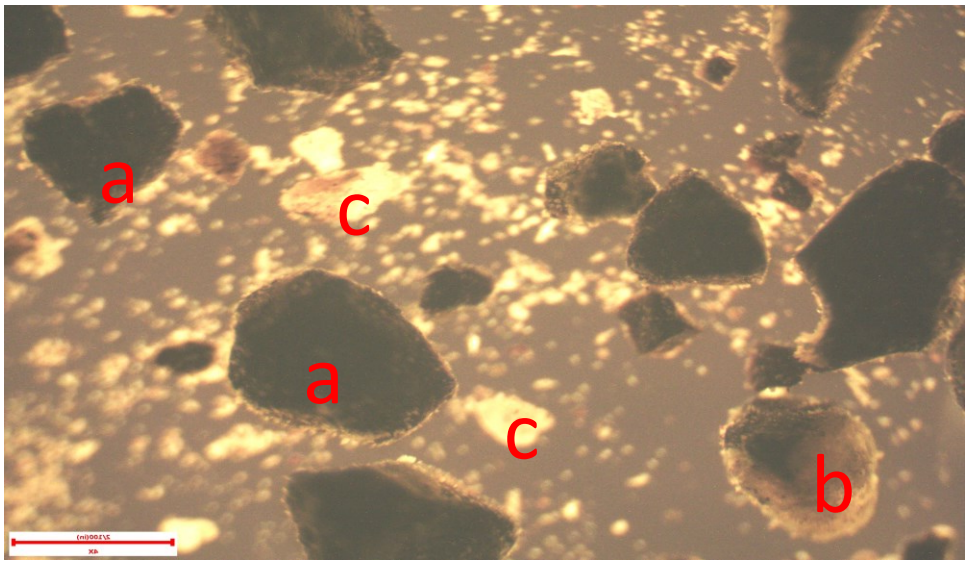

FIGURE 2. Photomicrography image of raw K-feldspar (a) quartz (b) albite (c) aluminium oxide.

3.2. Dissolution parameters optimization

3.2.1. Effects of sodium hydroxide concentration

A series of experiments was carried out to determine the influence of NaOH on the dissolution kinetics of K-feldspar. The concentration of NaOH varied from 0.5-2.5, as shown in Fig. 3. The highest SPS recovery was obtained from k-feldspar when 2.5M NaOH was used. This observation indicates that a highly concentrated alkaline solution is required to digest the K-feldspar and to extract silica.

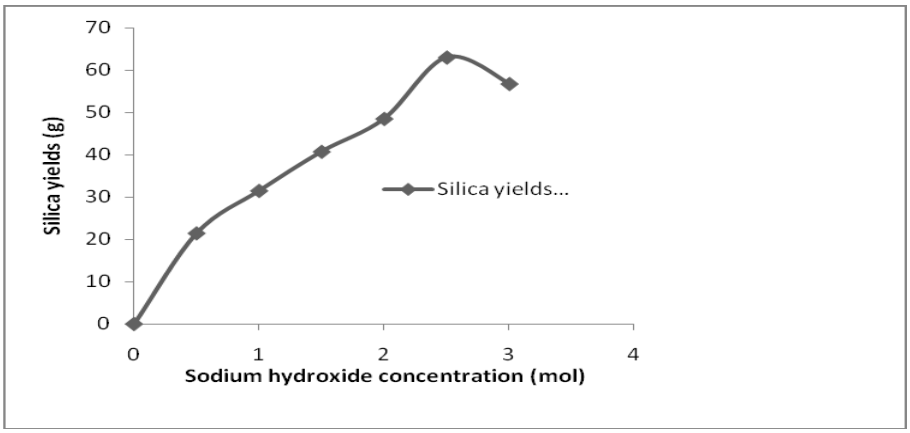

FIGURE 3. Profile of effect of concentration on silica extraction.

3.2.2. Effect of reaction temperature

The effect of leaching temperature (27–90°C) on the extent of k-feldspar ore dissolution was investigated. Other experimental conditions was kept constant at S/L of 20 g/L, 2.5 mol/L NaOH concentrations with moderate stirring (300 rpm) speed up to time interval of 120 minutes (Fig. 4).

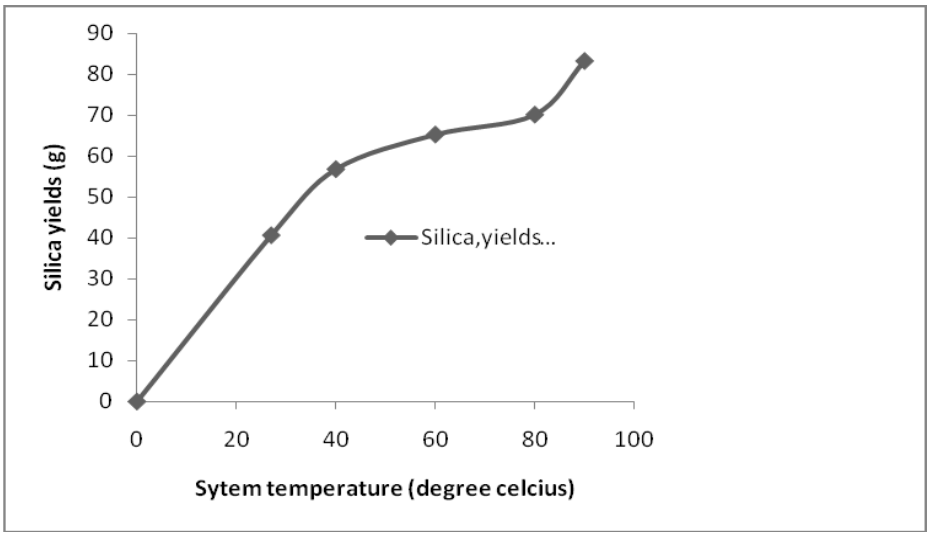

FIGURE 4. Profile of system temperature on silica extraction

From the result shown graphically in Fig. 4, it is evident that temperature plays an important role on the extent of K-feldspar ore dissolution. With increasing temperature, the dissolution increases. For example, at 90ºC, about 83.3 % of the initial 20 g/L k-feldspar ore was reacted within 120 minutes of reaction time. This is in line with the result of other similar studies which affirmed that increasing temperature of a system during ore dissolution speed up the rate of a reaction process [8]. However in this study, temperature above 90ºC was not considered.

3.2.3. Effect of particle size

Leaching experiment was carried out using three different particle size fractions of -75+90 µm, -90+112 µm, -112+145 µm. Other experimental conditions were kept constant at temperature 90 ºC, S/L of 20 g/L, 2.5 mol/L NaOH with moderate stirring (400 rpm) speed up to time intervals of 120 minutes (Fig. 5). This result affirmed that as ore fraction decreases from -112+145 µm to 63+75 µm, dissolution efficiency increases moderately. This result support liberation properties by mechanical milling that improve the surface area for reaction enabling chances.

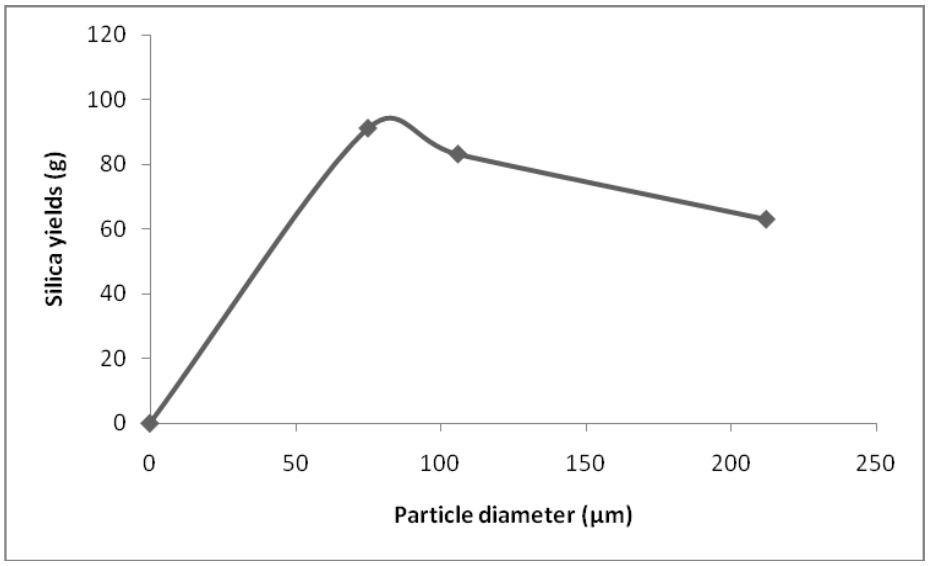

FIGURE 5. Effect of particle diameter on silica yield.

3.3. Kinetic analysis

In solid–fluid systems, the reaction rate is governed by one of the following kinetic mechanisms: diffusion through fluid film, diffusion through ash or product layer, or surface-controlled chemical reaction [16,17-18]. In a general form, the solid–fluid reaction can be represented as:

$$A_{(fluid)} + B_{(solid)} \rightarrow C_{(products)} \quad (3.1)$$

In acidic/basic leaching, the heterogeneous non-catalytic reaction for most mineral ore might be kinetically interpreted using the un-reacted Shrinking Core Model (SCM) [19,20]. The SCM is based on the description that solid particles are consumed by dissolution or reaction and as a result, the material being consumed is shrinking. Following the principle that dissolution process takes place from the outer surface of the ore particle, and as dissolution proceeds, the interface between the un-dissolved solid phase and solute free phase move towards the centre of the core, yielding the following three steps[21,22].

(i) diffusion of solute molecules from the solid-solid interface to the solid-liquid interface via the solute-free portion of the particle,

(ii) diffusion of solute molecules from the solid-liquid interface through the surface layer to the outer boundary of the surface layer; and

(iii) diffusion of solute molecules from the outer boundary of the surface layer to bulk liquid phase.

The rate equations for surface chemical reaction and diffusion through fluid film can be represented by eqn (3.2) and (3.3), respectively:

$$1 - 2/3\alpha - (1 - \alpha)^{2/3} = k_d t \quad (3.2)$$

$$1 - (1 - \alpha)^{1/3} = k_s t \quad (3.3)$$

Generally, it is assumed that α is the fraction of k-feldspar dissolved, and t is the reaction time (min), and k_S and k_d are the reaction rate constants for surface chemical reaction and diffusion through fluid film, respectively. In order to determine the rate limiting step for the leaching of silica from k-feldspar, the obtained experimental data were analysed using statistical and graphical approaches. From an analysis of correlation coefficients, it was determined that the leaching of k-feldspar in alkaline media follows a surface chemical reaction-controlled mechanism. Therefore, substituting the experimental data obtained from

Figures 3 and 4 into the kinetic equations (3.2–3.3). The calculated statistical average correlation of 0.65 and 0.94 respectively, showing that equation (3.3) gave better correlation. This indicates that the mechanism of k-feldspar leaching is closely follows the chemical controlled model and it was used in the estimation of some thermodynamics parameters such as reaction order and activation energy for the dissolution reaction as follows.

The treatment of dissolution data in Fig. 3 was done using (equation 3.3) to obtain the linear graph which later used to determine the order of reaction at defined concentrations of NaOH by plotting the value of $\ln k_s$ versus ln[NaOH] as depicted in Fig. 6.

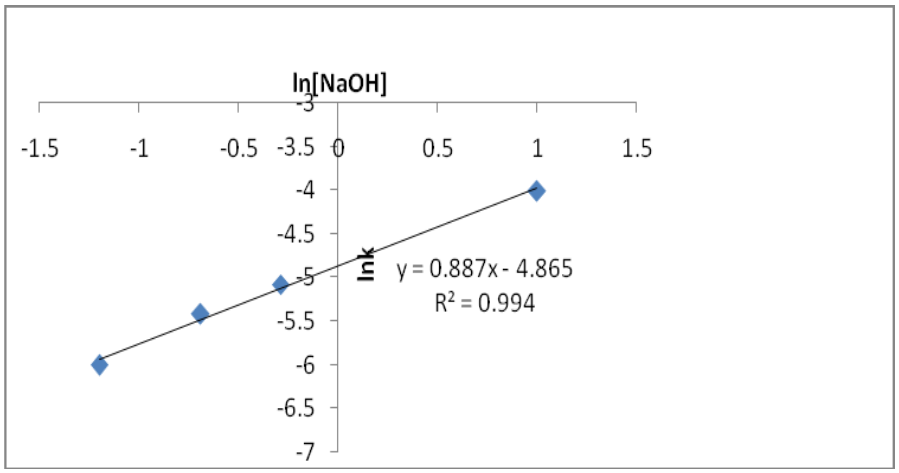

FIGURE 6. Relationship between ln*k* and ln*[NaOH]* for silica extraction.

The order of reaction derived from Fig. 6 gave 0.887 ~1.0 indicating a first order reaction at defined leachant concentrations. The temperature dependence of the reaction rate constant (dissolution activation energy) was calculated using the Arrhenius equation, the rate constant can be expressed as:

$$k_S = A_o e^{-Ea/RT} \tag{3.4}$$

Here, A_o is the Arrhenius constant, Ea the energy of activation, R the ideal gas constant, and T the reaction temperature. By comparing eqn (3.3) and (3.4), the integral rate expression can be written as

$$1 - (1 - \alpha)^{1/3} = A_o e^{-Ea/RT} t \tag{3.5}$$

In order to determine the values of the activation energy and Arrhenius constant, ln k_S and (1/T) values were plotted, as shown in Fig. 7.

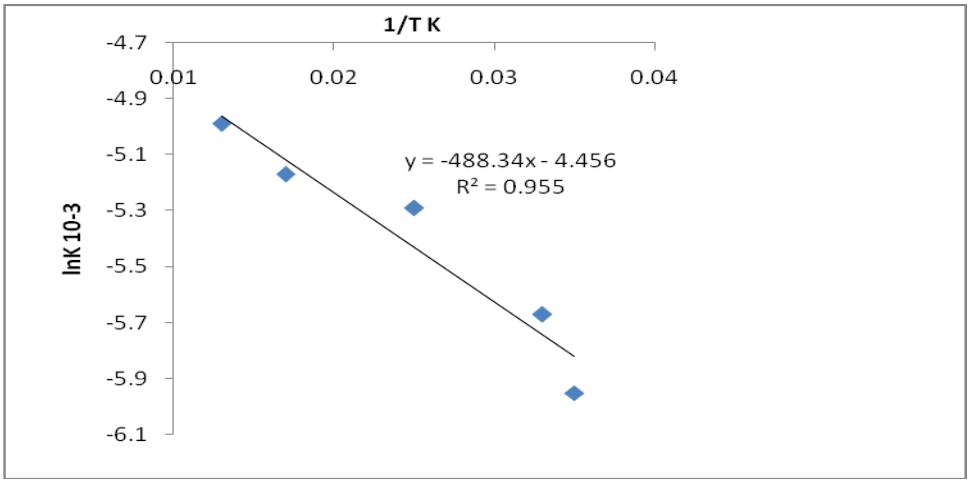

FIGURE 7. ln*k* versus 1/*T*.

Inserting the values for the activation energy and Arrhenius constant, eqn (8) can be written as

$$1 - (1 - \alpha)^{1/3} = 4.3357\ e^{-4063/RT}\ t \qquad (3.6)$$

The value of the activation energy (40.63 kJmol^{-1}) in equation (3.6) for the alkaline leaching of k-feldspar is in agreement with values obtained in previous studies of fluid–solid reaction systems [8, 23-24].

3.4. Purity analysis of PSP

Pure silica precipitate obtained from alkaline dissolution of K-feldspar was characterized by Fourier Infrared (FT-IR), XRD, SEM and thermogravimetric analysis (TGA). Fig. 8 exhibits the FT-IR spectra of extracted silica obtained after calcinations at 800°C for two hours.

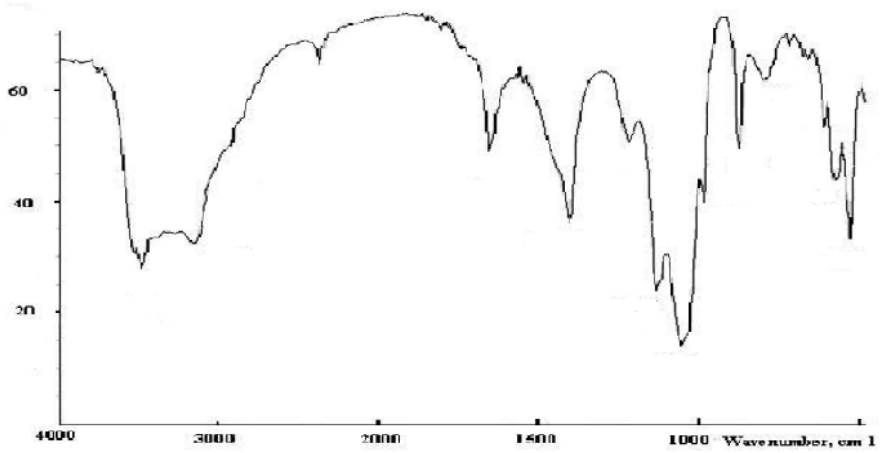

FIGURE 8. FT-IR spectral of precipitated silica.

The predominant band at 1100 cm^{-1} and the shoulder at 1189 cm^{-1} in Fig. 8 are associated with asymmetric stretching-vibrations of siloxane νs(Si-O-Si). The presence of bands at 474 cm^{-1} and 812 cm^{-1} was due to the presence of symmetric siloxane groups νs(Si-O-Si). The existence of a band at 950 cm^{-1} is associated with Si-OH groups; this band's existence is due to high concentrations of silanol groups with smaller particle sizes. The shoulder appeared at 3750 cm^{-1}, indicating the presence of hydrogen bonds that resulted from interaction between the silanol groups (Si-OH) located at the surface of the silica material. In the material, the band located at 1642 cm^{-1} is attributed to the O-H bending vibration of the adsorbed molecular water and its corresponding stretching vibration at 3452 cm^{-1}.

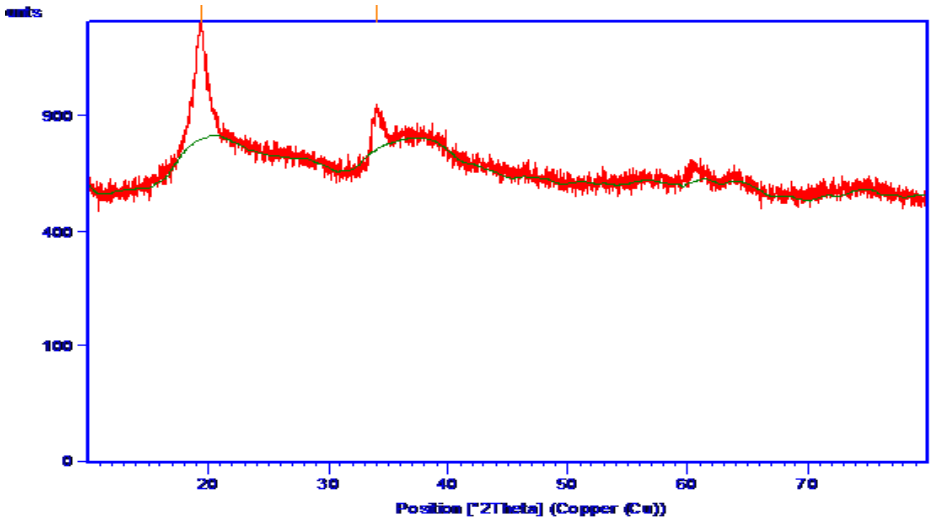

FIGURE 9. The XRD spectra of precipitated crystalline phase.

The XRD pattern of PSP shown in Fig. 9 shows that the PSP sample lacked any crystalline phase and exhibited an amorphous nature. The morphology of the PSP was studied by SEM (Jeol-5800LV). Fig. 10a shows the fluffy and porous nature of PSP, and that the most of the PSP particles were smaller than 1 mm. The EDX spectrum of APS (Fig. 10b) shows that the PSP sample was devoid of any inclusions or impurities. The thermal stability of PSP was determined by TGA using a heating rate of 10 °C min^{-1}. The TGA curve in Fig. 11 indicates two regions of weight loss, a lower temperature weight loss due to evaporation of weakly bonded (physisorbed) water molecules and a higher temperature loss during condensation of silanol groups.4 The overall weight loss of the APS sample was 11%; 8% weight loss occurred below 200 °C, while the remaining 3% took place between 200–500 °C.

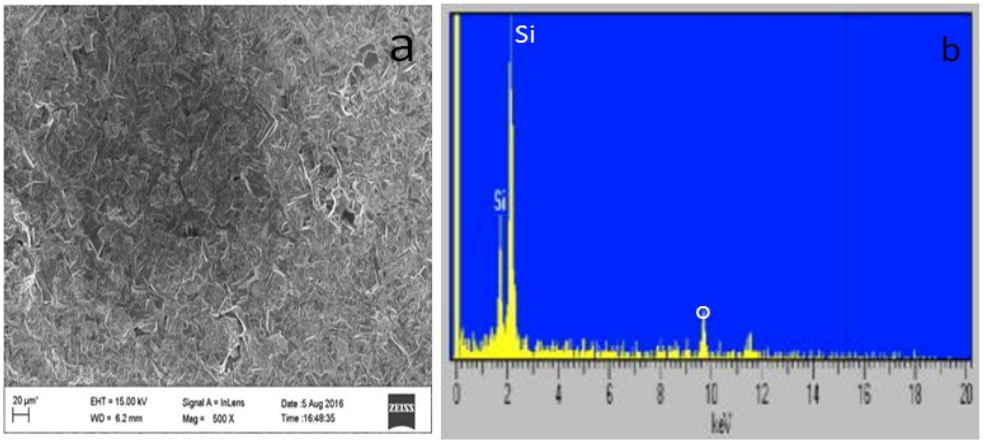

FIGURE 10. Microstructural Morphology of the PSP (a) SEM image (b) EDS of targeted point.

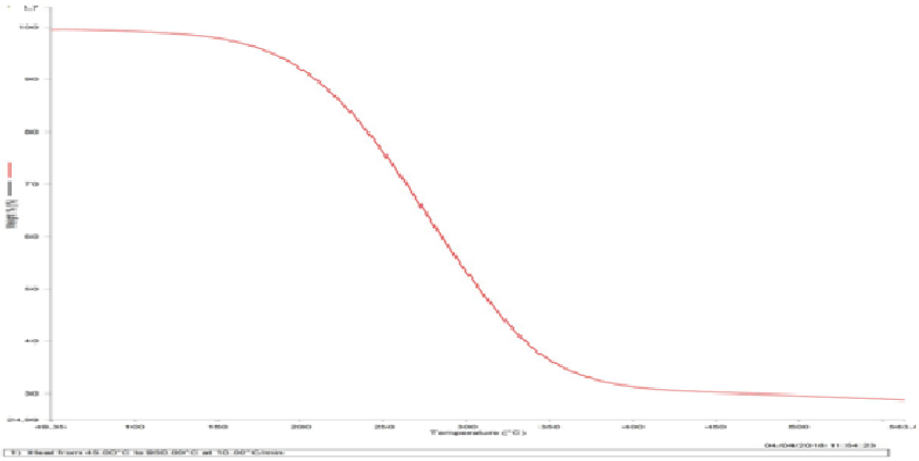

FIGURE 11. TGA spectra of precipitated silica heat from 45 °C – 950 °C at 10 °Cmin^{-1}.

3.5. Schematic diagram of pure silica precipitated process

A simple hydrometallurgical scheme was proposed for the extraction of silica from a Nigerian origin k- feldspar ore for industrial value addition (Fig. 12).

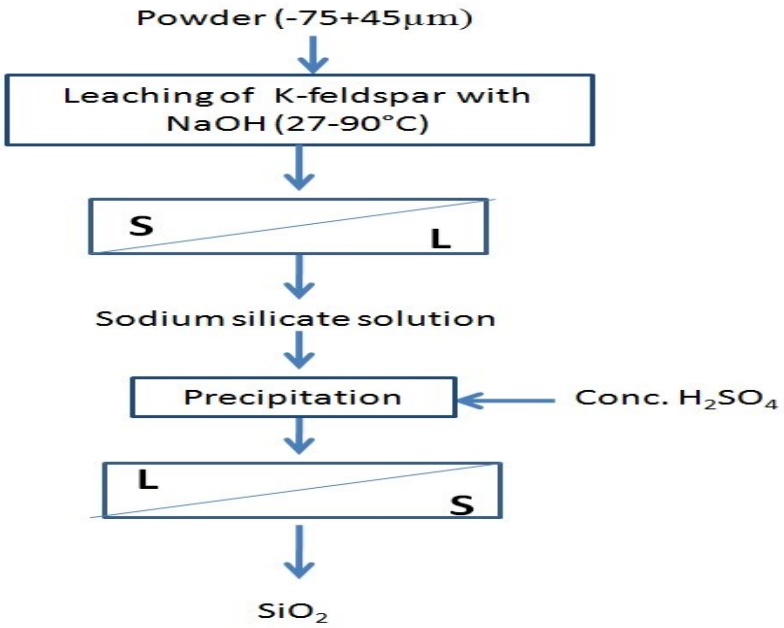

FIGURE 12. Schematic diagram of silica extraction from k-feldspar.

4. Conclusion

The process development for the extraction of pure silica from k-feldspar silicate mineral is unique in nature. Highly pure silica (SiO_2) powder was obtained through roast leaching and precipitation treatment of k- feldspar of Giri village, Nigeria, which contains an appreciable amount of silicate minerals. The conversion of k-feldspar powder into silica reached 83.3% as the process progresses. The leaching data obtained was analyzed by suitable Shrinking Core Model and the chemical controlled mechanism was found appropriate as the rate determine step for the dissolution process and the calculated activation energy (E_a) of 40.63 $kJmol^{-1}$ supported the proposed model. The FTIR and XRD technique of the synthesized product confirmed production of pure silica at optimal conditions and expected to improve revenue generation to aid Nigeria economic diversification and sustainability.

Özet

Nijerya, çok çeşitli mineral kaynağı olan Afrika ülkelerinden birisidir. Ülkenin tüm bölgelerindeki büyük mineral bolluğuna rağmen, bu kaynaklar ülke ekonomisine katkı sağlamak, sanayileşmeye yardımcı olmak ve gelir yaratmak için daha az kullanılmıştır. Bu nedenle, *ortoklaz* ($KAlSiO_8$: 96-740-9031), *albit* ($AlSiO_8$: 96-940-0741) ve *kuvars* (SiO_2 : 96-900-9667) safsızlıklarının bir karışımını içeren bir Nijerya k-feldispatının saf silika tozu (PSP) elde etmek için kullanımı, kavurma liçi ve birlikte çöktürme yöntemi ile incelendi. Liç sırasında, sızıntı suyu konsantrasyonu, parçacık büyüklüğü ve tepkime sıcaklığı gibi parametreler incelendi. Optimum liç koşullarında (2.0 mol/L NaOH, 90 °C), başlangıçta 10g/L mineralin %87' si 120 dakika içerisinde tepkimeye girdi. XRD ile analiz edilen tepkimeye girmemiş ürünün (~% 13.0) bazı tanımlanmış endüstriler için değerli bir yan ürün olarak hizmet verebilen silisyumlu safsızlıklar içerdiği bulundu. Optimal liçteki sızıntı suyu, endüstriyel değerde saf silika tozu elde etmek üzere derişik H_2SO_4 kullanılarak çöktürüldü.

References

[1] A. D. William R. A. Howie and W. S. Wise, Rock-forming minerals: Framework silicates: Slica minerals, feldspathoids and the zeolites. Geological Society, 3/5 (2004) 22-30.

[2] P. J. Heaney, Structure and chemistry of the low-pressure silica polymorphs. Reviews in Mineralogy, 29 (1994) 3-6.

[3] K. Kuniaki, T. Matsumoto and M. Imamura, Structural change of orthorhombic-I tridymite with temperature: A study based on second-order thermal-vibrational parameters. Zeitschrift für Kristallographie, 6 (1986) 12-17.

[4] J. W. Anthony, R. A. Bideaux, K. W. Bladh and M. C. Nichols, "Tridymite". Handbook of Mineralogy (PDF). III (Halides, Hydroxides, Oxides). Chantilly, VA, US, Mineralogical Society of America. 2 (2011) 32-54.

[5] S. Music, R. Filipovic-vincekovic and L. Sekovanic, Precipitation of amorphous SiO_2 particle and their properties. Brazillian Journal of Chemical Engineering, 128/1 (2011) 89-94.

[6] J. R. Martinez, S. Palomares, G. Ortega-Zarzosa, F. Ruiz and Y. Chumakov, Rietveld refinement of amorphous SiO_2 prepared via sol–gel method. Materials Letters, 60 (2006) 3520-3526.

[7] N. Moreno, X. Querol, F. Plana, J. M. Andres, M. Janssen and H. Nugteren, Pure zeolite synthesis from silica extracted from coal fly ashes. Journal of Chemical Technology and Biotechnology, 77 (2002) 274-279.

[8] R. Nadeem, R. Waseem, M. Silvia, A. Henry, V. Kumar and R. Ki-Hyun, Synthesis and characterization of amorphous precipitated silica from alkaline dissolution of olivine. RSC advance, 8 (2018) 32651-32658.

[9] G. Zhang., Y. Xu, D. Xu, D. Wang, Y. Xue and W. Su, Pressure-induced crystallization of amorphous SiO_2 with silicon-hydroxy group and the quick synthesis of coesite under lower temperature. High Pressure Research, 28 (2008) 641-648.

[10] E. R. Essien, O. A. Olaniyi, L. A. Adams and R. O. Shaibu, Sol-gel-derived porous silica: economic synthesis and characterization. Journal of Minerals and Materials Characterization and Engineering, 11 (2012) 976-981.

[11] M. Asmaa, K. Mariam, E. Adnane, K. Mohammed, H. Mohammed and A. Said, The synthesis and characterization of low-cost mesoporous silica SiO_2 from local pumice rock. Nanomaterial and Nanotechnology, 5(3) (2015) 1-7.

[12] K. Srivastava, N. Shringi, V. Devra and A. Rani, A facile method for production of amorphous silica from perlite under microwave irradiation. International Journal of IT, Engineering and Applied Sciences Research, 4 (2015) 18-24.

[13] A. Rani, S. Sanal, T. Jacob, G. Jacob, P. K. Desy and N. K. Manivarnan, Silica nano particles synthesized from boiler spent ash: Value addition to an industrial waste. Chemistry and Materials Research, 6 (2014) 93-99.

[14] K. M. Rani, P. N. Palanisamy, P. Sivakumar, Synthesis and characterization of amorphous nanosilica from biomass ash. International Journal of Advanced Technology in Engineering and Science 2 (2014) 71-76.

[15] U. Kalapathy, A. Proctor and J. Shultz, An improved method for production of silica from rice hull ash. Bioresource Technology, 85 (2002) 285-289.

[16] E. V. Todorova, G. E Chernev and S. P. Djambazov, Structure and properties of functionalized porous silica hybrid materials. Open Journal of Inorganic Non-Metallic Materials, (2014) 435-443.

[17] I. K.Ayinla, A. A. Baba, M. A. Raji, C. D. Uzondu, A. A. Mohammed and S. Girigisu, Quantitative leaching of potassium from K-feldspar ore bt Roast-leaching process. Journal of Chemical Society of Nigeria, 43/4 (2018) 825-832.

[18] O. Levenspiel, Chemical Reaction Engineering, 2nd ed. Wiley, New York, NK (1992) 5-12.

[19] A. Ekmekyapar, A. Celal, D. Nizamettin, K. Asim, B. Ahmet and C. Kadim, Reductive leaching of manganese ore. Russian Journal of Non-Ferrous Metals, 53/211 (2012) 76-84.

[20] H. Wei-Lun, L. Mon-Jyh and H. Jyh-Ping, Kinetic Leaching of ouka iron ore. International Journal of Chemical and Molecular Engineering, 3/5 (2009) 6-9.

[21] A. Alaoui, K. E Kacemi, K. E. Ass, Y. Darmane, S. Kitane. Mineral Processing and Extractive Metallurgy IMM Transactions, 125 (2016) 102-109.

[22] A. A. Baba, F. A. Adekola and R. B. Bale, Development of a pyro- and hydro metallurgical route to treat zinc-carbon batteries. Journal of Hazardous Materials, 171/1-3 (2009) 837-844.

[23] E. A. Abdel-Aal and M. M. Rashad, Kinetic study on the leaching of spent nickel oxide catalyst with sulfuric acid. Hydrometallurgy, 74 (2005) 189-194.
[24] I. K. Ayinla, Development of extraction methods and preparation of some industrial chromium compounds from a Nigeria chromite ore. pH.D. thesis, Department of Chemistry, University of Ilorin, Nigeria, 403 (2018).

Current Address: KURANGA I. AYINLA (Corresponding author): Department of Industrial Chemistry, University of Ilorin, P.M.B 1515, Ilorin-240003, Nigeria.
E-mail Address: ibkuranga@gmail.com, ayinla.ik@unilorin.edu.ng
ORCID: https://orcid.org/0000-0003-1988-3643

Current Address: ALAFARA A. BABA: Department of Industrial Chemistry, University of Ilorin, P.M.B 1515, Ilorin-240003, Nigeria.
E-mail Address: balafara@yahoo.com
ORCID: https://orcid.org/0000-0002-6978-7898

Current Address: SUBRAT KU. PADHY: Hydro & Electrometallurgy Department, CSIR-Institute of Minerals and Materials Technology,
E-mail Address: spadhy99@gmail.com
ORCID: https://:orcid.org/0000-0003-2415-0348

Current Address: OSENI ADIO: Department of Science Laboratory Technology, Kwara State Polytechnic, Ilorin, Nigeria
E-mail Address: adio.oseni@gmail.com
ORCID: https://:orcid.org/0000-0002-5122-9337

Current Address: KEHINDE A. ODELEYE: Department of Industrial Chemistry, University of Ilorin, P.M.B 1515, Ilorin-240003, Nigeria.
E-mail Address: adedoyinyink15@gmail.com
ORCID: https://:orcid.org/0000-0002-1525-9088

Current Address: BANKIM CH. TRIPATHY: Hydro & Electrometallurgy Department, CSIR- Institute of Minerals and Materials Technology,
E-mail Address: bankimtripathy@gmail.com
ORCID: https://orcid.org/0000-0002-4055-3203

INSTRUCTIONS TO CONTRIBUTORS

Communications Faculty of Sciences University of Ankara Series B Chemistry and Chemical Engineering is a peer reviewed journal which has been published since 1948 by Ankara University, accepts original research articles written in English in the fields of Chemistry and Chemical Engineering. Review articles written by eminent scientists can also be invited by the Editor.

The publication costs for Communications Faculty of Sciences University of Ankara Series B Chemistry and Chemical Engineering are covered by the journal, so authors do not need to pay an article-processing and submission charges. The PDF copies of accepted papers are free of charges and can be downloaded from the webside. Hard copies of the paper, if required, are due to be charged for the amount of which is determined by the administration each year.

Manuscripts should be typeset using the LATEX typesetting system or as a DOCX file. Authors may submit their manuscript and the Cover Letter via our submission system. A template of manuscript can be reviewed in https://dergipark.org.tr/tr/download/journal-file/16598. After the acceptance of manuscripts for publication, we will ask you to submit the TeX or Doc form of the manuscript prepared in accordance with the style of the Journal. Authors are required to submit their Open Researcher and Contributor ID (ORCID) 's which can be obtained from http://orcid.org as their URL address in the format http://orcid.org/xxxx-xxxx-xxxx-xxxx.

Acknowledgements should be given as short as possible at the end of the text. Formulas should be numbered consecutively in parentheses ( ). Footnotes should be avoided if possible, but when necessary, should be short and never contain any important part of the work and should be numbered consecutively by superscripts. All illustrations not including tables (photographs and other films, drawings, graphs, etc) must be labeled as "Figure #. Explanation".

Note that in the cover letter, authors should nominate three potential reviewers and the most appropriate Field Editor of the research. The editorial office may not use these nominations, but this may help to speed up the selection of appropriate reviewers.
In the cover letter you may enter details of anyone who you would prefer not to review your manuscript.

The proper position of each table and figure must be clearly indicated in the paper. All tables and figures must have a number (Table 1, Figure 1) and a caption or legend. References including comments must be numbered consecutively in order of first appearance in the text. The reference number should be put in brackets [] where referred to in the text. References should be listed at the end of the manuscript in the numbered order in which they appear in the text as follows:
[1] E. Bairamov and N. Ozalp, Uniform convergence and numerical computation of the Hubbell radiation rectangular source integral, Radiation Physics and Chemistry, 80 (2011), 1312–1315.
[2] Kelley, J. L., General Topology, Van Nostrand, 1970.
[3] G. Huve, K. Takahashi and M. Hashimoto, Brain activity recognition with a wearable fNIRS using neural networks, Mechatronics and Automation, (2017), 1573-1578.

The Editor may seek the advice of two, or three referees, depending on the response of the referees, chosen in consultation with appropriate members of the Editorial Board, from among experts in the field of specialization of the paper. The reviewing process is conducted in strict confidence and the identity of a referee is not disclosed to the authors at any point since we use a single-blind peer review process.

It is a fundamental condition that articles submitted to COMMUNICATIONS have not been previously published and will not be simultaneously submitted or published elsewhere. After the manuscript has been accepted for publication, the author will not be permitted to make any new additions to the manuscript.

Before publication the galley proof is always sent to the author for correction. Thus it is solely the author's responsibility for any typographical mistakes which occur in their article as it appears in the Journal. The contents of the manuscript published in the COMMUNICATIONS are the sole responsibility of the authors.

Research papers published in Communications Faculty of Sciences University of Ankara are archived in the Library of Ankara University (Volume 1-60) and Dergipark immediately following publication with no embargo.

C O M M U N I C A T I O N S

FACULTY OF SCIENCES
UNIVERSITY OF ANKARA

DE LA FACULTE DES SCIENCES
DE L'UNIVERSITE D'ANKARA

VOLUME: 61 **Number: 1-2** **YEAR: 2019**

Series B: Chemistry and Chemical Engineering